

Winter 2008

# Spectral effects of a calcium amendment on red spruce foliage at laboratory and stand scale

Will Robinson Kessler

*University of New Hampshire, Durham*

Follow this and additional works at: <https://scholars.unh.edu/thesis>

---

## Recommended Citation

Kessler, Will Robinson, "Spectral effects of a calcium amendment on red spruce foliage at laboratory and stand scale" (2008). *Master's Theses and Capstones*. 423.

<https://scholars.unh.edu/thesis/423>

This Thesis is brought to you for free and open access by the Student Scholarship at University of New Hampshire Scholars' Repository. It has been accepted for inclusion in Master's Theses and Capstones by an authorized administrator of University of New Hampshire Scholars' Repository. For more information, please contact [nicole.hentz@unh.edu](mailto:nicole.hentz@unh.edu).

SPECTRAL EFFECTS OF A CALCIUM AMENDMENT ON RED SPRUCE  
FOLIAGE AT LABORATORY AND STAND SCALE

BY

WILL ROBINSON KESSLER  
B.S., Cornell University, 2002

THESIS

Submitted to the University of New Hampshire  
in Partial Fulfillment of  
the Requirements for the Degree of

Master of Science  
in  
Natural Resources

December, 2008

UMI Number: 1463227

### INFORMATION TO USERS

The quality of this reproduction is dependent upon the quality of the copy submitted. Broken or indistinct print, colored or poor quality illustrations and photographs, print bleed-through, substandard margins, and improper alignment can adversely affect reproduction.

In the unlikely event that the author did not send a complete manuscript and there are missing pages, these will be noted. Also, if unauthorized copyright material had to be removed, a note will indicate the deletion.

**UMI**<sup>®</sup>

---

UMI Microform 1463227

Copyright 2009 by ProQuest LLC.

All rights reserved. This microform edition is protected against unauthorized copying under Title 17, United States Code.

ProQuest LLC  
789 E. Eisenhower Parkway  
PO Box 1346  
Ann Arbor, MI 48106-1346

This thesis has been examined and approved.



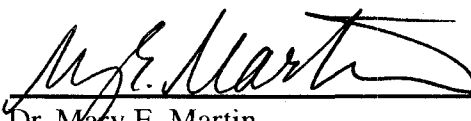
---

Thesis Director, Dr. Barrett N. Rock  
Professor of Natural Resources/EOS



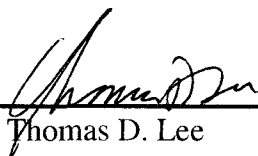
---

Dr. Richard A. Hallett  
Research Ecologist, U. S. Forest Service,  
Northern Research Station, Durham, NH



---

Dr. Mary E. Martin  
Research Assistant Professor EOS,  
Affiliate Assistant Professor of Natural Resources



---

Dr. Thomas D. Lee  
Associate Professor of Forest Ecology



---

Dr. Jana Albrechtová  
Associate Professor of Plant Physiology  
Charles University

---

November 17, 2008

DEDICATION

To my wife Marta.

## ACKNOWLEDGEMENTS

Without the help of several people, this thesis would probably still be sitting in its own special drawer. Sincere thanks are due to Gloria Quigley, Mike Gagnon, Danielle Haddad, and Tricia McCarthy. Nor can the role of a fine committee be understated in matters *macro* and *micro*. I offer my appreciation and admiration to Drs. Tom Lee, Jana Albrechtová, Mary Martin, Rich Hallett, and Barry Rock. Tim Fahey provided helpful guidance and comments on more than one occasion. Thanks also to my own family for their unwavering support and useful input.

This project was funded by a Space Grant Fellowship from the New Hampshire space Grant Consortium / NASA.

The work is a contribution to the Hubbard Brook Ecosystem Study, a joint undertaking of the U.S. Forest Service and The Cary Institute for Ecosystem Studies.

## TABLE OF CONTENTS

|                       |      |
|-----------------------|------|
| ACKNOWLEDGEMENTS..... | iv   |
| LIST OF TABLES.....   | vii  |
| LIST OF FIGURES.....  | viii |
| ABSTRACT.....         | ix   |

| CHAPTER | PAGE |
|---------|------|
|---------|------|

|                   |   |
|-------------------|---|
| INTRODUCTION..... | 1 |
|-------------------|---|

I. FOLIAR OXALIC ACID INCREASES IN RESPONSE TO CALCIUM-

|   |   |
|---|---|
| WOLLASTONITE APPLICATION IN A RED SPRUCE STAND..... | 2 |
|---|---|

|               |   |
|---------------|---|
| Abstract..... | 2 |
|---------------|---|

|                   |   |
|-------------------|---|
| Introduction..... | 2 |
|-------------------|---|

|              |   |
|--------------|---|
| Methods..... | 5 |
|--------------|---|

|              |    |
|--------------|----|
| Results..... | 10 |
|--------------|----|

|                 |    |
|-----------------|----|
| Discussion..... | 12 |
|-----------------|----|

|              |    |
|--------------|----|
| Summary..... | 17 |
|--------------|----|

|                       |    |
|-----------------------|----|
| Literature cited..... | 19 |
|-----------------------|----|

|                         |    |
|-------------------------|----|
| Tables and figures..... | 23 |
|-------------------------|----|

II. LABORATORY SPECTRAL RESPONSES AND STRESS INDICATORS IN

|   |  |
|---|--|
| CALCIUM-TREATED RED SPRUCE FOLIAGE AT THE HUBBARD BROOK |  |
|---|--|

|  |     |
|--|-----|
| EXPERIMENTAL FOREST.....   | 33  |
| Abstract.....  | 33  |
| Introduction.....  | 34  |
| Methods.....   | 36  |
| Results.....   | 40  |
| Discussion.....  | 43  |
| Summary.....   | 50  |
| Literature cited.....  | 52  |
| Tables and figures.....  | 57  |
|  |     |
| III. MEASUREMENT OF STAND SPECTRAL RESPONSES FOLLOWING<br>CALCIUM APPLICATION TO A SMALL FORESTED WATERSHED USING<br>LANDSAT TM IMAGERY..... | 69  |
| Abstract.....  | 69  |
| Introduction.....  | 70  |
| Methods.....   | 72  |
| Results.....   | 79  |
| Discussion.....  | 80  |
| Summary.....   | 86  |
| Literature cited.....  | 87  |
| Tables and figures.....  | 92  |
| CONCLUSION.....  | 103 |



## LIST OF TABLES

|  |       |
|--|-------|
| TABLE 1: Plot biometric description.....   | 23    |
| TABLE 2: Foliar chemistry effects by watershed.....                              | 24    |
| TABLE 3: Foliar chemistry correlations: calcium.....                             | 25    |
| TABLE 4: Foliar chemistry correlations: oxalate.....                             | 25    |
| TABLE 5: Synopsis of hyperspectral indices.....                                  | 57/58 |
| TABLE 6: Spectral index effects by watershed.....                                | 59/60 |
| TABLE 7: Correlations of hyperspectral indices with foliar calcium.....          | 61/62 |
| TABLE 8: Correlations of hyperspectral indices with foliar oxalate.....          | 63/64 |
| TABLE 9: List of Landsat imagery used.....                                       | 92    |
| TABLE 10: Coefficients of determination for image pair normalization.....        | 93    |
| TABLE 11: Mean coniferous pixel reflectance change, by watershed, 1999-2007..... | 93    |
| TABLE 12: Mean deciduous pixel reflectance change, by watershed, 1999-2007.....  | 93    |
| TABLE 13: Change in coniferous NDVI and TM5/4, by watershed, 1999-2007.....      | 94    |
| TABLE 14: Change in deciduous NDVI and TM5/4, by watershed, 1999-2007.....       | 94    |

## LIST OF FIGURES

|  |     |
|--|-----|
| FIGURE 1: Map of New Hampshire, HBEF, and the White Mountains.....                 | 26  |
| FIGURE 2: Partitioning of foliar samples into three needle age classes.....        | 27  |
| FIGURE 3: Mean annual basal area increment, by watershed.....                      | 28  |
| FIGURE 4: Foliar chemistry results by needle age class.....                        | 29  |
| FIGURE 5: Correlation of foliar chemicals with total foliar calcium.....           | 30  |
| FIGURE 6: Correlation of oxalate with other foliar chemicals.....                  | 31  |
| FIGURE 7: SEM imagery and EDS analysis results from red spruce needle section..... | 32  |
| FIGURE 8: Mean spectral reflectance curves, by needle age class.....               | 65  |
| FIGURE 9: Mean spectral reflectance curves, by watershed.....                      | 66  |
| FIGURE 10: Reflectance difference curves, by watershed.....                        | 67  |
| FIGURE 11: Reflectance sensitivity curves by watershed.....                        | 68  |
| FIGURE 12: Map of northern New England with Landsat scene footprint.....           | 92  |
| FIGURE 13: Infrared-color Landsat image of the Hubbard Brook valley.....           | 95  |
| FIGURE 14: Spring aerial photograph of watersheds 1 and 6, HBEF.....               | 96  |
| FIGURE 15: Photograph of spruce-fir stand on the Hubbard Brook ridge.....          | 97  |
| FIGURE 16: Aerial photo showing location of rain gauge ground-control points.....  | 98  |
| FIGURE 17: Topographic map of HBEF, showing watersheds and sampling plots.....     | 99  |
| FIGURE 18: Hyperspectral reflectance and difference curves for MNY needles.....    | 100 |
| FIGURE 19: Eight-year coniferous pixel reflectance change, by watershed.....       | 101 |
| FIGURE 20: Eight-year deciduous pixel reflectance change, by watershed.....        | 102 |

## ABSTRACT

### SPECTRAL EFFECTS OF A CALCIUM AMENDMENT ON RED SPRUCE FOLIAGE MEASURED AT LABORATORY AND STAND SCALE

by

Will Robinson Kessler

University of New Hampshire, December 2008

Three sets of measurements were made to determine the effects of an October 1999 whole-watershed Ca-application on the chemical and spectral properties of red spruce (*Picea rubens* Sarg.) foliage at the Hubbard Brook Experimental Forest. Results of our measurements showed significant differences between the Ca-treated watershed (WS1) and a nearby reference watershed (WS6). Foliar chemistry data collected in 2007 showed that concentrations of Ca, Sr, and oxalate remain higher in WS1, and the increase in oxalate is strongly linked to the level of total Ca, possibly by a Ca-oxalate crystal precipitation response. High-resolution laboratory spectral data measured from 400-2500 nm show a pan-spectral increase in reflectance in WS1 spruce. Satellite data from the Landsat TM and ETM+ instruments did not parallel laboratory spectral results, but showed a distinct increase in near-infrared reflectance between 1999-2007. See individual chapter abstracts for more complete summaries.

## INTRODUCTION

This work is presented as a series of three manuscripts investigating the physiological processes and optical characteristics of calcium (Ca) in red spruce foliage and forests. The objective of this study was to link direct measurements of foliar chemistry and laboratory reflectance spectra to satellite remote sensing data from a Ca-amended watershed in the Hubbard Brook Experimental Forest. Our hypotheses are (a) Ca-driven differences in red spruce foliar chemistry are persistent eight years following the Ca amendment of 1999, (b) Ca-treatment has significantly affected the laboratory spectral signature of fresh red spruce foliage in both fractioned and heterogeneous needle samples and (c) hyper-spectrally measured differences in red spruce foliar reflectance will be observed in the multispectral Landsat data collected from these two watershed areas. The three chapters of this study will address each of these hypotheses and specific sub-hypotheses in turn.

## CHAPTER I

### **Foliar oxalic acid increases in response to calcium-wollastonite application in a red spruce stand.**

**Abstract.** Foliar elemental and organic oxalate ion ( $C_2O_4^{2-}$ ) concentrations were measured in needles from red spruce (*Picea rubens* Sarg.) eight years following the large-scale application of wollastonite ( $CaSiO_3$ ) to a watershed at the Hubbard Brook Experimental Forest (HBEF) in the White Mountain region of New Hampshire. Total foliar Ca, Sr, and oxalate were significantly ( $P < 0.05$ ) higher in Ca-treated needles from 2005, 2007, and in composite samples of mixed needle-age classes. The Ca application has also resulted in marginally significant trends of increased Mg ( $P = 0.068$ ) and decreased Al ( $P = 0.073$ ). There was strong ( $R^2 = 0.813$ ) positive correlation between total foliar Ca and oxalate contents in all needle classes, and the linear relationship between Ca and oxalate may indicate the precipitation of  $CaC_2O_4$  (calcium oxalate) is a sequestration-detoxification response to the amendment. Scanning electron microscopy and energy dispersive X-ray spectroscopy confirmed the presence of  $CaC_2O_4$  crystal-sand deposits along the cell walls of mesophyll cavities.

### **Introduction**

Calcium (Ca) plays a role in several important plant processes, including: signal transduction, synthesis of proteins and defense compounds, stomatal regulation, formation and adhesion of cell walls by pectate construction, and uptake of other nutrients by fine roots (Kauss, 1987; Delhaize and Ryan, 1995; McLaughlin and

Wimmer, 1999). The northeastern United States has historically been a region of high acidic deposition ( $\text{SO}_x$  and  $\text{NO}_x$ ) and much evidence points to Ca depletion in acidic soils as the dominant, ensuing stress affecting the forest systems here (Shortle and Smith, 1988; Federer et al., 1989; Likens et al., 1996; DeHayes et al., 1999; Driscoll et al., 2001).

Several studies have measured the Ca status of coniferous forests, and red spruce (*Picea rubens* Sarg.) in particular, across New England to assess the potential for recovery from acid rain (McNulty et al., 1991; Lawrence et al., 1997; Bullen and Bailey, 2005). The minimum level for red spruce (i.e. 0.8-1.2 mg Ca  $\text{g}^{-1}$  dry weight foliage) presented by Swan (1971) is useful as a coarse indicator of the Ca requirement to avert visible foliar deficiency symptoms. However, particular mechanisms of Ca regulation are poorly understood at both small and large spatial scales, and experimental approaches have been useful in exploring the nature of foliar Ca pools in response to different factors at different levels.

On small scales, a number of studies have documented the direct sensitivity of foliage in species such as balsam fir (*Abies balsamea* L.), red spruce, and Norway spruce (*Picea abies* L.) to fluctuations in micro-environment in connection with Ca. Crystal deposits of calcium oxalate (CaOx) have been observed forming in response to experimental acid precipitation treatments in Norway and red spruce (Fink, 1991b; Turunen et al., 1995), and suggest a net immobilization of Ca in response to acidic leaching in needles. Moss et al. (1998) have also noted the formation of CaOx crystals in foliar tissues of red spruce growing at a high-damage stand in the White Mountains. These crystals were accompanied by signs of acute tissue damage to needle mesophyll

cells, and were probably an indication of needle exposure to ozone and acid-cloud chemistry. Similar work by DeHayes et al. (1997; 1999) argues that changes in the crystal-bound Ca oxalate pool is less important than is the likely source of the precipitable  $\text{Ca}^{2+}$ . After misting red spruce seedlings with pH 3.0 precipitation, Borer et al. (2005) measured changes in a more labile, membrane-associated pool (mCa), and suggest this triggered the subsequent observation of decreased stomatal aperture, stomatal response time, and net photosynthesis. Another study of red spruce foliage (Borer et al., 2004) focused on the control of free aluminum (Al) ions, which are harmful to membrane exchange processes and directly cytotoxic. This work documented positive correlations between acetic-acid-extractable (readily available) foliar Ca and a number of variables including: sequestration of foliar Al, total foliar Ca:Al ratios, resistance to winter freezing injury, and tolerance of low temperature. However, it was also found that the rate of Al sequestration was positively correlated with the rate of Ca sequestration.

In long-term research at the Hubbard Brook Experimental Forest, Likens et al. (1998) estimated that from 1940-1995, the exchangeable soil Ca pool diminished by roughly 70 percent. Recent work has cited such loss of Ca as an important though nebulous threat to the northeastern forests, potentially predisposing trees to other stresses such as tropospheric ozone, low temperature, mechanical stress, nutrient deficiency, aluminum toxicity, and pathogen attacks (Schaberg et al., 2001; McLaughlin and Wimmer, 1999; Horsley et al., 2002). In a recent survey of northeastern forest soil Ca levels from 1976-1997, Yanai et al. (1999) found no trends in forest floor Ca, suggesting that base cation losses have abated or cannot be detected.

Bailey et al. (2003) reported that historical decreases from the 1950s to the 2000s

in soil exchangeable Ca are unlikely as high as stream export data might suggest. They hypothesize that there is an unmeasured pool of Ca, such as Ca-oxalate crystals bound in organic matter, and point to the forest floor as a potential source of larger amounts of Ca than previously thought possible. In a separate hypothesis addressing the apparently missing Ca pool in these systems, Blum et al. (2002) have suggested that mycorrhizae enable tree root systems to selectively derive Ca directly from mineral deposits. However, Bullen and Bailey (2005) have used isotopic ratios in a mature spruce forest to identify the forest floor as the primary source of Ca found in trees, lending support to the oxalate source proposed by Bailey et al. (2003).

As part of an ongoing study of Ca nutrition in northeastern forest systems, we have compared the concentrations of eight major elements of red spruce foliage (Al, Ca, Fe, K, Mg, Mn, P, Sr), and of the oxalate anion ( $C_2O_4^{2-}$ ) in Ca-amended and reference stands. The present paper is the first in a series of three studies investigating the use of foliar spectral information to detect Ca gradients in red spruce forests. The objective of this study is to quantify residual differences in foliar chemistry following the 1999 application of mineral Ca, with particular emphasis on the relationship between the total and sequestered Ca pools. We hypothesize increased concentrations of total foliar Ca, Sr, and oxalate will still be measurable in the foliage of Ca-treated trees, and that foliar Al will have decreased as a result of raised soil pH.

## **Methods**

### *Study site and experimental background*

This work was carried out at the Hubbard Brook Experimental Forest (HBEF), located in



West Thornton, NH (43 ° 56' N, 71 ° 45' W, Figure 1). This valley consists of many small watersheds feeding the Hubbard Brook, and is characterized as a Northern Hardwood Forest Type common to the White Mountain region (Kricher and Morrison, 1988). At elevations below ~700 m American beech (*Fagus grandifolia* Ehrh.), yellow birch (*Betula alleghaniensis* Michx.) and sugar maple (*Acer saccharum* Marsh.) dominate, with a transition to red spruce (*Picea rubens* Sarg.), balsam fir (*Abies balsamea* L.), and paper birch (*Betula papyrifera* Marsh.) at higher elevations. The HBEF is part of the Long-Term Ecological Research (LTER) network and has been extensively characterized in its climate, hydrology, geology, soils, and biota beginning in 1955 (Likens and Bormann, 1995). Generally, the local parent material is granitic (schists, quartzites), with nutrient-poor Spodosol soils forming from a glacial till substrate (Barton et al., 1997). The forest receives approximately 140 cm of precipitation annually, with a deep winter snowpack contributing about 30 cm of this (Juice et al., 2006). This combination of low-Ca bedrock sources and moist climate results in poorly buffered soils (pH commonly < 4.5) with low available soil nutrient content below thick organic horizons (Fisk et al., 2006). A detailed description of the HBEF is available (Likens and Bormann, 1995), and is supported by extensive online resources (Hubbard Brook Ecosystem Study, 2008a).

Six watersheds in the northeast of the Hubbard Brook valley have been the focus of whole-watershed manipulations designed to investigate ecosystem processes such as mineral weathering, hydrologic export, nutrient cycling and storage, and response to timber harvest techniques (Johnson, 1995; Likens et al., 1996; 1998). A single watershed (WS6) has remained un-manipulated throughout the HBEF study, functioning as a

biogeochemical reference watershed. In October of 1999, an entire 11.8-ha watershed (WS1) was fertilized by helicopter with wollastonite ( $\text{CaSiO}_3$ ) at the rate of 0.12 kg Ca  $\text{m}^{-2}$  (Peters et al., 2004). This treatment was chosen as an approximately 100 % re-fertilization of the forest floor Ca pool following the heavy leaching of basic cations during periods of high acidic deposition in the mid- and late-1900s (Hawley et al., 2006).

#### *Plot selection and characterization*

Plots were chosen in each of two watersheds: the Ca-treated WS1, and an un-manipulated watershed used for destructive sampling immediately to the west of the reference WS6.

Peltic schists, meta-sandstone, and local grit underlie the coniferous zones of both watersheds, which are separated by roughly 1 km (Barton et al., 1997). Cluster plots of 3 trees were established, 6 clusters in each watershed, for a total sample size of 36 trees.

All trees were selected from within "spruce-fir" stands, i.e. those containing > 50 % red spruce and balsam fir as a fraction of total canopy. Selection was random, but immature, severely damaged (> 25 % crown damage or severe bole damage) and suppressed individuals were excluded from selections. We measured biometric data including total tree height and live crown fraction (Suunto\* clinometer; Vantaa, Finland), diameter at breast height (DBH), needle retention (single count, or average of three independent counts when necessary), and radial growth increment (increment corer; 1.35 m above ground). Radial increment was measured with a dendrochronometer, consisting of a stereoscopic dissecting microscope, a sliding stage micrometer (Velmax\* Series A 4000; East Bloomfield, NY), and a digitizer (Accu-Rite\* III; Jamestown, NY). Annual basal area increment (BAI) was calculated according to standard methods (see Duchesne et al.,

---

\* Use of brand names is for clarity and does not imply endorsement.

2003). Each tree's location was recorded with a differential global positioning system of < 1 m spatial accuracy (Trimble GPS Pathfinder\*; Sunnyvale, CA).

### *Foliar Chemistry*

Foliage was sampled as whole boughs taken from the middle canopy region, generally between 7-11 m in height, using a pole pruner. On 3 and 4 November 2006, a preliminary sampling was done on 7 trees: 3 from the Ca-treated watershed, and 4 from the reference area. The primary sampling for all 36 trees in this study was conducted 13 and 14 August 2007; at this point the foliar growth and nutrient allocation that accompanies the needle flush of red spruce had already occurred.

Following the counting of needle age-classes present, the sample was clipped into subsections, placed in a plastic zip-lock bag, and placed in a cooler at 7 °C, then moved to a refrigerator (7 °C) to await laboratory processing. Spectral analysis and processing was done within 48 h following sampling, where needles were separated into three sample classes. Air-drying for foliar chemical analyses was begun within 1 week of sample collections. The first sample class, mixed-needle year (MNY) or "bough," was a mixture of needle years, primarily including current-, second-, and third-year growth, but also years previous (Figure 2). The MNY sample was taken from the outer bough to represent the area of greatest relative exposure to sunlight. Third year (3Y) needles were taken from excised branchlets, and represent 2005 growth. Current year (CY) needles were sub-sampled similarly, and represent 2007 growth.

Needles from each sub-sample were weighed fresh before oven drying at 60 °C for 72 h, and reweighed dry. Moisture content for was determined to be the difference

---

\* Use of brand names is for clarity and does not imply endorsement.

between wet and dry weight, divided by the wet weight. Samples were then ground in a wiley mill with a #20 screen and stored in glass jars at 25 °C. Foliar digestion was done using nitric acid according to standard methods (EPA, 1996), and chemical determination was made by inductively coupled plasma atomic emission spectrometry (ICP-AES). Foliar element constituents analyzed include: Ca, magnesium (Mg), manganese (Mn), iron (Fe), strontium (Sr), phosphorus (P), potassium (K), and aluminum (Al). Standard foliar samples of known concentration (apple, peach, and pine; NIST standard reference materials #1547, #1515, and #1575a, respectively), blanks, and duplicate samples were run for quality control.

Foliar oxalate was analyzed by addition of a 1M hydrochloric-acid extractant. Ground sub-samples of 0.025 g received 3 mL of acid and were placed on a digesting block set to 25 °C, shaking at 1000 rpm, for 30 min. Following digestion, all samples were syringe filtered with a 0.45 µm filter (National Scientific Co.\* #F2500-1) and diluted 20x. A final syringe filtration was done with a filter of 0.2 µm (Pall Life Sciences\* #4192), and extracts were stored in scintillation vials at 7 °C before analysis by high-performance liquid chromatography (HPLC; Dionex\*, Sunnyvale, CA). Duplicate samples, standards, and a 0.1 g oxalate L<sup>-1</sup> spike were used for quality control purposes. Overall spike recovery was within 5 % error, at 104.8 %.

### *Scanning Electron Microscopy*

To explore the nature and location of crystal Ca deposits, scanning electron microscopy (SEM) images were made from CY needles from the 7 trees in the 2006 sampling. After refrigeration at 7 °C for 10 days, 15 needles were flash-frozen with liquid nitrogen to

---

\* Use of brand names is for clarity and does not imply endorsement.

facilitate a clean cut by razor cross-sectioning. Once cut, needle sections were mounted on a specimen stub using an adhesive, and sputter coated with platinum (Pt) to enhance visualization via electrostatic conduction. Image capture was done at a variety of magnifications ranging from 40-400x using an Amray 3300FE Scanning Electron Microscope (KLA Tencor\*, Milipitas, CA). Energy Dispersive X-ray Spectroscopy (EDS) was employed to identify the elemental composition of different targets, including isolated CaOx crystals.

## **Results**

### *Treatment comparison*

Biometric data for the 36 trees in this study did not significantly differ by watershed (Table 1). Trees had an overall mean DBH of 26.4 cm, a mean height of 14.5 m, a mean live crown fraction of 0.55, and mean needle retention of approximately 9 years. Basal area increment did not differ significantly by watershed. BAI data are grouped by watershed and presented from 1952-2007 to facilitate inter-annual comparison of high and low growth periods (Figure 3).

Results of analysis of variance (ANOVA) tests showed that for all foliar elements and oxalate, needle year was a significant determinant of foliar chemistry (Figure 4). Specifically, we noted a lower concentration of the re-translocated nutrients Mg, K, and P in third-year needles, compared to the current-year. Elements of lower mobility, including Ca, Mn, Sr, Al, and Fe, had accumulated in third-year needles. Oxalate concentrations were also higher in third-year foliage, compared to the current-year. In all analyses, the concentration of mixed-needle-year samples was between the current- and

---

\* Use of brand names is for clarity and does not imply endorsement.

third-year values (Table 2).

Two-way ANOVA test were done to assess the effect of the Ca treatment on needle chemistry, while accounting for the effect of needle age. Probabilities for F-tests of significance for each of the eight elements and oxalate are listed in Table 2. Significant ( $P < 0.05$ ) relationships were found for foliar Ca, Sr, and oxalate. For these ions, regardless of age class, needles in the Ca-amended watershed had higher concentrations than the reference samples. In addition, we found a marginally significant difference in foliar Mg and Al content between the two watersheds. Needles from Ca-treated trees tended to have higher Mg concentrations ( $P = 0.068$ ), but lower Al concentrations ( $P = 0.073$ ). Interactions between needle age and experimental treatment were not significant.

#### *Correlational relationships*

Multiple regressions of various foliar constituents on total foliar Ca, and needle age (a set of three dummy variables) showed four significant, positive relationships ( $P < 0.001$ ; Table 3; Figure 5). In order of ascending strength, correlations were found between Mn and Ca, Mg and Ca, Sr and Ca, and oxalate and Ca, when the effect of needle age was accounted for.

To explore the association of oxalate with elemental concentrations other than Ca, multiple regressions were run between foliar oxalate concentration and all cations except Ca, holding variation due to Ca and needle age constant (Table 4; Figure 6). Results show a significant positive relationship between oxalate and Mg ( $P = 0.014$ ;  $R^2 = 0.824$ ), oxalate and P ( $P < 0.001$ ;  $R^2 = 0.836$ ), and oxalate and K ( $P < 0.001$ ;  $R^2 = 0.879$ ).

### *SEM and anatomy*

A total of 47 images produced using the SEM revealed considerable detail of the red spruce needle in cross section (Figures 7a and 7c, with intact vascular cylinder, endodermis, mesophyll, resin ducts, epidermis, stomata, and sub-stomatal cavities all discernible at lower magnifications (40-100x). At higher-power magnifications (400x), cell lumens were distinguishable, and extracellular crystal sand was clearly visible along cell walls forming the interiors of substomatal cavities in the mesophyll. Crystals were observed in samples from both treatments, but not in every cross section. Crystals ranged widely in shape: from distinct polyhedrons and cuboids (Figure 7e), to less distinct, or "emergent" crystal sand visible in Figure 7d. Results of an EDS elemental analysis targeting a single crystal are shown in Figures 7e and 7f. Contents were identified as Pt (an artifact of the electrostatic coating process), Ca, oxygen (O), and carbon (C).

## **Discussion**

### *Elemental constituents*

Following the whole-watershed wollastonite treatment in 1999, spruce trees growing on Ca-amended soils show sustained differences in needle chemistry compared to those in reference stands. Our measurement of higher foliar Ca levels in the trees of watershed 1 is consistent with the transpiration-mass-flow model of Ca uptake in fine roots; i.e. roots in a higher-Ca medium will receive more Ca via diffusion from soil water of higher Ca concentrations. Increased foliar Ca content has been shown for the period of 1999-2002, following the treatment at HBEF for red spruce, balsam fir, and paper birch (Hubbard

Brook Ecosystem Study, 2008b), and correlations between foliar and soil Ca reported in a survey of similar sites across the region (McNulty et al., 1991). This study's measurement of higher Ca concentrations in current-year foliage suggests there is an enhanced available soil Ca pool present 8 years after the wollastonite addition.

The increased Sr concentration in foliage of Ca-treated trees was an expected result. Sr and Ca have the same valence characteristic, and Sr was present in the applied wollastonite at a proportion of 1:2900 (Sr:Ca; Peters et al., 2004). The significant differences in foliar Sr (Table 2) and correlation with foliar Ca (Table 3) are evidence of a proxy amendment accompanying the mineral addition. No nutritive effects of Sr are known in plants.

The marginally significant trend toward higher foliar Mg in watershed 1 was accompanied by a significant correlation of moderate strength with total foliar Ca. Within separate age classes and composite MNY samples, there was a clearly increasing Mg concentration with increasing Ca (Figure 5a), however, the causal relationship with the Ca amendment is unclear. One possibility is that trees from the treated plots experienced increased growth rates, leading to a greater increment of enzymatic and chlorophyllous Mg following treatment. However, the present study lacks evidence to support higher growth rates in these trees (Figure 3), and evidence from previous studies suggests any Ca-limitation effects for spruce are likely indirect (Schaberg et al., 2001). A more likely explanation is that the passive diffusion of Mg cations into red spruce roots has increased at higher pH. Spruce-fir zones of the HBEF valley have low pH ranges (3.5-4), and the addition of a mineral Ca source has increased the pH of the forest floor layer by at least 0.7 units (Fisk et al., 2006).



Observed decreases in foliar Al (Table 2) are probably also the result of higher pH in the Ca-treated soils. At soil pH below 5, there is increasing mobility of the Al<sup>3+</sup> ion, and direct effects on plant roots include: reduction and alteration of growth pattern, displacement of cations associated with membrane exchange sites, hampered root uptake capacity, and direct interference with enzymes in the apoplast and symplast (Delhaize and Ryan, 1995). The connection between soil acidity and Al-induced decline in spruce has been documented, and the competitive reduction in Ca supply to the tree is the primary mechanism (Shortle and Smith, 1988). A recent study notes a correlation between available foliar Ca, and Al sequestration in red spruce as evidence that effects of soil pH on Al toxicity may also have indirect, physiologically mediated aspects (Borer et al., 2004). The general decrease in total foliar Al following the Ca treatment seen in this study supports the argument of pH-driven alleviation of Al chemical stress.

There was also a weak positive correlation between total foliar Mn and Ca (Table 3; Figure 5), although our experimental data do not confirm this (Table 2). It is possible that root uptake processes are improved in spruce trees of higher Ca supply, and this effect could include raised rates of Mn uptake. The availability of this macronutrient does not strongly respond to increases in pH from 3.5 - 5.5, and so soil chemistry influence on foliar Mn concentration may be more directly related to other factors. Data from other studies of current-year spruce needle chemistry are also suggestive of a positive relationship between these two elements (Huntington et al., 1990). This relationship has not been well explored, and other possible reasons for this correlation of Mn with Ca in foliage are not apparent.

### *Calcium oxalate*

We measured significant differences in foliar oxalic acid 8 years post Ca-application across needle age class: the oxalate pool in watershed 1 foliage was greater in CY, 3Y, and MNY samples, by 53 %, 23 %, and 35 %, respectively (Table 2). Although the nature of this oxalate pool was uncertain, EDS analysis of a representative crystal (Figure 7e, 7f) showed elemental composition approximating that of  $\text{CaC}_2\text{O}_4$ . This EDS elemental analysis result was very similar to a graph produced from intercellular CaOx crystals by Hudgins et al. (2003). Furthermore, a strong correlation between total foliar Ca and oxalate ( $P < 0.001$ ,  $R^2 = 0.813$ ; Figure 5d) was found, suggesting an association of this anion with the needle's Ca pool. Calcium is known to readily precipitate in the presence of oxalate (Petrova et al., 2004), and many studies have documented the presence of intercellular CaOx in conifers. Moss et al. (1998) have observed CaOx crystals outside the cell walls of sub-stomatal cavities in red spruce mesophyll at a nearby site in New Hampshire. Horner and Wagner (1995) note that microscopic work has generally found conifers precipitating CaOx in the intercellular spaces, in contrast to the intracellular storage strategy of crystal idioblast cells in angiosperms. Fink (1991c) identified extracellular CaOx crystals in various conifer species, including red spruce, using microscopy and chemical staining procedures, noting that the crystals appear affixed to and originating from mesophyll cell walls. A number of studies have also noted the appearance of crystals in association with foliar damage from ozone pollution (Fink, 1991b), acidic precipitation (Moss et al., 1998), and cement dust (Cesar et al., 2004).

Other work has related the presence of visible CaOx or a large insoluble Ca

fraction in foliage to belowground Ca supply (Fink, 1991a; Gülpen et al., 1995; Borer et al., 2004; Littke and Zabowski, 2007). In the cytoplasm, Ca precipitates inorganic phosphate and therefore must be maintained at concentrations sufficiently low to avoid disruption of energy transfer processes (ATP, ADP). Oxalic acid also has phytotoxic properties, but may be synthesized in the symplast of plants from different precursors including: oxaloacetate, glycolate, and L-ascorbic acid (Franceschi and Loewus, 1995; Gülpen et al., 1995), prior to extrusion into the apoplast. Considering that Ca enters the plant by passive uptake processes, whereas oxalate is actively synthesized and represents a resource allocation, it is more likely that a tree regulates the precipitation of excess Ca via oxalate, than *vice versa* (Fink, 1991a; Gülpen et al., 1995; McLaughlin and Wimmer, 1999). An experiment by Nakata (2003) showed that in plants with a genetic mutation for oxalate hyperproductivity, excessive CaOx crystallization reduces chlorophyll content and overall plant growth. Our measurement of increased oxalate content following an experimental Ca addition, coupled with the observed tendency of CaOx to precipitate in the extracellular spaces agrees, in the case of red spruce, with this hypothesis of oxalate mediated Ca regulation.

Some Ca necessarily exists unbound to oxalate, e.g bound as Ca-pectate within the middle lamella, residing on membrane surfaces, or acting in signal transduction. In addition, oxalate may be associated with other ionic constituents, for example bound to Mn, Fe, Sr, and Al, as insoluble precipitates (Horner and Wagner, 1995). This makes estimation of chemical fractionation relationships difficult, however, it is interesting to note the slope of the oxalate-Ca relationship (Table 3) was found to be 2.28, which approximates the molar mass ratio of 2.20 for oxalate to Ca in a crystal of CaOx (88 g

C<sub>2</sub>O<sub>4</sub> : 20 g Ca).

Aside from Ca regulation, other hypotheses of oxalate function in plant tissues include: ion balance, plant protection against herbivory, detoxification of heavy metals, structural support, and light gathering and reflection (Horner and Wagner, 1995; Nakata, 2003). We found that, accounting for variation due to needle age and Ca content, there were significant relationships between oxalic acid and three elements: Mg, P, and K (Table 3). Franceschi and Loweus (1995) suggest the generation of oxalate anions may be the necessary result of positive charge potentials of the vacuole. The positive relationship of oxalate with three primary contributors (Mg, K, and P) to vacuolar charge contents lends support to this hypothesis, and the formation of insoluble Mg-oxalate is also a possibility (Table 4). Surprisingly, Table 4 also indicates we found no significant correlations between oxalate and the heavier ions that it has directly precipitated (Mn, Fe, Sr, Al).

### **Summary**

The addition of mineral Ca has had a sustained effect on the foliar chemistry of red spruce at HBEF. Eight years following the application of wollastonite (CaSiO<sub>3</sub>) we observed significantly higher total foliar Ca and Sr, better access to the mineral nutrients Mg and Mn, and lower rates of Al uptake in the Ca-treated watershed compared to the reference. These responses are likely due to the combined effects of increased soil pH and improved membrane structure and function in fine roots. Experimental and correlational data show that a significant response to increased Ca levels in red spruce is the production of oxalic acid, which leads to the precipitation of insoluble crystal Ca-

oxalate. We observed sand-like crystals, shown to be CaOx, lining the exterior of cell walls in mesophyll sub-stomatal cavities, where they appear to be the product of a secretion-precipitation reaction. The oxalate-bound Ca is recalcitrant, dissolving only at very low pH levels, and is likely to remain physiologically inactive once formed (DeHayes et al., 1997). However, the role of these crystals likely extends beyond the simple process of Ca detoxification, and there may be a benefit to the prolonged storage of Ca in base-poor conifer systems.

## Literature cited

- Bailey SW, Buso DC, Likens GE (2003) Implications of sodium mass balance for interpreting the calcium cycle of a forested ecosystem. *Ecology* 84: 471-484.
- Barton CC, Camerlo RH, Bailey SW (1997) Bedrock geologic map of the Hubbard Brook Experimental Forest and maps of fractures and geology in roadcuts along interstate 93, Grafton County, New Hampshire, Sheet 1, Scale 1:12,000; Sheet 2, Scale 1:200: U.S. Geological Survey Miscellaneous Investigations Series Map I-2562.
- Borer CH, Schaberg PG, DeHayes DH, Hawley GJ (2004) Accretion, partitioning, and sequestration of calcium and aluminum in red spruce foliage: implications for tree health. *Tree Physiology* 24: 929-939.
- Borer CH, Schaberg PG, DeHayes DH (2005) Acidic mist reduces foliar membrane-associated calcium and impairs stomatal responsiveness in red spruce. *Tree Physiology* 25: 673-680.
- Blum JD, Klaue A, Nezat CA, Driscoll CT, Johnson CE, Siccama TG, Eagar C, Fahey TJ, Likens GE (2002) Mycorrhizal weathering of apatite as an important calcium source in base-poor forest ecosystems. *Nature* 417: 729-731.
- Bullen TD and Bailey SW (2005) Identifying calcium sources at an acid deposition-impacted spruce forest: a strontium isotope, alkaline earth element multi-tracer approach. *Biogeochemistry* 74: 63-99.
- Cesar V, Lepeduš H, Ljubešić (2004) Histochemical observations on the needles of Norway spruce trees affected by cement dust pollution. *Phyton* 44: 203-214.
- DeHayes DH, Schaberg PG, Hawley GJ, Borer CH, Cummings JR, Strimbeck GR (1997) Physiological implications of seasonal variation in membrane-associated calcium in red spruce mesophyll cells. *Tree Physiology* 17: 687-695.
- DeHayes DH, Schaberg PG, Hawley GJ, Strimbeck GR (1999) Acid rain impacts on calcium nutrition and forest health. *Bioscience* 49: 789-800.
- Delhaize E and Ryan PR (1995) Aluminum toxicity and tolerance in plants. *Plant Physiology* 107: 315-321.
- Driscoll CT, Lawrence GB, Bulger AJ, Butler TJ, Cronan CS, Eagar C, Lambert KF, Likens GE, Stoddard JL, Weathers KL (2001) Acidic deposition in the northeastern United States: sources and inputs, ecosystem effects, and management strategies. *Bioscience* 51: 180-198.
- Duchesne LR, Ouimet R, Morenau C (2003) Assessment of sugar maple

health based on basal area growth pattern. *Canadian Journal of Forest Research* 33: 2074-2080.

- EPA (1996) Microwave assisted acid digestion of siliceous and organically-based matrices, Method 3052. U.S. Environmental Protection Agency, Washington, D.C.
- Federer CA, Hornbeck JW, Tritton LM, Martin CW, Pierce RS, Smith CT (1989) Long-term depletion of calcium and other nutrients in eastern US forests. *Environmental Management* 13: 593-601.
- Fink S (1991a) The micromorphological distribution of bound calcium in needles of Norway spruce [*Picea abies* (L.) Karst.]. *New Phytologist* 119: 33-40.
- Fink S (1991b) Unusual patterns in the distribution of calcium oxalate crystals in spruce needles and their possible relationships to the impacts of pollutants. *New Phytologist* 119: 41-51.
- Fink S (1991c) Comparative microscopical studies on the patterns of calcium oxalate distribution in the needles of various conifer species. *Botanica Acta* 104: 306-315.
- Fisk MC, Kessler WR, Goodale A, Fahey TJ, Groffman PM, Driscoll CT (2006) Landscape variation in microarthropod response to calcium addition in a northern hardwood forest ecosystem. *Pedobiologia* 50: 69-78.
- Franceschi VR and Loewus FR (1995) Oxalate function and biosynthesis in plants and fungi. In: Kahn SR (ed) *Calcium oxalate in biological systems*. CRC Press, New York.
- Gülpen M, Türk S, Fink S (1995) Ca nutrition in conifers. *Zeitschrift für Pflanzenernährung und Bodenkunde* 158: 519-527.
- Hawley GJ, Schaberg PG, Eagar C, Borer CH (2006) Calcium addition at the Hubbard Brook Experimental Forest reduced winter injury to red spruce in a high-injury year. *Canadian Journal of Forest Research* 36: 2544-2549.
- Horner HT and Wagner BL (1995) Calcium oxalate formation in higher plants. In: Kahn SR (ed) *Calcium oxalate in biological systems*. CRC Press, New York.
- Horsley SB, Long RP, Bailey SW, Hallett RA, Wargo PM (2002) Health of eastern North American sugar maple forests and factors affecting decline. *Northern Journal of Applied Forestry* 19: 34-44.
- Hubbard Brook Ecosystem Study (2008a) Hubbard Brook Ecosystem Study. <http://www.hubbardbrook.org/> Cited 20 September 2008

- Hubbard Brook Ecosystem Study (2008b) Watershed 1 and 6 temporal canopy leaf chemistry. <http://www.hubbardbrook.org/data/> Cited 15 September 2006
- Hudgins JW, Kreckling T, Franceschi VR (2003) Distribution of calcium oxalate crystals in the secondary phloem of conifers: a constitutive defense mechanism? *New Phytologist* 159: 677-690.
- Huntington TG, Peart DR, Hornig J, Ryan DF, Russo-Savage S (1990) Relationships between soil chemistry, foliar chemistry, and condition of red spruce at Mount Moosilauke, New Hampshire. *Canadian Journal of Forest Research* 20: 1219-1227.
- Johnson CE (1995) Soil nitrogen status eight years after whole-tree clear-cutting. *Canadian Journal of Forest Research* 25: 1346-1355.
- Juice SM, Fahey TJ, Siccama TG, Driscoll CT, Denny EG, Eagar C, Cleavitt NL, Minocha R, Richardson AD (2006) Response of sugar maple to calcium addition to northern hardwood forest. *Ecology* 87:1267-1280.
- Kauss H (1987) Some aspects of calcium-dependent regulation in plant metabolism. *Annual Review of Plant Physiology and Molecular Biology* 38: 42-72.
- Kricher JC and Morrison G (1988) *Eastern forests*. Houghton-Mifflin, Boston.
- Lawrence GB, David MB, Bailey SW, Shortle WC (1997) Assessment of soil calcium status in red spruce forests in the northeastern United States. *Biogeochemistry* 38: 19-39.
- Likens GE and Bormann FH (1995) *Biogeochemistry of a forested ecosystem*, 2nd ed. Springer-Verlag, New York.
- Likens GE, Driscoll CT, Buso DC (1996) Long-term effects of acid rain: response and recovery of a forest ecosystem. *Science* 272: 244-246.
- Likens GE, Driscoll CT, Buso DC, Siccama TG, Johnson CE, Lovett GM, Fahey TJ, Reiners WA, Ryan DF, Martin CW, Bailey SW (1998) The biogeochemistry of calcium at Hubbard Brook. *Biogeochemistry* 41: 89-173.
- Littke KM and Zabowski D (2007) Influence of calcium fertilization on Douglas-fir foliar nutrition, soil nutrient availability, and sinuosity in coastal Washington. *Forest Ecology and Management* 247: 140-148.
- McLaughlin SB and Wimmer R (1999) Calcium physiology and terrestrial ecosystem processes. *New Phytologist* 142: 373-417.
- McNulty SG, Aber JD, Boone RD (1991) Spatial changes in forest floor and foliar



chemistry of spruce-fir forests across New England. *Biogeochemistry* 14: 13-29.

Moss DM, Rock BN, Bogle AL, Bilkova J (1998) Anatomical evidence of the development of damage symptoms across a growing season in needles of red spruce from central New Hampshire. *Environmental and Experimental Botany* 39: 247-262.

Nakata PA (2003) Advances in our understanding of calcium oxalate crystal formation and function in plants. *Plant Science* 164: 901-909.

Peters SC, Blum JD, Driscoll CT, Likens GE (2004) Dissolution of wollastonite during the experimental manipulation of Hubbard Brook watershed 1. *Biogeochemistry* 67: 309-329.

Petrova EV, Gvozdev NV, Rashkovich LN (2004) Growth and dissolution of calcium oxalate monohydrate (COM) crystals. *Journal of Optoelectronics and Advanced Materials* 6: 261-268.

Schaberg PG, DeHayes DH, Hawley GJ (2001) Anthropogenic calcium depletion: a unique threat to forest ecosystem health? *Ecosystem Health* 7: 214-228.

Shortle WC and Smith KT (1988) Aluminum-induced calcium deficiency syndrome in declining red spruce. *Science* 240: 1017-1018.

Swan HSD (1971) Relationships between nutrient supply, growth, and nutrient concentrations in the foliage of white and red spruce. *Pulp and Paper Research Institute of Canada, Pointe Claire.*

Turunen M, Huttunen S, Back J, Lamppu J (1995) Acid-rain induced changes in cuticles and Ca distribution in Scots pine and Norway spruce seedlings. *Canadian Journal of Forest Research* 25: 1313-1325.

Yanai RD, Siccama TG, Arthur MA, Federer CA, Friedland AJ (1999) Accumulation and depletion of base cations in forest floors in the northeastern United States. *Ecology* 80: 2774-2787.

| Plot              | Watershed  | DBH (cm)    | Needle retention (y) | Tree height (m) | Live crown fraction |
|-------------------|------------|-------------|----------------------|-----------------|---------------------|
| 1                 |            | 20.1 (3.04) | 7.5 (1.30)           | 14.7 (0.30)     | 0.57 (0.06)         |
| 2                 |            | 25.0 (3.96) | 11.2 (0.25)          | 14.0 (2.35)     | 0.47 (0.19)         |
| 3                 | #1         | 27.5 (7.2)  | 10.1 (1.60)          | 16.6 (4.24)     | 0.63 (0.12)         |
| 4                 | Ca-treated | 26.5 (9.45) | 8.6 (0.44)           | 14.0 (1.37)     | 0.47 (0.26)         |
| 5                 |            | 27.5 (5.32) | 6.3 (1.58)           | 13.6 (2.34)     | 0.57 (0.15)         |
| 6                 |            | 26.4 (10.6) | 9.2 (1.39)           | 12.5 (1.20)     | 0.51 (0.15)         |
| Watershed 1 mean: |            | 25.5 (6.54) | 8.8 (1.99)           | 14.2 (2.35)     | 0.54 (0.15)         |
| 7                 |            | 26.3 (3.37) | 7.7 (1.09)           | 13.4 (3.63)     | 0.42 (0.10)         |
| 8                 |            | 22.6 (6.02) | 9.2 (3.07)           | 14.1 (3.54)     | 0.61 (0.22)         |
| 9                 | West of #6 | 29.3 (6.77) | 7.8 (1.95)           | 15.3 (2.18)     | 0.53 (0.19)         |
| 10                | Reference  | 37.3 (3.95) | 12.8 (1.39)          | 18.4 (1.01)     | 0.73 (0.08)         |
| 11                |            | 28.2 (9.71) | 9.7 (2.38)           | 15.6 (3.91)     | 0.50 (0.13)         |
| 12                |            | 19.7 (6.53) | 8.6 (1.74)           | 12.0 (4.41)     | 0.55 (0.14)         |
| West of 6 mean:   |            | 27.2 (7.87) | 9.3 (2.62)           | 14.8 (3.48)     | 0.56 (0.16)         |
| Total mean:       |            | 26.4 (7.19) | 9.1 (2.32)           | 14.5 (2.94)     | 0.55 (0.15)         |

*Table 1.* Mean biometric characteristics (averages of three trees) across 12 plots; standard deviations given in parentheses. Values for watersheds (n = 18), and study (n = 36) are also shown. No significant ( $P < 0.05$ ) differences were found between watersheds.

| Analyte | Watershed | ----- mg / g dry weight ----- |         |         | P           |
|---------|-----------|-------------------------------|---------|---------|-------------|
|         |           | CY                            | 3Y      | MNY     |             |
| Ca      | 1         | 1.77                          | 3.85    | 3.22    | 0.0015**    |
|         | 6         | 1.44                          | 3.26    | 2.59    |             |
| oxalate | 1         | 5.39                          | 8.08    | 7.18    | < 0.0001*** |
|         | 6         | § 3.53                        | 6.57    | 5.32    |             |
| Sr      | 1         | 0.00172                       | 0.00403 | 0.00339 | 0.0141*     |
|         | 6         | 0.00108                       | 0.00340 | 0.00258 |             |
| Mg      | 1         | 0.654                         | 0.465   | 0.520   | 0.0682#     |
|         | 6         | 0.635                         | 0.425   | 0.473   |             |
| Mn      | 1         | 0.754                         | 1.37    | 1.31    | 0.3215      |
|         | 6         | 0.802                         | 1.61    | 1.31    |             |
| Al      | 1         | 0.0144                        | 0.0325  | 0.0280  | 0.0727#     |
|         | 6         | 0.0210                        | 0.0367  | 0.0285  |             |
| P       | 1         | 1.15                          | 0.802   | 0.923   | 0.2777      |
|         | 6         | 1.18                          | 0.835   | 0.952   |             |
| K       | 1         | 5.87                          | 3.13    | 4.10    | 0.1924      |
|         | 6         | 5.53                          | 3.04    | 3.91    |             |
| Fe      | 1         | 0.0187                        | 0.0250  | 0.0256  | 0.1835      |
|         | 6         | 0.0204                        | 0.0273  | 0.0245  |             |

\*\*\* Significant at  $P < 0.0001$

\*\* Significant at  $0.0001 \leq P < 0.01$

\* Significant at  $0.01 \leq P < 0.05$

# Marginally significant at  $0.05 \leq P < 0.10$

*Table 2.* Results of a two-way ANOVA for each of nine analytes in red spruce foliage, along with means ( $n = 18$ , except § where  $n = 17$ ) for both the Ca-treated watershed (#1), and west of reference watershed (#6), by needle-age class. *P*-values are for the significance of a partial effect of watershed treatment on element/oxalate concentration. Ca, Sr, and oxalate were significantly higher in all WS1 needles compared to the reference, while Mg showed a marginally significant increase. Al showed a marginally significant decrease following the Ca-treatment.

| Dependent var.               | Slope   | <i>t</i> | <i>P</i> | <i>R</i> <sup>2</sup> |
|------------------------------|---------|----------|----------|-----------------------|
| Sr (mg g <sup>-1</sup> d.w.) | 0.00131 | 12.24    | <0.001   | 0.716                 |
| Mg                           | 0.0562  | 5.65     | <0.001   | 0.559                 |
| Mn                           | 0.333   | 7.25     | <0.001   | 0.520                 |
| oxalate                      | 2.278   | 18.16    | <0.001   | 0.813                 |
| Al                           | 0.0011  | 0.89     | 0.374    | -                     |
| Fe                           | -0.0002 | -0.54    | 0.598    | -                     |
| K                            | -0.0603 | -0.64    | 0.521    | -                     |
| P                            | 0.0009  | 0.05     | 0.959    | -                     |

*Table 3.* Results of multiple regressions of elemental/oxalate concentrations on total foliar Ca and needle age. Slopes, *t*-values for test of significance, and probabilities describe the partial relationship of each analyte with foliar Ca. Coefficients of determination (listed only for significant relationships) show the strength of the model's prediction. Oxalate showed the strongest relationship with Ca, followed by Sr, Mg, and Mn.

| Independent var.             | Slope  | <i>t</i> | <i>P</i> | <i>R</i> <sup>2</sup> |
|------------------------------|--------|----------|----------|-----------------------|
| Mg (mg g <sup>-1</sup> d.w.) | 3.02   | 2.51     | 0.014    | 0.824                 |
| K                            | 0.792  | 7.45     | <0.001   | 0.879                 |
| P                            | 2.55   | 3.74     | <0.001   | 0.836                 |
| Sr                           | -110.2 | -0.96    | 0.341    | -                     |
| Mn                           | 0.420  | 1.58     | 0.118    | -                     |
| Al                           | -1.88  | -0.18    | 0.854    | -                     |
| Fe                           | 16.0   | 0.57     | 0.570    | -                     |

*Table 4.* Results of multiple regressions of oxalate on various foliar element concentrations, accounting for the effect of total foliar Ca and needle age. Slopes, *t*-values for test of significance, and probabilities describe the partial relationship of each analyte with foliar oxalate. Coefficients of determination (listed only for significant relationships) show the strength of the model's prediction. K showed the strongest relationship with oxalate, followed by P and Mg.

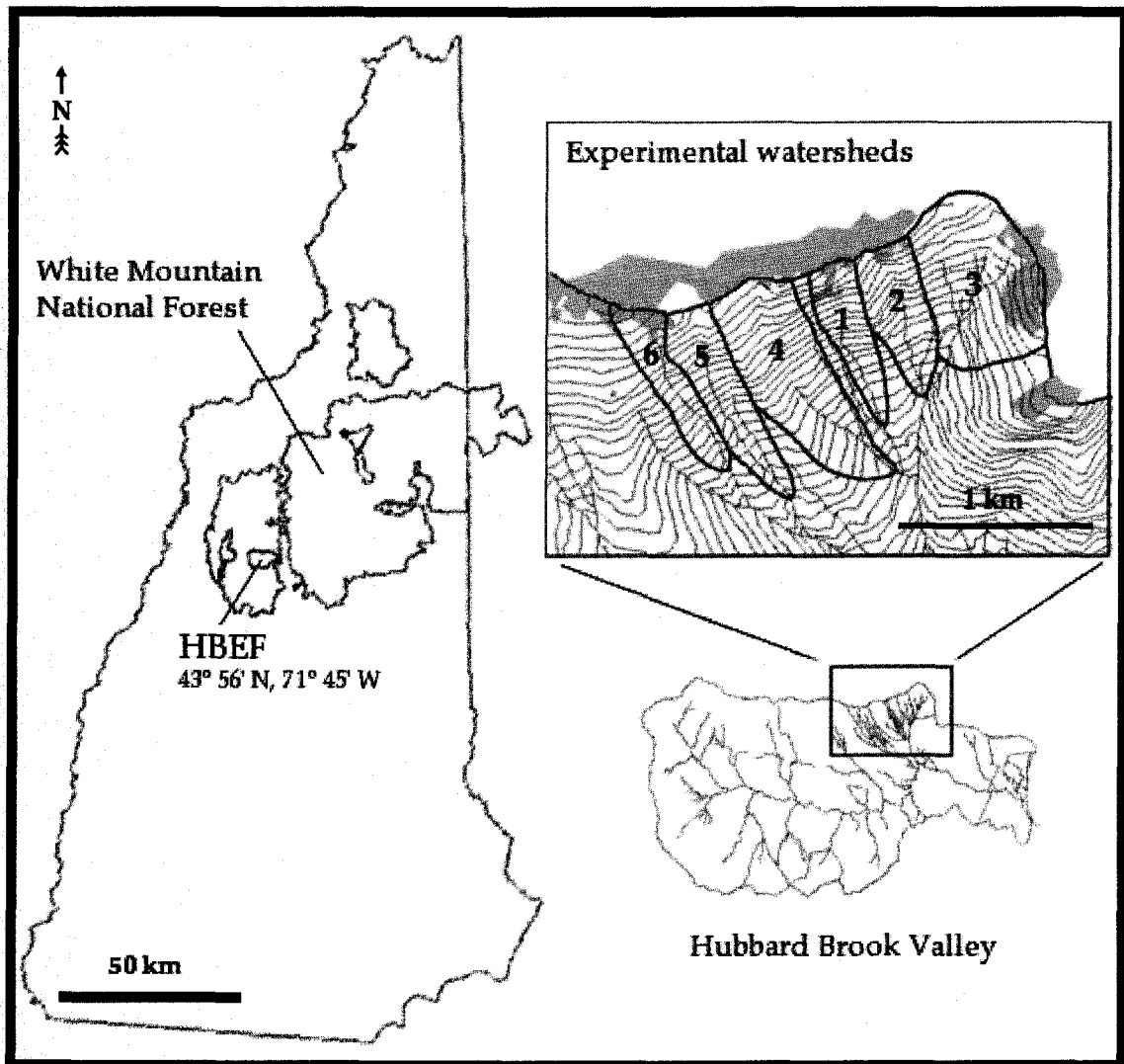


*Figure 1.* Location of experimental watersheds in the Hubbard Brook Experimental Forest (HBEF), within the White Mountains of New Hampshire. Watershed #1 received a Ca-wollastonite treatment in October 1999; watershed #6 is the biogeochemical reference area. The gray regions (inset) show the location of spruce-fir stands along the ridge of these watersheds.



*Figure 2.* Photo of red spruce bough, November 2006. Sample partitioning included foliage from the current (2007) and third (2005) years' growing seasons (shown as CY and 3Y; solid lines), as well as a mixed-needle-year sample (MNY; dashed line), which includes foliage from current- through fifth-years, and occasionally higher age classes.

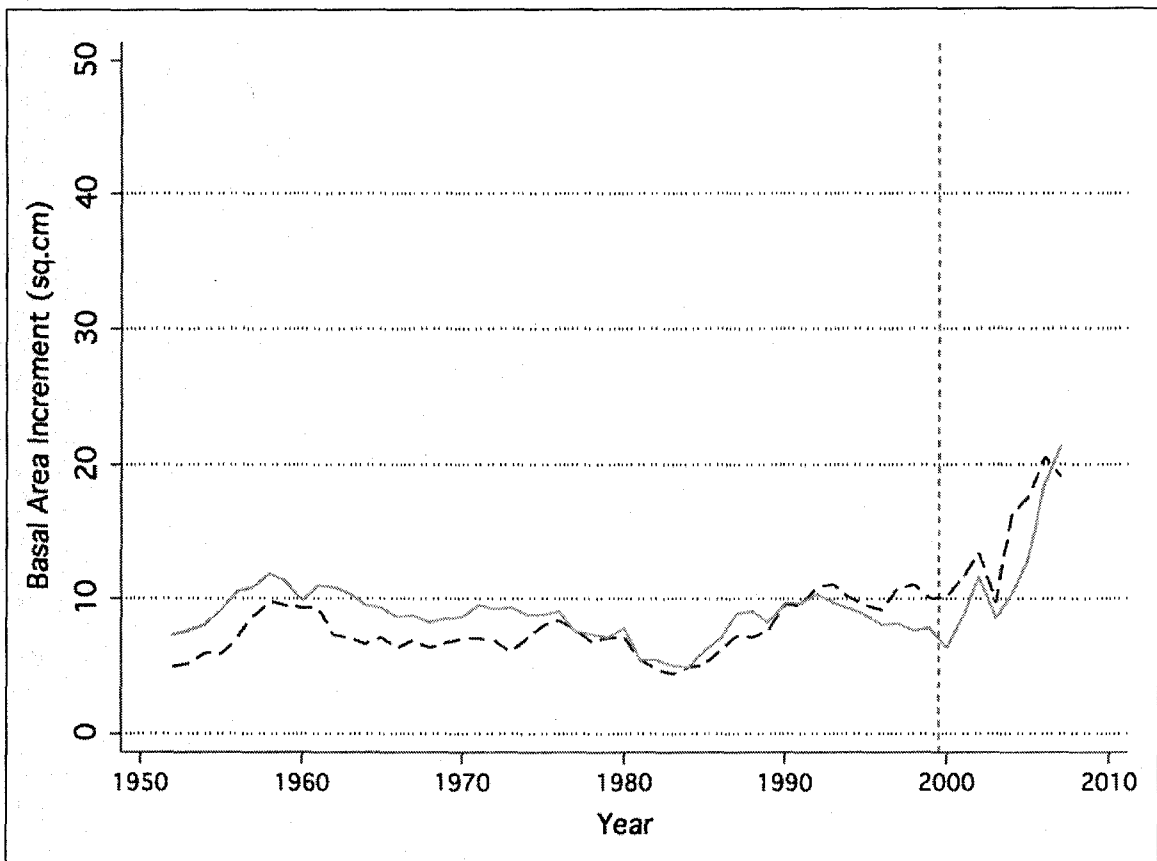


Figure 3. Mean ( $n = 18$ ) basal area increment in red spruce of the Ca-treated (WS1; dashed line), and reference stands (WS6; solid line) at HBEF. The vertical dashed reference line (October 1999) indicates the time of Ca application. Year-by-year t-test found no significant ( $P < 0.05$ ) differences by watershed in the years from 1952 and 2007.

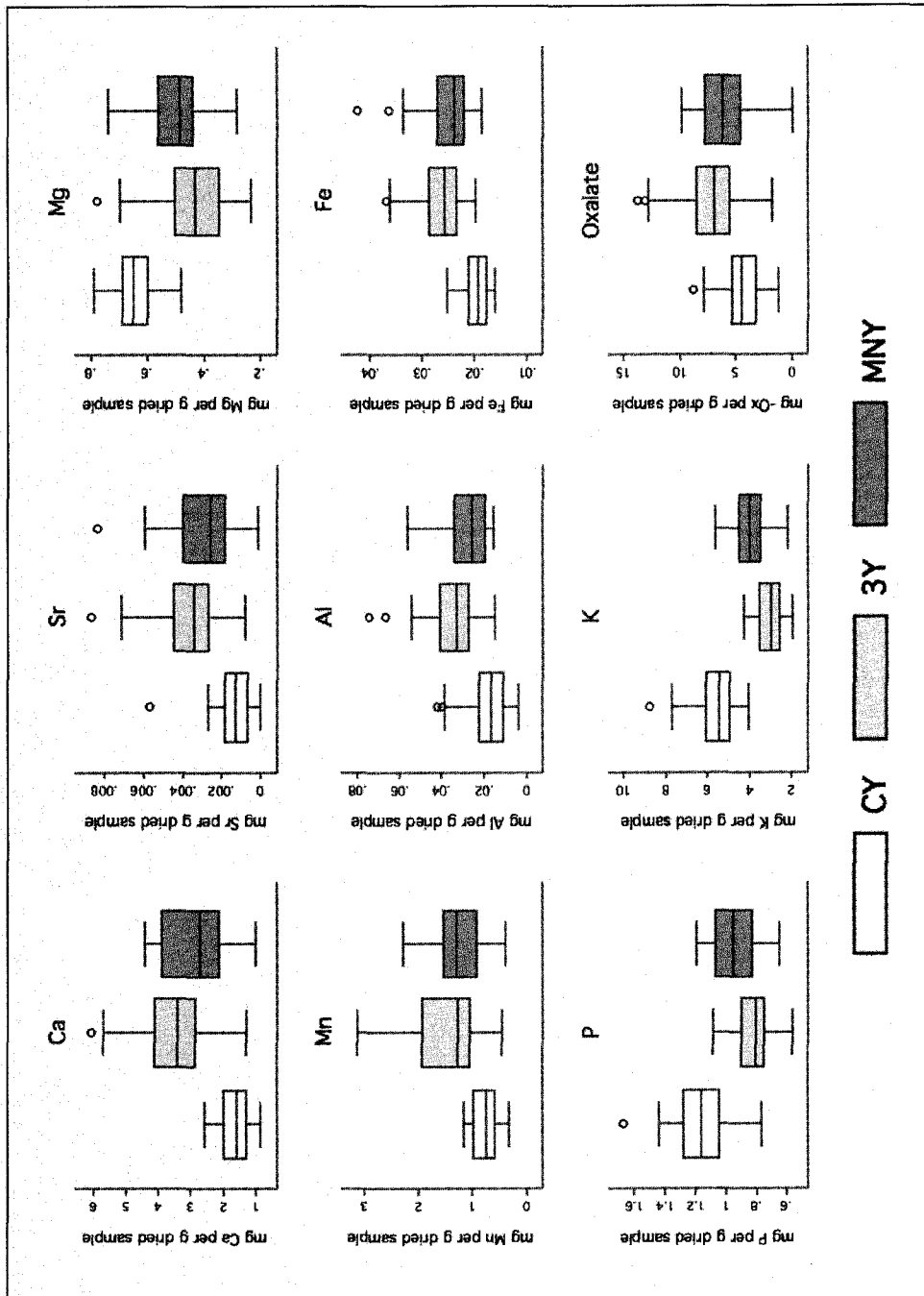
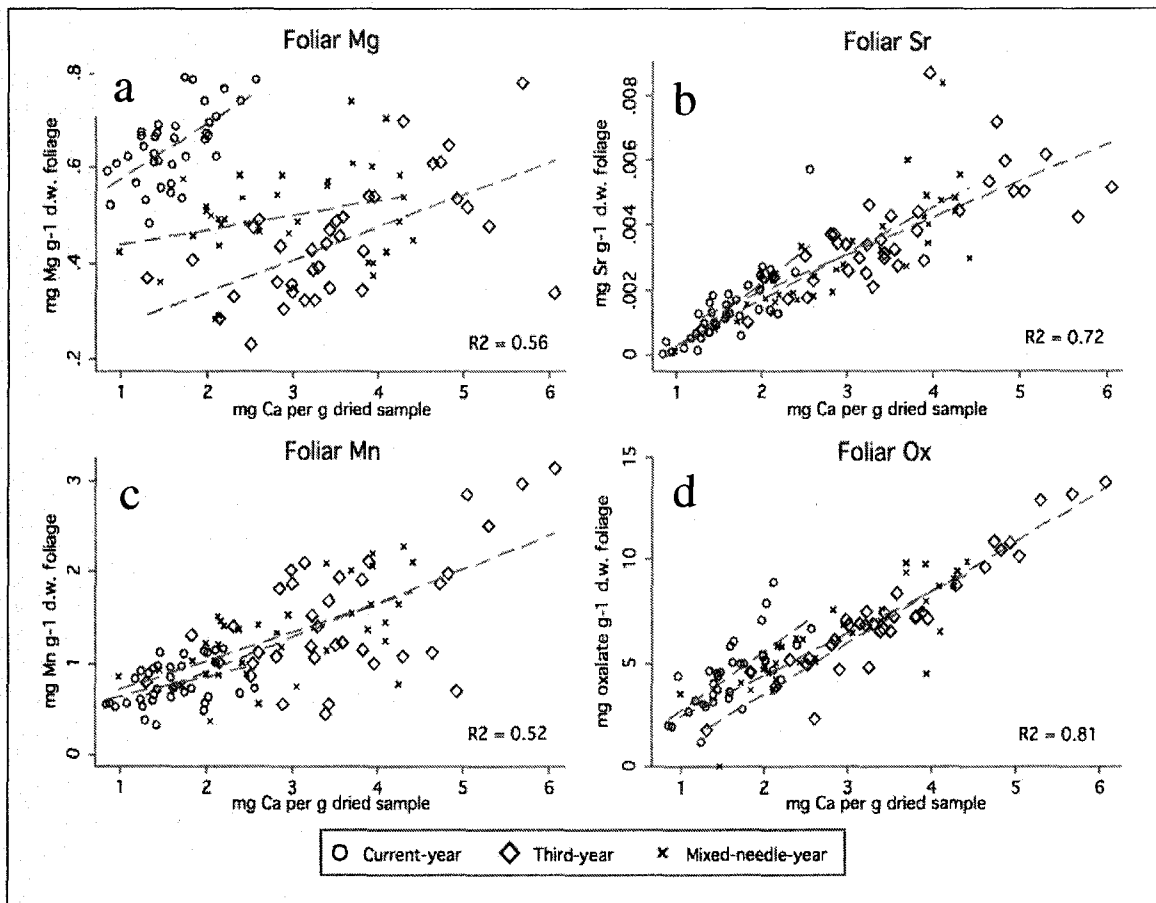


Figure 4. Box-and-whisker plots of foliar chemistry results by needle age class. Categories are current-year (CY), third-year (3Y), and mixed-needle-year (MNY). Two-way ANOVA showed a significant ( $P < 0.0001$ ) effect of needle age class on concentration for all analytes.





**Figure 5.** Scatter plots of 2007 foliar chemistry ( $n = 108$ ) where significant correlation with total foliar Ca was found in multiple regression. Sample points are labeled by needle age class: CY (circles), 3Y (diamonds), and MNY (crosses).  $R^2$  values are from multiple regression, accounting for effects of needle age, while trend lines indicate the linear model for an individual age class.

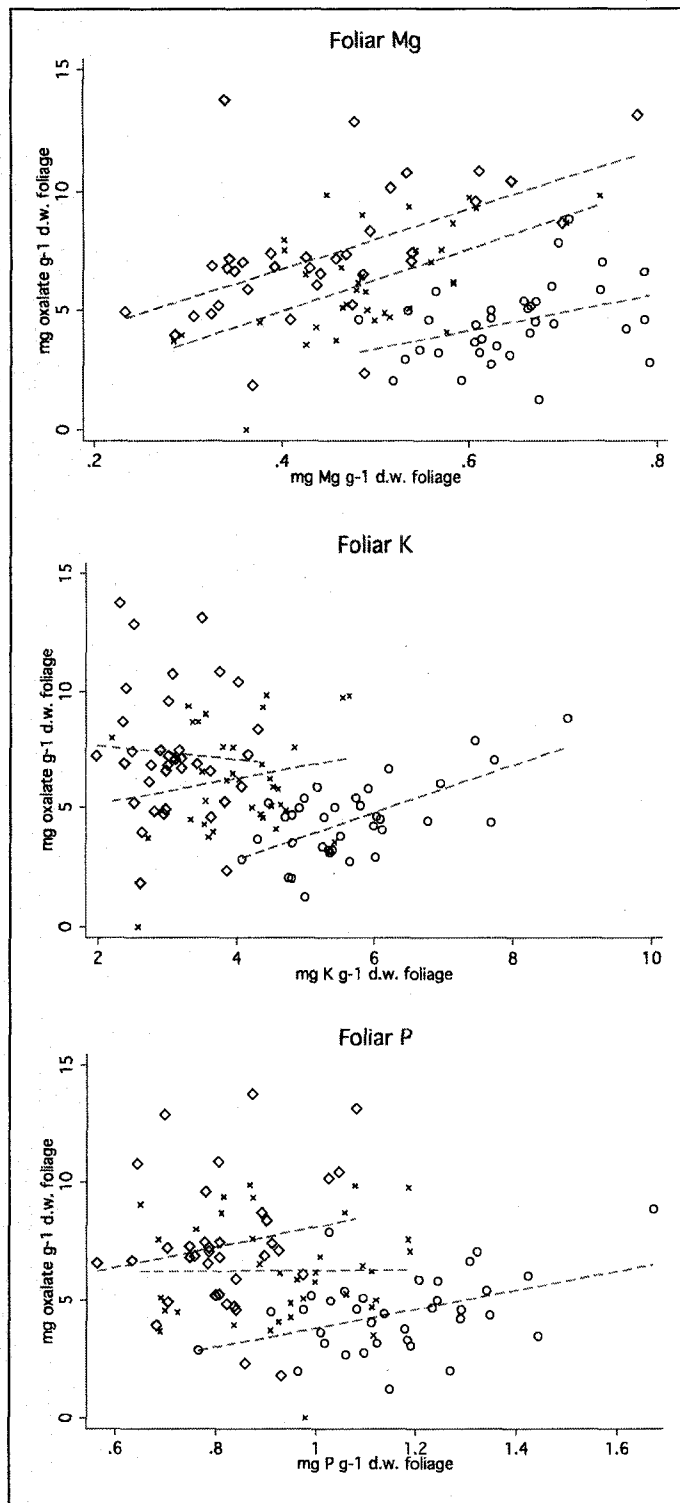
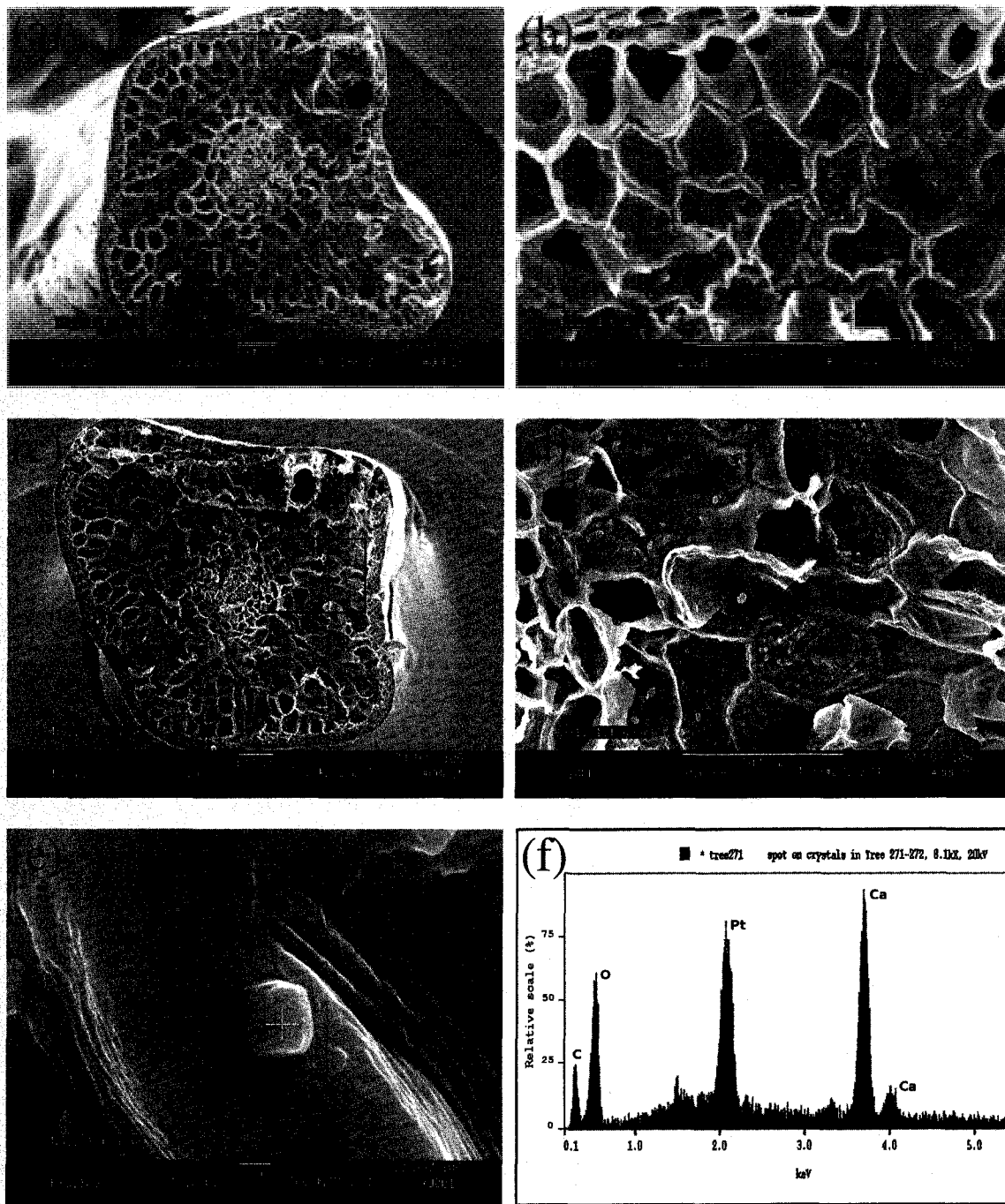


Figure 6. Scatter plots of 2007 foliar chemistry ( $n = 108$ ) where significant correlation between foliar oxalate and a non-Ca element was found. Sample points are labeled by needle age class: CY (circles), 3Y (diamonds), and MNY (crosses).  $R^2$  values are from multiple regression, accounting for effects of Ca concentration and needle age. Dashed trend lines indicate the linear model for an individual age class.



*Figure 7.* Scanning electron micrographs of current-year red spruce needles collected from the Ca-treated watershed (a-d). The boxed regions in a and c correspond to the areas displayed in panes b and d, respectively. Results of energy-dispersive X-ray spectroscopy (EDS) analysis are shown in panes e and f. Peaks shown correspond to the elemental composition of the target (Ca, O, C), and to the Pt coating applied to needle sections.

## CHAPTER II

### **Laboratory spectral responses and stress indicators in calcium-treated red spruce foliage at the Hubbard Brook Experimental Forest.**

**Abstract.** Optical properties of conifers associated with soils of varying calcium (Ca) availability have not been characterized at either large or small scale in forest systems, but could provide basis for the remote assessment of this important stand nutrient. Following the 1999 application of Ca-wollastonite to a ~2.5-ha coniferous stand in central New Hampshire, we measured visible and infrared (400-2500 nm) needle reflectance of fresh red spruce (*Picea rubens* Sarg.) foliage using a high-resolution laboratory spectroradiometer. Foliage collected from Ca-treated and reference watershed trees in August 2007 was measured in current-year, third-year, and mixed-needle-year sub-samples, and spectral data were analyzed for correlations with needle chemical properties. Current-year and third-year needle spectra did not show strong differences between treatments. Mixed-needle-year samples from the treatment watershed had significantly higher reflectance compared to the reference samples, and these differences were also observed in simulated Landsat bands 1-5 and 7 ( $P < 0.1$ ). Reflectance at infrared wavelengths showed weak, positive correlation with foliar concentrations of the oxalate anion, and a connection between extracellular Ca-oxalate crystal deposition in spruce foliar tissue and increased refraction and reflection is hypothesized. Surprisingly, a number of spectral indices suggested the Ca-treated trees are experiencing stress, possibly due to the active precipitation of a large Ca influx from soils of manipulated Ca availability.

## Introduction

Airborne multispectral and hyperspectral instruments have been used to detect signs of forest damage and estimate ecosystem processes (Rock et al., 1986; Wessman et al., 1988; Martin and Aber, 1997; Albrechtová et al., 2001; Entcheva Campbell et al., 2004; Ollinger and Smith; 2005). These studies rely on the spectral characteristics of organic compounds, green biomass, and foliar damage, which in turn depend on the interaction of incident solar radiation with leaf constituents, such as water, pigments, lignin, and cellulose, as well as tissue geometry (Gates et al., 1965; Tucker, 1980; Curran et al., 1992).

Forests of northeastern North America have experienced reduced soil calcium (Ca) pools following periods of acidic deposition and base cation leaching in the late twentieth century (Federer et al., 1989; Likens et al., 1998; Driscoll et al., 2001). Calcium is a vital plant nutrient functioning in photosynthesis, intercellular signal transduction, synthesis of proteins and reparatory compounds, stomatal regulation, cell-wall pectate formation, lignin production, and nutrient acquisition in fine roots (McLaughlin and Wimmer, 1999). Deficiencies in Ca have contributed to particularly heavy damage in coniferous forest systems, and this damage has been spectrally measured in red spruce (*Picea rubens* Sarg.) and balsam fir (*Abies balsamea* L.) communities in the Adirondack Mountains of New York (Rock et al., 1989), Green Mountains of Vermont, and White Mountains of New Hampshire (Vogelmann and Rock, 1988).

At laboratory scale, the correlation between foliar constituents and spectra

provides the basis for remote sensing applications. Peterson et al. (1988) noted that chemical bond structures can affect reflectance signatures, and used this to develop predictive equations for foliar biochemistry. Others (Curran et al., 1992; Vogelmann et al., 1993) have also been successful in detecting relationships between fresh leaf reflectance at certain wavelengths and chemical constituents including chlorophyll, starch, the protein amaranthin, and water content. One spectral index widely employed in remote prediction of canopy chlorophyll and damage is the red-edge inflection point (REIP), which correlates strongly with the amount of chlorophyll pigment in leaves (Vogelmann et al., 1993; Filella and Peñuelas, 1994; Entcheva Campbell et al., 2004).

A few studies have addressed the connections between Ca and foliar spectra. Hallett et al. (1997) have shown a predictive relationship between near infrared reflectance and Ca content in dried, ground foliage of pine and oak. Other work has addressed the influence of Ca on foliar spectra of fresh plants in agricultural systems. Mutanga et al. (2005) have shown correlations between Ca and reflectance properties occurring across a range of Ca concentrations in a forage grass (*Cenchrus ciliaris* L.). Ayala-Silva and Beyl (2005) induced Ca-deficiency in wheat (*Triticum aestivum* L.), and observed enhanced chlorosis and reflectance in visible wavelengths, although this result was similar to symptoms of deficiencies in other nutrients, such as nitrogen, magnesium, potassium, and phosphorus. Possible linkages between foliar Ca and hyperspectral data, however, remain uncharacterized in base-poor coniferous forest systems.

The treatment of an 11.8-ha forested watershed of the Hubbard Brook Experimental Forest (HBEF) with wollastonite ( $\text{CaSiO}_3$ ) in October of 1999 was designed to investigate the effects of a re-fertilization of forest soils that have been

historically reduced in Ca (Peters et al., 2004). In this experiment, Hawley et al. (2006) have measured decreased winter injury in the Ca-treated red spruce, while Juice et al. (2006) have shown improved crown vigor and seedling regeneration occurring in treated sugar maples (*Acer saccharum* Marsh.). Neither multispectral nor hyperspectral effects of the Ca amendment have been quantified for any species in this ecosystem study.

The objective of this work is to determine the spectral effects of the Ca application on red spruce at HBEF by measuring needles from the treated and reference areas with a high-resolution laboratory spectroradiometer. Multispectral and hyperspectral vegetation stress indices in the visible (400-750 nm), near-infrared (750-1350 nm), and infrared (1350-2500 nm) regions of the spectrum will also be compared to foliar chemistry, with the objective of supporting any experimental differences with correlational relationships. We hypothesize that needles of Ca-treated spruce trees will have benefited from the enhanced nutrient supply and responded with increased photosynthetic efficiency (greater chlorophyll absorption), and decreased signs of stress effects in visible, red-edge, and near infrared spectral indices.

## **Methods**

### *Experimental background and plot selection*

The present study was done at the Hubbard Brook Experimental Forest (HBEF), in the White Mountain National Forest, located in New Hampshire at 43 ° 56' N, 71 ° 45' W. The HBEF is a forested valley, comprising several small watersheds that drain into the east-flowing Hubbard Brook (elev. 200 m at outlet), and hills (elev. 600 - 1000 m) defining the northern and southern boundaries of the catchment (Barton et al., 1997).

American beech (*Fagus grandifolia* Ehrh.), yellow birch (*Betula alleghaniensis* Michx.) and sugar maple are the dominant broadleaf species at low to intermediate elevations, whereas red spruce, balsam fir, and paper birch (*Betula papyrifera* Marsh.) become more prevalent toward the ridges, and on north-facing slopes.

Following historical losses of base cation nutrients from the forest soils at HBEF, a whole-watershed Ca amendment was executed to assess the effect on forest dynamics of replenishing this soil pool by approximately 100 percent. The 11.8-ha watershed 1 received an aerial application of wollastonite ( $\text{CaSiO}_3$ ) at a rate of  $0.12 \text{ kg Ca m}^{-2}$  in October of 1999 (Peters et al., 2004). A biogeochemical reference watershed of similar geology, topography, and hydrology (watershed 6) is situated 1 km away, received no treatment, and is used in comparative studies (Likens and Bormann, 1995).

Red spruce trees were selected from coniferous stands in both the Ca-treated watershed (WS1) and an area adjacent to watershed 6 (WS6). No destructive sampling is permitted within WS6, so this study's reference samples were selected from trees along the ridge west of WS6, designated here as "west of six" (Wo6). Six plots were established in each watershed, and each plot contained three trees, for a total of 36 trees. Trees were selected randomly from mature, exposed individuals not having visible signs of canopy damage. A biometric description of these trees is submitted in a separate paper (Chapter I).

#### *Foliar collection and chemistry*

On 13 and 14 August 2007, foliage was sampled from branches within the mid-canopy assimilative zone of the crown using an extendable pole-pruner. All samples were



immediately placed in plastic zip-lock bags in a hand cooler with frozen blue ice, and transported to the laboratory, where they were stored at 7 °C. Spectroscopic processing took place within 48 h of collection, and oven drying for moisture content and chemical analyses within 1 week. All foliar samples were analyzed for the elements aluminum (Al), Ca, iron (Fe), potassium (K), magnesium (Mg), manganese (Mn), phosphorus (P), strontium (Sr), and the organic oxalate ion ( $C_2O_4^{2-}$ ). Detailed methodology for analyses of chemical and moisture content is described separately (Chapter I).

### *Needle spectroscopy*

Spectra were generated using the Visible/Infrared Intelligent Spectroradiometer (VIRIS), which is a portable, table-top spectroradiometer model GER 2600 (Geophysical Environmental Research Corp.\*, Millbrook, NY) currently supported by Spectravista\* Corp. (Poughkeepsie, NY). The VIRIS underwent a wavelengths and radiometric calibration prior to this study, on 27 November 2006. Spectral curves produced were of 3 / 1.5 nm spectral resolution (full-width half max / bandwidth sampling interval) in the visible and near-infrared regions (400-1020 nm), and of 25 / 15 nm spectral resolution at longer wavelengths (1020-2580 nm). The instrument consists of a dual silicon/lead-sulfide detector oriented perpendicular the sample tray, at a distance of 50 cm. A 1000 W hemispherical light source provides illumination from 50 cm away, at a 45° angle. A white spectralon reference target was scanned after every 16th spectrum to provide a 95-99 % reflectance value for radiometric calibration (Labsphere Corp.\*, North Sutton, NH).

Samples were arranged in a flat black sample dish, for maximum foliar

---

\* Use of brand names is for clarity and does not imply endorsement.

representation in the detector field of view, a minimum of 3 needle layers deep.

Scanning was done in a darkened, black-walled room, on a black matte table to minimize ambient reflectance signal. Each sample consisted of 3 scans, with a 120° rotation of the sample dish between scans, in order to account for spectral variation due to needle-branch orientation. The 3 scans were averaged to produce 1 spectral curve for each sample. An initial scan was done of a mixed-needle-year (MNY) bough from the most recent 3 to 5 years of growth. The un-partitioned sample was chosen to represent the foliage contributing to nadir-viewing satellite imagery. Boughs were then separated into current-year (CY) and third-year (3Y) sub-samples in order to quantify the spectral properties of 2007 and 2005 foliage, respectively.

For each sample, 32 indices were calculated using bands at different wavelengths. These included simulations of multispectral indices: Landsat Thematic Mapper (TM) bands 1-5 and 7, Normalized Difference Vegetation Index (NDVI), TM band 5/4 ratio (TM5/4), and TM band 4/3 ratio (TM4/3), as well as 23 hyperspectral indices generated according to equations, given in Table 5.

### *Statistical analysis*

All analyses were performed on unsmoothed reflectance data, using the Stata 10 data analysis software package (StataCorp\*, College Station, TX). Nested t-tests were done within needle age groups (n = 36) for foliar chemical measurements, for all spectral bands from 400-2500 nm, and for each of the 32 indices. A band-wise synopsis of the location and strength of significant differences between treatments was done using reflectance difference and sensitivity graphs after Carter (1993). For a given wavelength

---

\* Use of brand names is for clarity and does not imply endorsement.

(*B*), these metrics state:

$$\text{Reflectance difference}_{(B)} = R_{(B) \text{ TREATED}} - R_{(B) \text{ REFERENCE}} \quad [1]$$

$$\text{Reflectance sensitivity}_{(B)} = (R_{(B) \text{ TREATED}} - R_{(B) \text{ REFERENCE}}) / R_{(B) \text{ REFERENCE}} \quad [2]$$

where  $R_{\text{REFERENCE}}$  corresponds to spectra from Wo6 trees, and the  $R_{\text{TREATED}}$  to WS1 trees.

Correlations were tested first using ordinary least squares (OLS) methods within each needle class ( $n = 36$ ), and second, using multiple regression with binary dummy variables for needle age for all samples across age class ( $n = 108$ ).

## **Results**

### *Foliar chemistry*

Accounting for differences due to needle age class, analyses showed that in WS1 foliage, there is significantly ( $P < 0.05$ ) higher total foliar Ca, Sr, and oxalate, and that oxalate and foliar Ca are strongly positively correlated ( $P < 0.001$ ,  $R^2 = 0.831$ ). Full results of foliar chemistry measurements, including eight elemental analytes, along with scanning electron microscope imagery, are presented separately (Chapter I).

### *Spectral results*

Needle spectra collected on 13 and 15 August 2007 were averaged by age class (CY, 3Y, or MNY), and showed differences throughout the visible, near infrared (NIR), and infrared regions. Reflectance of CY needles was greatest in the visible and near-infrared

regions, while 3Y needle reflectance were equal to CY at infrared wavelengths beyond 1400 nm (Figure 8). In the visible region MNY and 3Y spectral curves tended to be more similar, and of lower reflectance than the CY, however, there was higher reflectance in the green and lower reflectance in the red portions of the MNY spectrum compared to the 3Y. The "red-well" area from 600-700 nm also appeared to broaden in 3Y needles compared to CY, and to broaden and deepen in MNY samples compared to CY. The near-infrared "plateau" region (about 750-1300 nm) also exhibited differences. In this region, current-year needles had a distinctly negative-sloping spectral shape due to reduced reflectance at 1300 nm relative to reflectance at 800 nm, while third-year needles tended to have a flatter form in this same region due to similar reflectance at 800 and 1300 nm. Needles of MNY samples appeared of intermediate slope, with higher percent reflectance than 3Y below ~1200 nm, and consistently lower reflectance at longer wavelengths.

Table 6 contains the results of t-tests of difference, along with *P* values for significance, for all indices computed. Within CY needles, four indices significantly differed by treatment: reflectance in simulated Thematic Mapper bands 5 (TM5) and 7 (TM7), Thematic Mapper band 5/4 moisture ratio (TM5/4), and the red/green ratio (RDGR) were lower in Ca-treated samples compared to the reference (Figure 9a, Table 6). Within 3Y needle spectra, we found no significant differences between Ca-treated and un-treated samples (Figure 9b, Table 6).

Comparing treatments within MNY needle scans (Table 6), the following areas of reflectance were significantly ( $P < 0.05$ ) higher in samples from WS1: simulated Thematic Mapper bands 1, 2, 3, 5, and 7 (band 4;  $P = 0.08$ ), NIR bands 2 and 3, and red-

edge (RE) bands 1, 2, and 3. Indices for NIR slope (NIR3/1), the red-well minimum reflectance, green peak maximum reflectance, Carter-Miller stress (CM1 and CM2), and the structure independent pigment index (SIPI) were also higher in Ca-treated foliage. Measurements of the RE3/1 ratio and the chlorophyll normalized difference index (CNDI) were both lower for trees growing in the treated watershed 1. Averaged spectral curves showing areas of overlap and divergence within the MNY spectra are also presented (Figure 9c).

The CY reflectance difference curve shows a significantly lowered reflectance for Ca-treated spectra at most wavelengths greater than 1370 nm (Figure 10a). Sensitivity of these reflectance differences appears to peak slightly in the infrared regions centered around 1500, 1950, and 2400 nm (Figure 11a). Graphs of significant differences in MNY samples indicate the opposite trend, where Ca-treated needles have a higher percent reflectance in areas of the spectrum including the visible and far-red (400-739 nm), near-infrared (928-1325 nm), and infrared (1325-2500 nm), but excluding the near infrared region from 740-927 nm (Figure 10c). These differences appeared strongest in the visible region, particularly in green wavelengths centered at 631 nm, and at local peak around 699 nm (Figure 11c).

#### *Correlations with total foliar calcium*

The results of OLS and multiple regression analyses done between spectral indices and total foliar Ca levels are presented in Table 7. Multiple regression accounts for variation in an index due to needle age, and showed significant ( $P < 0.05$ ) positive relationships between RDGR (red/green ratio) and Ca, SIPI (structure-independent pigment index) and

Ca, and chlorosis index (YLGR or yellow/green ratio) and Ca, while a negative correlation was found between the water band index (WBI) and needle Ca. Individual regressions within an age class showed significant positive relationships between NIR2 and Ca, and RE3 and Ca in CY needles, between YLGR, RDGR, and SIPI and Ca in 3Y needles, and a negative correlation between WBI and Ca in MNY samples.

#### *Correlations with foliar oxalate*

Relationships found between spectral indices and foliar oxalate (Ox) are presented in Table 8. Multiple regression showed a positive relationship between reflectance in the NIR2 and NIR3 regions and Ox, SIPI and Ox, and a negative relationship of WBI with Ox concentrations. In CY samples we found positive correlations between NIR3/1, RE3/1, green peak  $\lambda$ , and Ox, as well as a negative correlation between CM2 (Carter-Miller red/blue stress index) and Ox. In 3Y samples we found positive correlations between YLGR, RDGR, and SIPI and Ox. Significant positive correlations in MNY needles were seen between TM4, TM5, and TM7 reflectance, and green peak  $\lambda$ , and Ox, while a negative relationship was seen between WBI and Ox.

#### **Discussion**

A previous component of this study found the WS1 spruce foliage have accrued elevated levels of both foliar Ca and oxalate 8 years following the 1999 wollastonite application (Chapter I). Spectral data collected from the same foliage strongly suggest there is an age-dependent effect on needle and whole bough optical properties resulting from the Ca addition in red spruce. A primary objective herein was to empirically determine whether

needle spectral properties might be related to enhanced Ca supply for purposes of remote sensing in coniferous forests. Our results, at least from the heterogeneous MNY samples, suggest this potential is realistic, and a direct link between needle chemistry and optical properties is presented in theory. Satellite spectral data collected *in situ* are based on the reflectance properties of tree boughs, which were simulated by the MNY foliar samples of this study. Several findings point to the interplay of needle age, stress physiology, and reflectance properties, and these will be discussed in turn.

#### *Indications of stress following Ca treatment*

A suite of spectral indices was employed in this study, each of which has been related to some aspect or agent of plant stress, e.g. desiccation: WBI (Tucker, 1980), TM5/4 (Carter, 1991), atmospheric pollution: TM5/4, NIR3/1 (Rock et al., 1986), insect damage: CM1 (Pontius et al., 2005), REIP (Vogelmann et al., 1993), root pruning: CNDI, YLGR (Luther and Carrol, 1999), nutrient deficiency: PRI (Gamon et al., 1997), REIP, RE3/1, YLGR (Adams et al., 1999), elevation: REIP, PRI, CNDI (Richardson et al., 2001) and herbicide application: CM1, CM2 (Carter and Miller, 1994). Recent studies have measured red-edge properties associated with Ca supply, finding positive correlations with the red-edge inflection point (Ayala-Silva and Beyl, 2005) and red-edge slope (Mutanga et al., 2005). This is expected, as the red-edge region (680-750 nm) identifies the transition from high chlorophyll absorbance in the red to high infrared reflectance associated with a leaf tissue's structural components, water content, and chlorophyll content. The physiological role of Ca in the pectate composition of cell walls, the function of the photosystem-II apparatus, and carbohydrate synthesis could have

significant impact on this region of the spectrum. Healthier plants of higher chlorophyll levels will produce a deeper, and broader chlorophyll well in the 600-700 nm range and have a steeper red-edge of longer wavelength, both indicating normal chlorophyll concentrations at low stress levels (Vogelmann et al., 1993; Fillela and Peñuelas, 1994; Pontius et al., 2005).

The red spruce stands of watershed one (WS1) at Hubbard Brook have shown signs of improved vigor since the Ca addition, evidenced by reduction in winter injury (Hawley et al., 2006). Needle fluorescence ( $F_v/F_m$ ), which positively relates to photosynthetic efficiency in the PS-II center (Krause and Weis, 1991) and to cold tolerance in red spruce trees (Adams and Perkins, 1993), has increased in WS1 spruce (Boyce, 2007), providing spectral corroboration of this finding by Hawley et al. (2006).

Surprisingly, our hypothesis that high-resolution spectral data from the Ca-treated trees would show reduced signs of stress, was not supported. Moreover, our data suggest the opposite trend; that the Ca-treated stands are experiencing physiological stress. In mixed-needle-year scans, which exhibited the strongest and broadest differences between treatments (Figure 10c), we observed eight indices that suggest the presence of stress in WS1 needles. Significant ( $P < 0.05$ ) differences in red-edge associated indices included: RE1, RE2, RE3, RE3/1, CM1, CM2, SIPI, and CNDI (Table 6), and the NIR3/1 senescence ratio was also higher in WS1. Additionally, four indices showed marginally significant stress evidence in MNY samples: TM5/4, REIP,  $RW_{\lambda}$ , and PRI (Table 6).

A study by Carter (1993), measuring the spectral effects of treatments including herbicide, competition, pathogen attack, ozone, insufficient mycorrhizae, and dehydration, concluded there are sensitivity maxima in the visible regions 535-640 nm



(the green peak) and 685-700 nm (the red well), with a local minimum near 670 nm. The present study's results for Ca-treated MNY samples show these three sensitivity features distinctly within the increased reflectance effect (Figure 11c). Finally, significant positive correlations between total foliar Ca and SIPI and YLGR in multiple regression (Table 7) suggest carotenoid pigments may contribute to these treatment effects in the green-yellow and blue regions of the spectrum. The increased plant allocation to pigments such as xanthophylls, anthocyanins, and carotenes, relative to chlorophylls a and b may be related to decreases in photosynthetic efficiency (Peñuelas and Fillela, 1998; Richardson et al., 2001; Sims and Gamon, 2002). Although Boyce (2007) measured increased photosystem efficiency as indicated by greater fluorescence in WS1 spruce trees, our finding of decreased PRI suggests ( $P = 0.055$ ) the opposite pattern, with respect to positive correlations reported between PRI and  $F_v/F_m$  (Gamon et al., 1997; Richardson et al., 2001). Physiological measurements that may indicate stress in trees, including basal area increment, needle moisture content, and needle retention, did not differ by watershed (Chapter I).

#### *Mixed-needle-year boughs more reflective*

Compared to limited treatment effects on 3Y needle reflectance (Figure 10b) and CY effects occurring at wavelengths primarily past 1400 nm (Figure 10a), the significant reflectance increases in spectra for MNY samples existed across almost the entire spectrum measured from 400 to 2500 nm (Figure 9c, Figure 10c). Of the 12 band-average indices simulating the Landsat Thematic Mapper bands, as well as near infrared, and red-edge bands, 10 were significantly higher in WS1, and two approached a

significant increase (TM4,  $P = 0.080$ ; NIR1,  $P = 0.073$ ).

There is a possibility this increase in reflectance is an indirect effect of the Ca treatment related to water. Some studies have shown forest liming to bring about a change in root distribution to favor the richer surface soils, thereby reducing access to water in the lower soil profiles (McLaughlin and Wimmer, 1999). Although evidence exists that broad increases in infrared reflectance similar to those in the present study accompany drought effects (Carter, 1991; 1993; Kokaly and Clark, 1999), we did not see a moisture content effect in foliage in this experiment. Furthermore, no significant correlations were found between needle moisture content and either Ca or oxalate concentration. Both Ox and total Ca did, however, correlate negatively with the water band index (WBI), which has been shown to positively respond to water loss (Peñuelas and Fillela, 1998; Pontius et al., 2005).

Reflectance differences measured in the infrared (TM5, TM7, NIR2, NIR3; increased in WS1;  $P < 0.05$ ) and near infrared (WBI; decreased in WS1;  $P = 0.067$ ) provide conflicting evidence of water effects in MNY needles. Furthermore, the TM7 band was found to positively correlate with needle moisture content in a multiple regression accounting for needle age ( $R^2 = 0.707$ ;  $P = 0.027$ ). Finally, the absorptive properties of water are greatly diminished in the visible and near infrared regions ( $< 1300$  nm; Tucker, 1980), where we found significant reflectance increases. On the spectral effects of water in plant tissues, Carter (1991) has stated there are primary and secondary effects; the primary are attributable to the radiative absorption properties of the water molecule, and secondary effects result from the interaction of water and a second factor, such as carbohydrates contained in cell walls, tissue architecture and microstructure, or

pigments. Though the above results suggest the spectral differences by watershed have a more direct causal link to Ca supply, they do not allow rejection of water effects outright.

Plant spectral reflectance in the near infrared region is due to structural heterogeneity in foliar tissues (Gates et al., 1965; Peterson et al., 1988; Rock et al., 1994). Specifically, the effect of water-air, water-cell, and cell-air boundaries on incident radiation entering the leaf is a scattering due to differences of refractive indices.

Gausman (1974) noted the refractive index of the cell wall in a number of plants to be  $\approx 1.425$ , while that of water is 1.333; air, 1. Crystal sand deposits of CaOx appear to have accumulated in red spruce foliage following the addition of Ca at Hubbard Brook (Chapter I), and their position on the external surfaces of mesophyll cells might influence foliar optical properties through increased scattering and reflectance due to greater variation in refractive index. A monaxial crystal of CaOx has two refractive indices, whereas a biaxial crystal of CaOx has three refractive indices, reported as 1.49, 1.56, and 1.65 (Peterson and Kuhn, 1965). As an alternative to the hypothesis of a water-mediated Ca effect, we propose that increased reflectance in WS1 foliage is due to accumulations of refractive extracellular Ca-oxalate crystals in multiple years of needles.

#### *Current-year and third-year trends*

As in MNY samples, CY showed no correlation between moisture content and reflectance in the TM5 region, and in TM7 there was a weak positive correlation with moisture ( $R^2 = 0.102$ ,  $P = 0.057$ ), suggesting either an interrelationship between water, Ca, and reflectance properties (i.e. a secondary water effect), or that this reflectance effect is unrelated to needle moisture.

Opposite effects of the Ca-addition were seen in current-year needles compared to the MNY, evidenced by reduced reflectance in TM5 and TM7 regions ( $P = 0.049$  and  $P = 0.01$  respectively). Reflectance sensitivity measurements agree with this result, showing a significant reduction of CY needle reflectance in Ca-treated trees (Figures 10a, 11a). Across needle years, reflectance difference and sensitivity curves show a general reversal of the Ca effect, changing from decreased reflectance to increased reflectance from CY, 3Y, to MNY (Figures 10, 11). As CaOx tends to accumulate in older needle tissues (Gülpen et al., 1995; DeHayes et al., 1997; Borer et al., 2004), this agrees with the hypothesized connection between crystal presence and enhanced reflectance. The decreased fraction of CY needles in samples of the mixed-needle boughs could also relate to the reversal of this effect. It is not clear whether the amounts of oxalate we measured in 3Y needles (Chapter I) would be sufficient to expect increases in the associated spectral curves, although none were observed here (Figure 9b, 10b).

Cytoplasmic Ca levels in plants are kept low (0.1 – 100  $\mu\text{M}$ ; McLaughlin and Wimmer, 1999) compared to those of the cell interstices, by active processes that may include the biosynthesis and cellular extrusion of oxalate from precursors such as oxaloacetate, L-ascorbic acid, and glycolate (Franceschi and Loewus, 1995; Gülpen et al., 1995). The increased production of oxalic acid seen in red spruce trees in the Ca-amended watershed at HBEF was likely in response to an over-abundance of Ca. A change in allocation strategy may be required to actively maintain cytoplasmic Ca at low levels by the precipitation of excess Ca in the needle apoplast, and this re-allocation may then represent a physiological stress to the tree (McLaughlin and Wimmer, 1999). Our data suggest that spectral impacts of extracellular CaOx crystallization become

significant only when a number of aged needles are viewed simultaneously (i.e. in MNY scans), whereas in CY and 3Y age classes, this impact is not apparent. Non-significant stress related features in wavelengths 535-700 nm of the visible region, however, were seen in the youngest needle class (Figure 11a), and these features were strengthened in 3Y (Figure 11b), and in MNY samples (Figures 11c). If this stress were apparent to the nascent foliage of a given growing season, but before significant crystal accumulation had occurred, then unchanged reflectance in the infrared region would be expected, even as stress related areas of the visible spectrum had begun to respond positively. In Ca-treated mixed-needle-year samples, there were several indices that suggested lower chlorophyll, greater accessory pigments (carotenes and xanthophylls), and lower photosynthetic efficiency, possibly related to the trees' response to the physiological stress of high Ca influx through time. The causes of a decrease in infrared reflectance (Landsat TM5 and TM7 bands) of current-year needles from the Ca application site are not clear.

### **Summary**

The 1999 Ca-wollastonite amendment in WS1 of Hubbard Brook has caused changes in the spectral properties of red spruce foliage measured in 2007. Mixed-needle-year reflectance increased in the visible, near infrared, and short-wave infrared (400-2500 nm), but earlier needle years from the 2005 (3Y) and 2007 (CY) growing seasons did not show the same differences, suggesting that an accumulating Ca pool affects reflectance additively over multiple seasons. Increased refraction by calcium oxalate crystal deposits on the external cell walls is the potential cause of this effect in older needle age classes.

Spectral differences, particularly in the visible and red-edge transition wavelengths, may be a sign these trees are experiencing a Ca-superabundance stress, where photosynthetic function has yielded to increased oxalate synthesis for the maintenance of cytoplasmic Ca at physiological levels.

## Literature cited

- Adams GT and Perkins TD (1993) Assessing cold tolerance in *Picea* using chlorophyll fluorescence. *Environmental and Experimental Botany* 33: 377-382.
- Adams ML, Philpot WD, Norvell WA (1999) Yellowness index: an application of spectral second derivatives to estimate chlorosis of leaves in stressed vegetation. *International Journal of Remote Sensing* 20: 3663-3675.
- Albrechtová J, Rock BN, Soukupová J, Entcheva P, Šolcová B, Polák T (2001) Biochemical, histochemical, structural and reflectance markers of damage in Norway spruce from the Krušné hory Mts. used for interpretation of remote sensing data. *Journal of Forest Science* 47: 26-33.
- Ayala-Silva T and Beyl CA (2005) Changes in spectral reflectance of wheat leaves in response to specific macronutrient deficiency. *Advances in Space Research* 35: 305-317.
- Barton CC, Camerlo RH, Bailey SW (1997) Bedrock geologic map of the Hubbard Brook Experimental Forest and maps of fractures and geology in roadcuts along interstate 93, Grafton County, New Hampshire, Sheet 1, Scale 1:12,000; Sheet 2, Scale 1:200: U.S. Geological Survey Miscellaneous Investigations Series Map I-2562.
- Borer CH, Schaberg PG, DeHayes DH, Hawley GJ (2004) Accretion, partitioning, and sequestration of calcium and aluminum in red spruce foliage: implications for tree health. *Tree Physiology* 24: 929-939.
- Boyce RL (2007) Chlorophyll fluorescence response of red spruce and balsam fir to a watershed calcium fertilization experiment in New Hampshire. *Canadian Journal of Forest Research* 37: 1518-1522.
- Carter GA (1991) Primary and secondary effects of water content on the spectral reflectance of leaves. *American Journal of Botany* 78: 916-924.
- Carter GA (1993) Responses of leaf spectral reflectance to plant stress. *American Journal of Botany* 80: 239-243.
- Carter GA and Miller RL (1994) Early detection of plant stress by digital imaging within narrow stress-sensitive wavebands. *Remote Sensing of Environment* 50: 295-302.
- Curran PJ, Dungan JL, Macler BA, Plummer SE, Peterson DL (1992) Reflectance spectroscopy of fresh whole leaves for the estimation of chemical concentration. *Remote Sensing of Environment* 39: 153-166.

- DeHayes DH, Schaberg PG, Hawley GJ, Borer CH, Cummings JR, Strimbeck GR (1997) Physiological implications of seasonal variation in membrane-associated calcium in red spruce mesophyll cells. *Tree Physiology* 17: 687-695.
- Driscoll CT, Lawrence GB, Bulger AJ, Butler TJ, Cronan CS, Eagar C, Lambert KF, Likens GE, Stoddard JL, Weathers KL (2001) Acidic deposition in the northeastern United States: sources and inputs, ecosystem effects, and management strategies. *Bioscience* 51: 180-198.
- Entcheva Campbell PK, Rock BN, Martin ME, Neefus CD, Irons JR, Middletown EM, Albrechtová J (2004) Detection of initial damage in Norway spruce canopies using hyperspectral airborne data. *International Journal of Remote Sensing* 25: 5557-5583.
- Federer CA, Hornbeck JW, Tritton LM, Martin CW, Pierce RS, Smith CT (1989) Long-term depletion of calcium and other nutrients in eastern US forests. *Environmental Management* 13: 593-601.
- Filella I and Peñuelas J (1994) The red edge position and shape as indicators of plant chlorophyll content, biomass and hydric status. *International Journal of Remote Sensing* 15: 1459-1470.
- Franceschi VR and Loewus FR (1995) Oxalate function and biosynthesis in plants and fungi. In: Kahn SR (ed) *Calcium oxalate in biological systems*. CRC Press, New York.
- French CS and Young VMK (1956) Spectra of photosynthetic pigments. In: Hollaender A (ed) *Radiation Biology*. McGraw-Hill, New York.
- Gamon JA, Serrano L, Surfus JS (1997) The photochemical reflectance index: an optical indicator of photosynthetic radiation use efficiency across species, functional types, and nutrient levels. *Oecologia* 112: 492-501.
- Gates DM, Keegan HJ, Schleter JC, Weidner VR (1965) Spectral properties of plants. *Applied Optics* 4: 11-20.
- Gausman HW, Allen WA, Escobar DE (1974) Refractive index of plant cell walls. *Applied Optics* 13: 109-111.
- Gitelson A and Merzlyak MN (1994) Spectral reflectance changes associated with autumn senescence of *Aesculus hippocastanum* L. and *Acer platanoides* L. leaves: spectral features and relation to chlorophyll estimation. *Journal of Plant Physiology* 143: 286-292.
- Gülpen M, Türk S, Fink S (1995) Ca nutrition in conifers. *Zeitschrift für Pflanzenernährung und Bodenkunde* 158: 519-527.



- Hallett RA, Hornbeck JW, Martin ME (1997) Predicting elements in white pine and red oak foliage with visible-near infrared reflectance spectroscopy. *Journal of Near Infrared Spectroscopy* 5: 77-82.
- Hawley GJ, Schaberg PG, Eagar C, Borer CH (2006) Calcium addition at the Hubbard Brook Experimental Forest reduced winter injury to red spruce in a high-injury year. *Canadian Journal of Forest Research* 36: 2544-2549.
- Juice SM, Fahey TJ, Siccama TG, Driscoll CT, Denny EG, Eagar C, Cleavitt NL, Minocha R, Richardson AD (2006) Response of sugar maple to calcium addition to northern hardwood forest. *Ecology* 87:1267-1280.
- Kokaly RF and Clark RN (1999) Spectroscopic determination of leaf biochemistry using band-depth analysis of absorption features and stepwise multiple linear regression. *Remote Sensing of Environment* 67: 267-287.
- Krause GH and Weis E (1991) Chlorophyll fluorescence and photosynthesis: the basics. *Annual Review of Plant Physiology and Plant Molecular Biology* 42: 313-349.
- Likens GE and Bormann FH (1995) *Biogeochemistry of a forested ecosystem*, 2nd ed. Springer-Verlag, New York.
- Likens GE, Driscoll CT, Buso DC, Siccama TG, Johnson CE, Lovett GM, Fahey TJ, Reiners WA, Ryan DF, Martin CW, Bailey SW (1998) The biogeochemistry of calcium at Hubbard Brook. *Biogeochemistry* 41: 89-173.
- Luther JE and Carroll AL (1999) Development of an index of balsam fir vigor by foliar spectral reflectance. *Remote Sensing of Environment* 69: 241-252.
- Martin ME and Aber JD (1997) High spectral resolution remote sensing of forest canopy lignin, nitrogen, and ecosystem processes. *Ecological Applications* 7: 431-443.
- McLaughlin SB and Wimmer R (1999) Calcium physiology and terrestrial ecosystem processes. *New Phytologist* 142: 373-417.
- Mutanga O, Skidmore AK, Kumar L, Ferwerda J (2005) Estimating tropical pasture quality at canopy level using band depth analysis with continuum removal in the visible domain. *International Journal of Remote Sensing* 26:1093-1108.
- Ollinger SV and Smith ML (2005) Net primary production and canopy nitrogen in a temperate forest landscape: an analysis using imaging spectroscopy, modeling, and field data. *Ecosystems* 8: 760-778.
- Peñuelas J and Filella I (1998) Visible and near-infrared reflectance techniques for diagnosing plant physiological status. *Trends in Plant Science* 3: 151-156.

- Peters SC, Blum JD, Driscoll CT, Likens GE (2004) Dissolution of wollastonite during the experimental manipulation of Hubbard Brook Watershed 1. *Biogeochemistry* 67: 309-329.
- Peterson DL, Aber JD, Matson PA, Card DH, Swanberg N, Wessman C, Spanner M (1988) Remote sensing of forest canopy and leaf biochemical contents. *Remote Sensing of Environment* 24: 85-108.
- Peterson BJ and Kuhn RJ (1965) Optical characterization of crystals in tissue: cystine and calcium oxalate monohydrate. *American Journal of Clinical Pathology* 43: 401-408.
- Pontius J, Hallett RA, Martin ME (2005) Assessing hemlock decline using visible and near-infrared spectroscopy: indices comparison and algorithm development. *Applied Spectroscopy* 59: 836-843.
- Richardson AD, Berlyn GP, Gregoire TG (2001) Spectral reflectance of *Picea rubens* (Pinaceae) and *Abies balsamea* (Pinaceae) needles along an elevational gradient, Mt. Moosilauke, New Hampshire, USA. *American Journal of Botany* 88: 667-676.
- Rock BN, Vogelmann JE, Williams DL, Vogelmann AF, Hoshizaki T (1986) Remote detection of forest damage. *Bioscience* 36: 439-445.
- Rock BN, Vogelmann JE, DeFeo NJ (1989) The use of remote sensing for the study of air pollution effects in forests. In: *Biologic markers of air-pollution stress and damage in forests*. National Academy Press, Washington, DC.
- Rock BN, Williams DL, Moss DM, Lauten GN, and Kim M (1994) High-spectral resolution field and laboratory optical reflectance measurements of red spruce and eastern hemlock needles and branches. *Remote Sensing of Environment* 47: 176-189.
- Rouse JW, Haas RH, Schell JA, Deening DW (1973) Monitoring vegetation systems in the great plains with ERTS, Third ERTS Symposium, NASA SP-351 I: 309-317.
- Sims DA and Gamon JA (2002) Relationships between leaf pigment content and spectral reflectance across a wide range of species, leaf structures, and developmental stages. *Remote Sensing of Environment* 81: 337-354.
- Tucker CJ (1980) Remote sensing of leaf water content in the near infrared. *Remote Sensing of Environment* 10: 23-32.
- Vogelmann JE and Rock BN (1988) Assessing forest damage in high-elevation coniferous forests in Vermont and New Hampshire using Thematic Mapper data.

Remote Sensing of Environment 24: 227-246.

Vogelmann JE, Rock BN, Moss DM (1993) Red edge spectral measurements from sugar maple leaves. *International Journal of Remote Sensing* 14: 1563-1575.

Wessman CA, Aber JD, Peterson DL, Melillo JM (1988) Remote sensing of canopy chemistry and nitrogen cycling in temperate forest ecosystems. *Nature* 335: 154-156.

| Index  | Abbr.         | Formula   | Physiological significance in plants  |
|--|---------------|---|---|
| Landsat band 1 (simulated)<br>band 2<br>band 3<br>band 4<br>band 5<br>band 7   | TM1           | mean R450:520 nm                                    | High absorbance due to carotenes, xanthophylls, chlorophylls } (French & Young, 1956)<br>Area of relatively low chlorophyll absorbance<br>High absorbance due to chlorophylls a and b<br>Reflection/refraction from cellulose, lignin, and cell-water interstices (see NIR refs.)<br>Water absorption, lignin/cellulose (Tucker, 1980; Carter, 1991; Kokaly & Clark, 1999)            |
|  | TM2           | mean R520:600 nm                                    |   |
|  | TM3           | mean R630:690 nm                                    |   |
|  | TM4           | mean R690:900 nm                                    |   |
|  | TM5           | mean R1550:1750 nm                                  |   |
|  | TM7           | mean R2080:2350 nm                                  |   |
|  | TM4/TM3 ratio | Landsat TM4 / TM3                                   |   |
| Norm. Diff. Veg. Index<br>TM5/TM4 ratio  | NDVI          | (TM4 - TM3) / (TM4 + TM3)                           | Plant biomass characteristic (Rouse et al., 1973)<br>Water content, leaf age class, foliar biomass (Rock et al., 1986)  |
|  | TM5/4         | Landsat TM5/TM4                                     |   |
| Red edge 1<br>Red edge 2<br>Red edge 3<br>Near-infrared band 1<br>Near-infrared band 2<br>Near-infrared band 3<br>NIR3/NIR1 ratio<br>RE3/RE1 ratio | RE1           | mean R695:705                                       | Chlorophyll content and fluorescence (Vogelmann et al., 1993; Filella & Peñuelas, 1994)<br>Cellulose, lignin, cell-water interfaces (Gates et al., 1965; Gausman et al., 1974; Peterson et al., 1988; Rock et al., 1994)<br>Leaf age class, senescence, stress (Albrechtová et al., 2001)<br>Chlorophyll content, fluorescence, plant moisture and biomass (Filella & Peñuelas, 1994) |
|  | RE2           | mean R715-726                                       |   |
|  | RE3           | mean R734:746                                       |   |
|  | NIR1          | mean R794:900                                       |   |
|  | NIR2          | mean R1030:1060                                     |   |
|  | NIR3          | mean R1250:1325                                     |   |
| NIR3/1   | ----          |   |   |
| RE3/1  | ----          |   |   |
| Red well<br>Red well band<br>Green peak<br>Green peak band   | Rwell         | R <sub>MIN</sub> 600:700                            | Maximum red absorption by chlorophyll<br>Wavelength of the max. chlorophyll absorbance feature<br>Maximum green reflectance by photosynthetic and photo-protective pigments<br>Wavelength of max. green reflectance   |
|  | RW_λ          | λ R <sub>MIN</sub> 600:700                          |   |
|  | Gpeak         | R <sub>MAX</sub> 500:600                            |   |
|  | GP_λ          | λ R <sub>MIN</sub> 500:600                          |   |
| Red-edge inflection point<br>Chlorosis index<br>Red-green ratio<br>Green shoulder ratio<br>Red shoulder ratio                                      | REIP          | λ (700:740), where $dR^2/d^2λ = 0$                  | Chlorophyll content, fluorescence, plant moisture and biomass (Vogelmann et al., 1993)<br>Foliar yellowing, age class, senescence (Adams et al., 1999)<br>Anthocyanin/chlorophyll ratio (Sims & Gamon, 2002)<br>Normalized maximum green pigment reflectance<br>Normalized maximum red absorption by chlorophyll  |
|  | CHLR          | mean R580:620 / R <sub>MAX</sub> 530:570            |   |
|  | RDGR          | R <sub>MIN</sub> 600:700 / R <sub>MAX</sub> 530:570 |   |
|  | GSHD          | R <sub>MAX</sub> 500:700 / mean R750:780            |   |
|  | RSHD          | R <sub>MIN</sub> 600:700 / mean R750:780            |   |

Table 5. Synopsis of indices. R = percent reflectance at a given wavelength. Continued on following page.

| Index                                   | Abbr. | Formula                                     | Physiological significance in plants   |
|---|-------|---|--|
| Carter/Miller index 1                   | CM1   | $R_{695} / R_{760}$                         | Chlorophyll content and fluorescence, general plant stress (Carter & Miller, 1994)                         |
| Carter/Miller index 2                   | CM2   | $R_{695} / R_{420}$                         |  |
| Chlorophyll normalized difference index | CNDI  | $(R_{750} - R_{705}) / (R_{750} + R_{705})$ | Chlorophyll a content (Gitelson & Merzlyak, 1994)  |
| Structure-independent pigment index     | SIPI  | $(R_{800} - R_{445}) / (R_{800} - R_{680})$ | Carotenoid/chlorophyll a ratio (Peñuelas & Fillela, 1998)  |
| Photochemical reflectance index         | PRI   | $(R_{531} - R_{570}) / (R_{531} + R_{570})$ | Xanthophyll activity, photosynthetic radiation-use efficiency, CO <sub>2</sub> uptake (Gamon et al., 1997) |
| Water band index                        | WBI   | $R_{970} / R_{900}$                         | Plant moisture content (Pontius et al., 2005)  |

Table 5 continued.

| Needle-age class..... | CY (2007) |       |       |        | 3Y (2005) |       |       |       | MNY (whole-bough) |         |   |     |     |
|-----------------------|-----------|-------|-------|--------|-----------|-------|-------|-------|-------------------|---------|---|-----|-----|
|                       | Index     | Units | WS1   | Wo6    | P         | WS1   | Wo6   | P     | WS1               | Wo6     | P | WS1 | Wo6 |
| TM1                   | %         | 3.74  | 3.62  | 0.384  | 3.17      | 3.14  | 0.709 | 3.23  | 2.93              | 0.021*  |   |     |     |
| TM2                   | %         | 6.98  | 6.54  | 0.145  | 5.81      | 5.57  | 0.274 | 6.26  | 5.43              | 0.010*  |   |     |     |
| TM3                   | %         | 3.98  | 3.87  | 0.443  | 3.79      | 3.62  | 0.247 | 3.52  | 3.05              | 0.004** |   |     |     |
| TM4                   | %         | 59.2  | 58.8  | 0.742  | 44.0      | 44.8  | 0.399 | 49.0  | 45.9              | 0.080#  |   |     |     |
| TM5                   | %         | 24.4  | 25.5  | 0.049* | 25.5      | 25.8  | 0.640 | 21.5  | 19.3              | 0.003** |   |     |     |
| TM7                   | %         | 14.8  | 16.3  | 0.010* | 16.1      | 16.8  | 0.281 | 11.7  | 10.6              | 0.005** |   |     |     |
| NIR1                  | %         | 60.0  | 59.6  | 0.731  | 44.8      | 45.6  | 0.423 | 49.9  | 46.7              | 0.073#  |   |     |     |
| NIR2                  | %         | 58.8  | 57.9  | 0.368  | 47.4      | 47.4  | 0.942 | 51.8  | 46.9              | 0.011*  |   |     |     |
| NIR3                  | %         | 45.2  | 45.4  | 0.718  | 42.0      | 41.9  | 0.993 | 42.3  | 38.0              | 0.005** |   |     |     |
| RE1                   | %         | 9.39  | 9.29  | 0.812  | 8.46      | 8.27  | 0.615 | 7.96  | 6.84              | 0.005** |   |     |     |
| RE2                   | %         | 26.1  | 25.6  | 0.560  | 21.0      | 20.9  | 0.972 | 21.4  | 19.2              | 0.011*  |   |     |     |
| RE3                   | %         | 44.4  | 43.9  | 0.591  | 33.4      | 33.9  | 0.458 | 36.3  | 33.7              | 0.046*  |   |     |     |
| TM5/TM4               | .         | 0.412 | 0.434 | 0.020* | 0.580     | 0.576 | 0.747 | 0.440 | 0.421             | 0.094#  |   |     |     |
| TM4/TM3               | .         | 15.0  | 15.4  | 0.373  | 11.7      | 12.5  | 0.128 | 14.1  | 15.2              | 0.067#  |   |     |     |
| NDVI                  | .         | 0.874 | 0.877 | 0.427  | 0.841     | 0.850 | 0.107 | 0.866 | 0.875             | 0.057#  |   |     |     |
| NIR3/1                | .         | 0.754 | 0.762 | 0.346  | 0.938     | 0.920 | 0.109 | 0.849 | 0.815             | 0.022*  |   |     |     |
| RE3/1                 | .         | 4.77  | 4.78  | 0.934  | 3.99      | 4.16  | 0.279 | 4.63  | 4.93              | 0.044*  |   |     |     |
| Rwell                 | %         | 3.48  | 3.42  | 0.660  | 3.34      | 3.23  | 0.370 | 2.96  | 2.62              | 0.014*  |   |     |     |
| RW_λ                  | nm        | 669   | 668   | 0.132  | 669       | 668   | 0.271 | 671   | 670               | 0.086#  |   |     |     |
| Gpeak                 | %         | 8.26  | 7.72  | 0.124  | 6.67      | 6.43  | 0.321 | 7.32  | 6.37              | 0.011*  |   |     |     |
| GP_λ                  | nm        | 553   | 552   | 0.697  | 553       | 552   | 0.547 | 553   | 552               | 0.073#  |   |     |     |
| REIP                  | nm        | 726   | 726   | 0.380  | 724       | 726   | 0.123 | 726   | 727               | 0.085#  |   |     |     |

Key to significance  
# 0.10 > P ≥ 0.05  
\* 0.05 > P ≥ 0.01  
\*\* 0.01 > P  
\*\*\* 0.01 > P

Key to units  
% percent reflectance  
nm wavelength / band  
. unitless

Table 6. Mean spectral indices for current-year (CY), third-year (3Y), and multiple-needle-year (MNY) red spruce foliage from a Ca-treated (WS1) and reference (Wo6) watershed at the HBEF, along with probabilities for a Student's t difference of means (n = 18 per treatment). Continued on following page.

| Index | Units | CY (2007) |       |        | 3Y (2005) |         |        | MNY (whole-bought) |        |        |
|-------|-------|-----------|-------|--------|-----------|---------|--------|--------------------|--------|--------|
|       |       | WSI       | Wo6   | P      | WSI       | Wo6     | P      | WSI                | Wo6    | P      |
|       |       |           |       |        |           |         |        |                    |        |        |
| YLGR  | .     | 0.654     | 0.656 | 0.647  | 0.721     | 0.705   | 0.084# | 0.676              | 0.664  | 0.112  |
| RDGR  | .     | 0.423     | 0.444 | 0.041* | 0.505     | 0.503   | 0.912  | 0.409              | 0.412  | 0.825  |
| GSHD  | .     | 0.151     | 0.141 | 0.065# | 0.167     | 0.156   | 0.092# | 0.164              | 0.152  | 0.081# |
| RSHD  | .     | 0.061     | 0.060 | 0.796  | 0.080     | 0.075   | 0.133  | 0.0634             | 0.0599 | 0.155  |
| CM1   | .     | 0.132     | 0.132 | 0.982  | 0.168     | 0.160   | 0.280  | 0.139              | 0.127  | 0.038* |
| CM2   | .     | 1.32      | 1.34  | 0.669  | 1.55      | 1.51    | 0.557  | 1.35               | 1.23   | 0.041* |
| CNDI  | .     | 0.599     | 0.602 | 0.782  | 0.542     | 0.557   | 0.267  | 0.591              | 0.614  | 0.046* |
| SIPI  | .     | 0.995     | 0.996 | 0.737  | 1.01      | 1.01    | 0.408  | 0.995              | 0.990  | 0.015* |
| PRI   | .     | 0.015     | 0.019 | 0.306  | 3.07e-3   | 9.95e-3 | 0.122  | 0.008              | 0.016  | 0.055# |
| WBI   | .     | 0.913     | 0.910 | 0.388  | 0.971     | 0.975   | 0.334  | 0.927              | 0.938  | 0.061# |

Table 6 continued.

| Needle-age class.....CY (2007) | 3Y (2005) |        |                | MNY (whole-bough) |        |                | Multiple regression |        |                |        |
|--------------------------------|-----------|--------|----------------|-------------------|--------|----------------|---------------------|--------|----------------|--------|
|                                | Index     | Coeff. | R <sup>2</sup> | P                 | Coeff. | R <sup>2</sup> | P                   | Coeff. | R <sup>2</sup> | P      |
| TM1                            | 0.175     | 0.028  | 0.333          | 0.839             | 0.436  | 0.034          | 0.280               | 0.221  | 0.481          | 0.342  |
| TM2                            | 0.038     | 0.007  | 0.635          | 0.289             | 0.130  | 0.019          | 0.429               | 0.014  | 0.476          | 0.885  |
| TM3                            | 0.088     | 0.009  | 0.577          | 0.479             | 0.390  | 0.044          | 0.222               | 0.271  | 0.487          | 0.136  |
| TM4                            | 0.017     | 0.017  | 0.454          | 0.683             | 0.050  | 0.074          | 0.110               | 0.029  | 0.485          | 0.187  |
| TM5                            | -0.022    | 0.009  | 0.594          | 0.572             | 0.105  | 0.070          | 0.120               | 0.057  | 0.486          | 0.156  |
| TM7                            | -0.053    | 0.053  | 0.177          | 0.737             | 0.222  | 0.072          | 0.114               | 0.028  | 0.478          | 0.568  |
| NIR1                           | 0.042     | 0.103  | 0.057#         | 0.978             | 0.009  | 0.003          | 0.772               | 0.014  | 0.478          | 0.508  |
| NIR2                           | 0.051     | 0.120  | 0.038*         | 0.452             | 0.016  | 0.010          | 0.564               | 0.027  | 0.485          | 0.197  |
| NIR3                           | 0.056     | 0.083  | 0.089#         | 0.758             | 0.017  | 0.007          | 0.625               | 0.023  | 0.481          | 0.359  |
| RE1                            | 0.097     | 0.082  | 0.090#         | 0.252             | 0.095  | 0.014          | 0.492               | 0.010  | 0.476          | 0.890  |
| RE2                            | 0.054     | 0.099  | 0.062#         | 0.169             | 0.040  | 0.013          | 0.512               | 0.009  | 0.477          | 0.805  |
| RE3                            | 0.048     | 0.111  | 0.047*         | 0.422             | 0.016  | 0.004          | 0.711               | 0.011  | 0.477          | 0.692  |
| TM5/TM4                        | -2.90     | 0.040  | 0.245          | 0.249             | 0.107  | 0.000          | 0.982               | 1.80   | 0.479          | 0.452  |
| TM4/TM3                        | -0.020    | 0.005  | 0.676          | 0.506             | 0.006  | 0.000          | 0.948               | -0.029 | 0.478          | 0.590  |
| NDVI                           | -1.77     | 0.002  | 0.776          | 0.307             | -0.968 | 0.000          | 0.928               | -5.56  | 0.481          | 0.316  |
| NIR3/1                         | 0.591     | 0.002  | 0.822          | 0.184             | 2.26   | 0.011          | 0.536               | 3.38   | 0.487          | 0.153  |
| RE3/1                          | 0.121     | 0.015  | 0.484          | 0.778             | 0.156  | 0.006          | 0.668               | 0.129  | 0.479          | 0.496  |
| Rwell                          | 0.124     | 0.012  | 0.522          | 0.231             | 0.501  | 0.050          | 0.192               | 0.415  | 0.495          | 0.054# |
| RW_λ                           | 0.020     | 0.017  | 0.477          | 0.787             | 0.064  | 0.023          | 0.377               | 0.016  | 0.478          | 0.614  |
| Gpeak                          | 0.032     | 0.006  | 0.644          | 0.208             | 0.111  | 0.018          | 0.436               | 0.004  | 0.476          | 0.961  |
| GP_λ                           | 0.065     | 0.083  | 0.089#         | 0.961             | 0.157  | 0.080          | 0.096#              | 0.057  | 0.486          | 0.172  |
| REIP                           | -0.012    | 0.005  | 0.698          | 0.167             | 0.016  | 0.000          | 0.895               | 0.028  | 0.481          | 0.356  |

Table 7. Results of least-squares (OLS; columns 1-3) and multiple regressions (column 4) of spectral indices on total foliar Ca. Coefficients of determination are for the single predictor index in OLS groups, and for the needle age-index model in multiple regressions. (#) 0.10 > P ≥ 0.05; (\*) 0.05 > P ≥ 0.01; (\*\*) 0.01 > P. Continued on following page.



| Needle-age class..... | CY (2007) |        |                | 3Y (2005) |        |                | MNY (whole-bough) |        |                | Multiple regression |        |                |         |
|-----------------------|-----------|--------|----------------|-----------|--------|----------------|-------------------|--------|----------------|---------------------|--------|----------------|---------|
|                       | Index     | Coeff. | R <sup>2</sup> | P         | Coeff. | R <sup>2</sup> | P                 | Coeff. | R <sup>2</sup> | P                   | Coeff. | R <sup>2</sup> | P       |
| YLGR                  | 2.73      | 0.008  | 0.615          | 0.615     | 14.2   | 0.145          | 0.022*            | 6.90   | 0.028          | 0.330               | 10.4   | 0.515          | 0.005** |
| RDGR                  | 0.188     | 0.000  | 0.936          | 0.936     | 7.68   | 0.177          | 0.011*            | 2.56   | 0.015          | 0.483               | 4.96   | 0.513          | 0.006** |
| GSHD                  | 6.98      | 0.071  | 0.116          | 0.116     | -8.59  | 0.023          | 0.381             | 7.95   | 0.031          | 0.307               | 2.12   | 0.477          | 0.641   |
| RSHD                  | 17.7      | 0.059  | 0.155          | 0.155     | -1.15  | 0.000          | 0.950             | 16.6   | 0.017          | 0.450               | 7.30   | 0.479          | 0.494   |
| CM1                   | -3.56     | 0.015  | 0.472          | 0.472     | 0.479  | 0.000          | 0.953             | -1.83  | 0.001          | 0.850               | -1.00  | 0.477          | 0.827   |
| CM2                   | -0.875    | 0.079  | 0.096#         | 0.096#    | -0.671 | 0.012          | 0.525             | 0.186  | 0.001          | 0.843               | -0.386 | 0.479          | 0.459   |
| CNDI                  | 1.90      | 0.018  | 0.432          | 0.432     | 2.37   | 0.008          | 0.599             | 1.44   | 0.003          | 0.755               | 1.95   | 0.480          | 0.409   |
| SIP1                  | 6.73      | 0.006  | 0.650          | 0.650     | 40.4   | 0.125          | 0.034*            | 28.0   | 0.034          | 0.281               | 32.0   | 0.513          | 0.006** |
| PRI                   | 0.540     | 0.000  | 0.935          | 0.935     | -11.1  | 0.019          | 0.426             | -19.7  | 0.066          | 0.129               | -11.0  | 0.489          | 0.110   |
| WBI                   | -5.89     | 0.030  | 0.310          | 0.310     | -23.1  | 0.053          | 0.178             | -19.5  | 0.121          | 0.037*              | -16.5  | 0.512          | 0.007** |

Table 7 continued.

| Index   | Needle-age class.....CY (2007) |                |        | 3Y (2005) |                |        | MNY (whole-bough) |                |        | Multiple regression |                |        |
|---------|--------------------------------|----------------|--------|-----------|----------------|--------|-------------------|----------------|--------|---------------------|----------------|--------|
|         | Coeff.                         | R <sup>2</sup> | P      | Coeff.    | R <sup>2</sup> | P      | Coeff.            | R <sup>2</sup> | P      | Coeff.              | R <sup>2</sup> | P      |
| TM1     | -0.313                         | 0.005          | 0.678  | -0.739    | 0.006          | 0.662  | 1.63              | 0.086          | 0.082# | 0.426               | 0.220          | 0.493  |
| TM2     | -0.232                         | 0.015          | 0.479  | -0.985    | 0.055          | 0.168  | 0.436             | 0.038          | 0.258  | -0.076              | 0.220          | 0.773  |
| TM3     | -0.624                         | 0.028          | 0.340  | 0.533     | 0.007          | 0.633  | 1.18              | 0.072          | 0.115  | 0.456               | 0.222          | 0.348  |
| TM4     | -0.017                         | 0.001          | 0.849  | -0.106    | 0.012          | 0.524  | 0.179             | 0.173          | 0.012* | 0.085               | 0.232          | 0.137  |
| TM5     | -0.060                         | 0.004          | 0.712  | 0.160     | 0.015          | 0.478  | 0.379             | 0.164          | 0.014* | 0.204               | 0.244          | 0.052# |
| TM7     | -0.209                         | 0.055          | 0.176  | 0.095     | 0.005          | 0.675  | 0.700             | 0.129          | 0.031* | 0.073               | 0.220          | 0.568  |
| NIR1    | 0.037                          | 0.005          | 0.677  | -0.029    | 0.001          | 0.863  | 0.115             | 0.074          | 0.108  | 0.073               | 0.228          | 0.196  |
| NIR2    | 0.162                          | 0.079          | 0.101  | 0.146     | 0.020          | 0.414  | 0.109             | 0.083          | 0.088# | 0.123               | 0.254          | 0.023* |
| NIR3    | 0.235                          | 0.095          | 0.072# | 0.134     | 0.013          | 0.517  | 0.110             | 0.056          | 0.164  | 0.131               | 0.245          | 0.049* |
| RE1     | 0.090                          | 0.005          | 0.695  | -0.384    | 0.025          | 0.354  | 0.412             | 0.048          | 0.199  | 0.053               | 0.216          | 0.777  |
| RE2     | 0.081                          | 0.015          | 0.490  | -0.341    | 0.051          | 0.187  | 0.231             | 0.077          | 0.101  | 0.063               | 0.219          | 0.511  |
| RE3     | 0.058                          | 0.010          | 0.560  | -0.204    | 0.027          | 0.340  | 0.160             | 0.078          | 0.098# | 0.068               | 0.222          | 0.344  |
| TM5/TM4 | -2.47                          | 0.002          | 0.804  | 17.0      | 0.069          | 0.122  | -0.157            | 0.000          | 0.989  | -4.97               | 0.216          | 0.736  |
| TM4/TM3 | 0.179                          | 0.023          | 0.387  | -0.153    | 0.008          | 0.611  | 0.089             | 0.005          | 0.691  | 13.5                | 0.251          | 0.029* |
| NDVI    | 25.9                           | 0.031          | 0.316  | -24.6     | 0.026          | 0.344  | 7.00              | 0.002          | 0.781  | 0.820               | 0.236          | 0.103  |
| NIR3/1  | 20.4                           | 0.113          | 0.048* | 24.9      | 0.087          | 0.081# | 5.11              | 0.011          | 0.553  | 0.851               | 0.232          | 0.139  |
| RE3/1   | 1.41                           | 0.116          | 0.045* | 0.496     | 0.007          | 0.621  | 0.733             | 0.022          | 0.391  | 0.820               | 0.236          | 0.103  |
| Rwell   | -0.741                         | 0.026          | 0.358  | 1.33      | 0.034          | 0.285  | 1.56              | 0.086          | 0.082# | 0.851               | 0.232          | 0.139  |
| RW_λ    | 0.043                          | 0.005          | 0.683  | -0.093    | 0.009          | 0.582  | 0.088             | 0.008          | 0.609  | 0.0013              | 0.215          | 0.988  |
| Gpeak   | -0.182                         | 0.013          | 0.520  | -0.994    | 0.071          | 0.117  | 0.393             | 0.041          | 0.236  | -0.068              | 0.216          | 0.763  |
| GP_λ    | 0.340                          | 0.150          | 0.022* | -0.020    | 0.000          | 0.916  | 0.501             | 0.146          | 0.022* | 0.202               | 0.241          | 0.063# |
| REIP    | -0.088                         | 0.014          | 0.502  | 0.215     | 0.058          | 0.159  | -0.090            | 0.014          | 0.496  | 0.038               | 0.217          | 0.642  |

Table 8. Results of least-squares (OLS; columns 1-3) and multiple regressions (column 4) of spectral indices on total foliar oxalate. Coefficients of determination are for the single predictor index in OLS groups, and for the needle age-index model in multiple regressions. (#) 0.10 > P ≥ 0.05; (\*) 0.05 > P ≥ 0.01; (\*\*) 0.01 > P. Continued on the following page.

| Needle-age class..... | CY (2007) |                |         | 3Y (2005) |                |         | MNY (whole-bough) |                |        | Multiple regression |                |         |
|-----------------------|-----------|----------------|---------|-----------|----------------|---------|-------------------|----------------|--------|---------------------|----------------|---------|
|                       | Coeff.    | R <sup>2</sup> | P       | Coeff.    | R <sup>2</sup> | P       | Coeff.            | R <sup>2</sup> | P      | Coeff.              | R <sup>2</sup> | P       |
| YLGR                  | -27.7     | 0.051          | 0.193   | 33.4      | 0.123          | 0.036*  | 1.19              | 0.000          | 0.943  | 15.3                | 0.234          | 0.116   |
| RDGR                  | -0.893    | 0.000          | 0.923   | 20.5      | 0.192          | 0.008** | 4.97              | 0.010          | 0.563  | 12.5                | 0.267          | 0.008** |
| GSHD                  | 19.6      | 0.037          | 0.268   | -20.3     | 0.019          | 0.419   | 11.5              | 0.012          | 0.532  | 2.68                | 0.216          | 0.822   |
| RSHD                  | 45.3      | 0.025          | 0.363   | 17.4      | 0.004          | 0.712   | -0.163            | 0.000          | 0.997  | 17.0                | 0.218          | 0.545   |
| CM1                   | -38.9     | 0.110          | 0.051#  | -2.16     | 0.000          | 0.917   | -13.3             | 0.010          | 0.555  | -12.4               | 0.223          | 0.307   |
| CM2                   | -6.02     | 0.237          | 0.003** | -2.36     | 0.023          | 0.381   | -0.816            | 0.004          | 0.712  | -2.55               | 0.242          | 0.061#  |
| CNDI                  | 18.2      | 0.100          | 0.064#  | 7.96      | 0.014          | 0.490   | 7.09              | 0.013          | 0.512  | 9.82                | 0.234          | 0.116   |
| SIPI                  | 22.0      | 0.004          | 0.713   | 101.8     | 0.122          | 0.037*  | 51.9              | 0.021          | 0.397  | 76.8                | 0.261          | 0.013*  |
| PRI                   | 18.2      | 0.015          | 0.485   | -21.9     | 0.011          | 0.540   | -19.0             | 0.011          | 0.540  | -10.4               | 0.218          | 0.567   |
| WBI                   | -24.0     | 0.032          | 0.305   | -54.2     | 0.044          | 0.217   | -46.9             | 0.127          | 0.033* | -42.3               | 0.266          | 0.009** |

Table 8 continued.

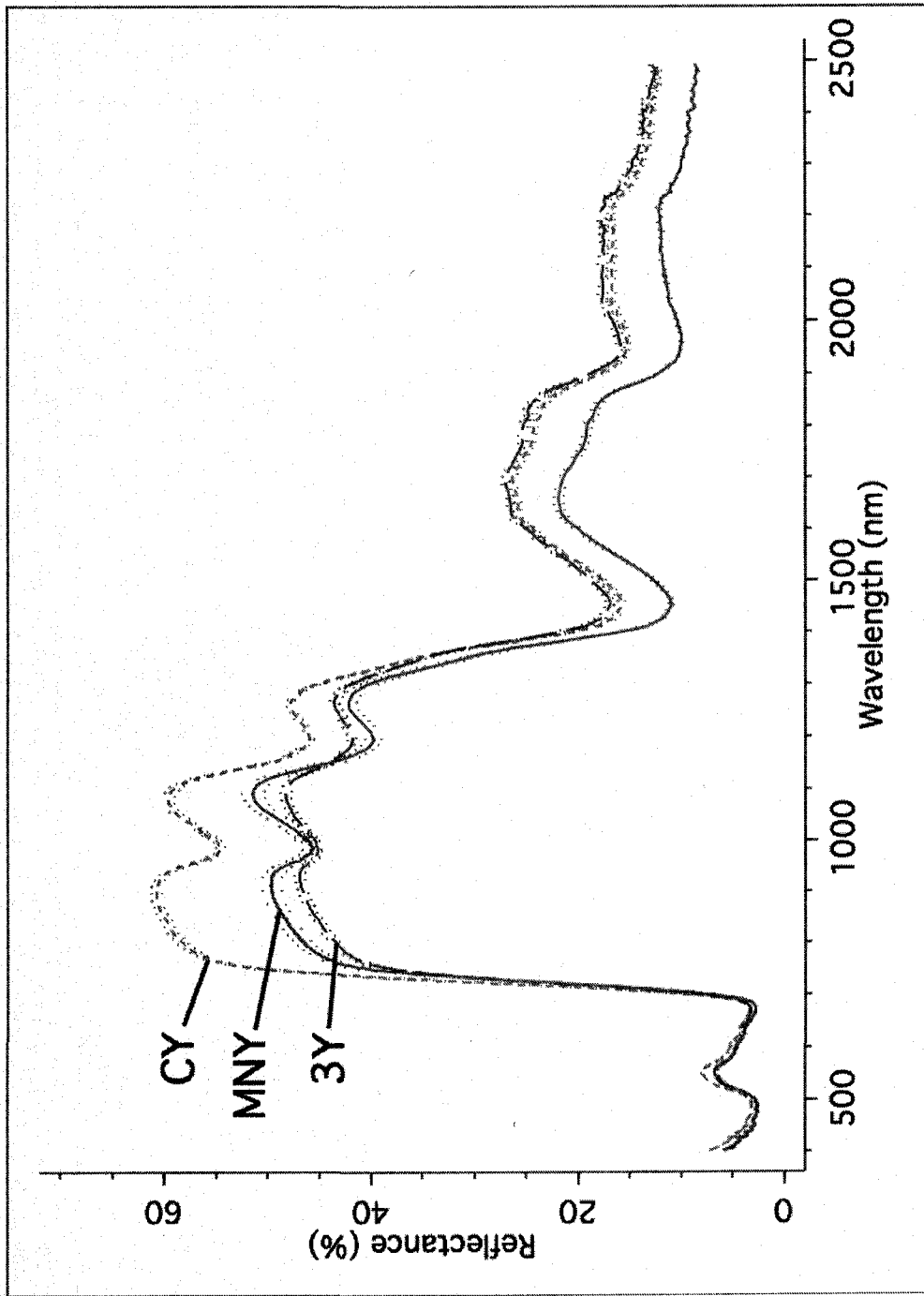


Figure 8. Mean (n = 36) reflectance across watershed, for current-year (CY), third-year (3Y), and mixed-year (MNY) samples scanned with the GER 2600. Finely dotted lines show +/- standard error of measurement for each age class.

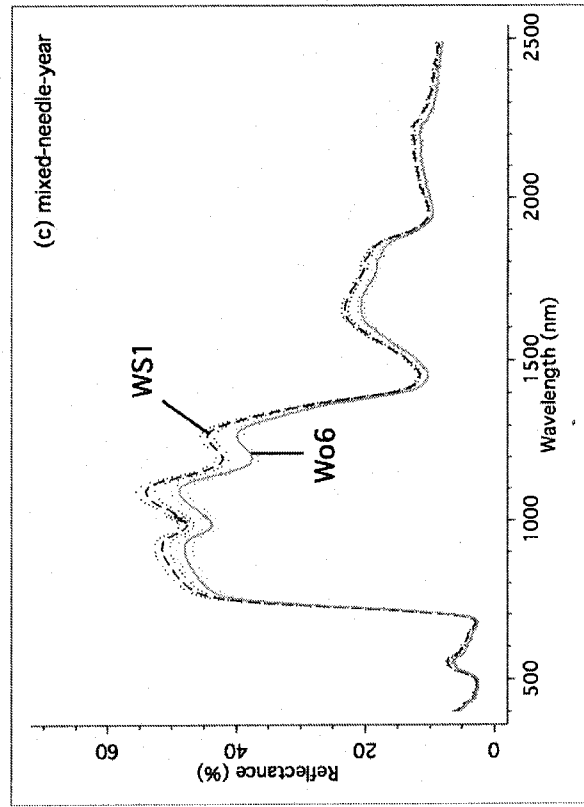
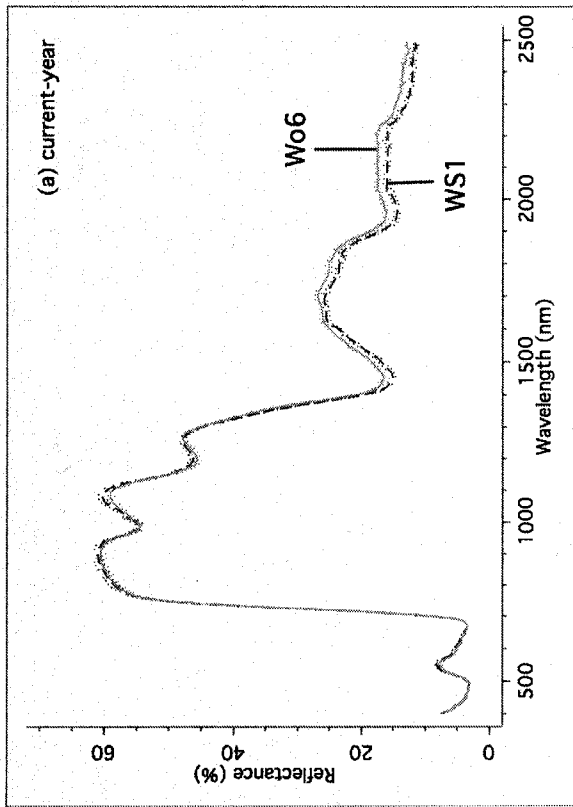
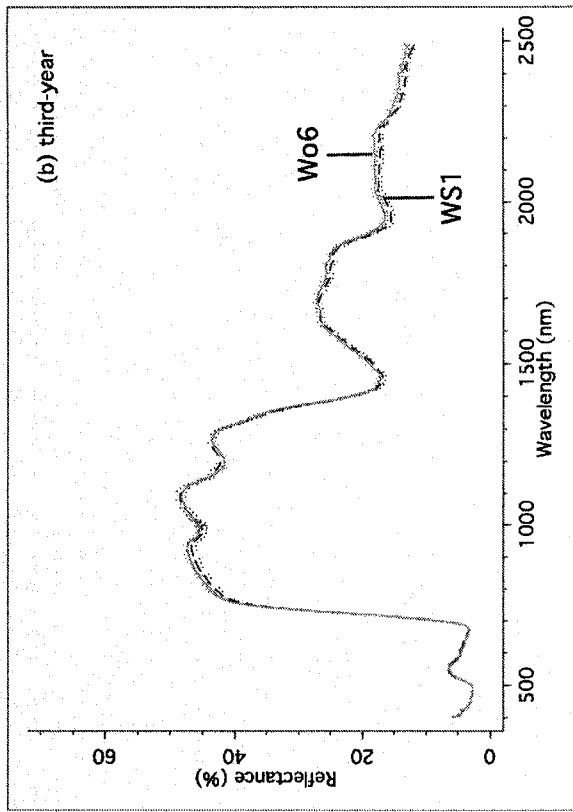


Figure 9. Mean ( $n = 18$ ) reflectance curves for Ca-treated (WS1) and reference (Wo6) needles in (a) current-year (b) third-year and (c) mixed-needle-year samples. Finely dotted lines show  $\pm$  standard error of measurement for each age class.

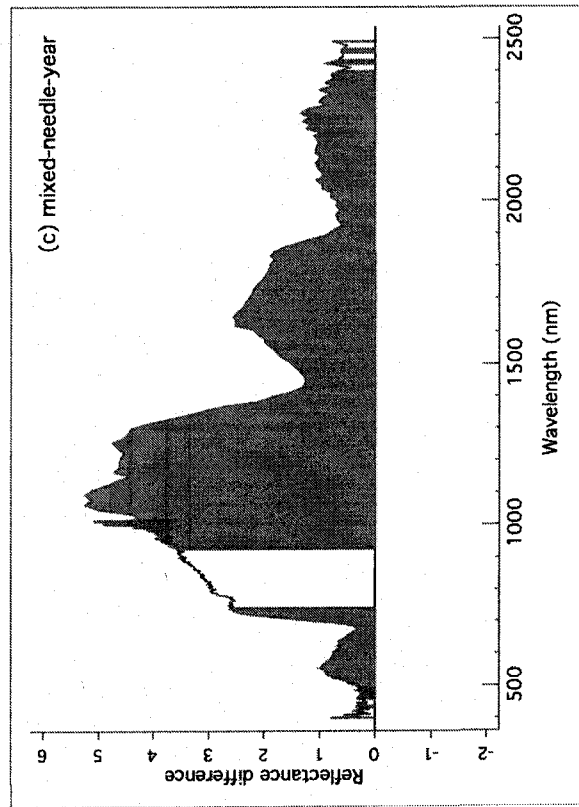
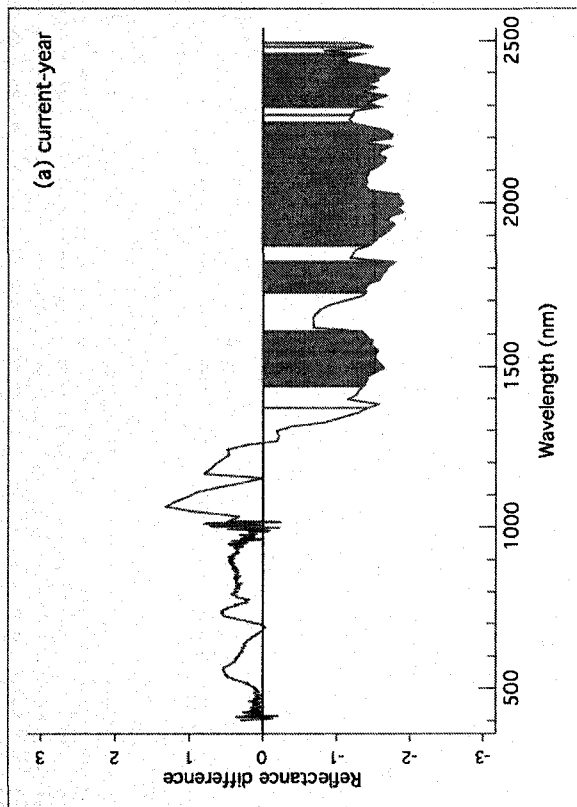
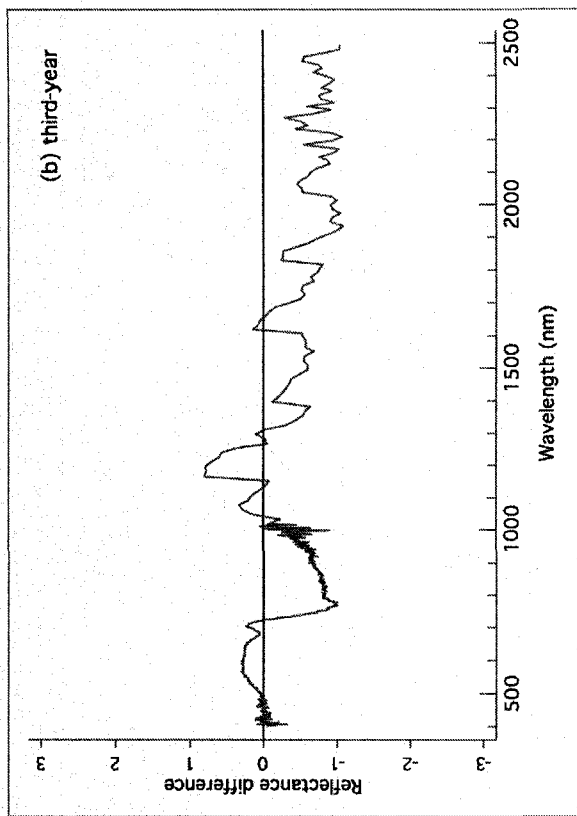


Figure 10. Reflectance curves, showing the difference in reflectance between reference and Ca-amended needles for (a) current-year (b) third-year and (c) mixed-needle-year samples. Shaded areas of the spectrum indicate significant differences ( $P < 0.05$ ) between treatments.

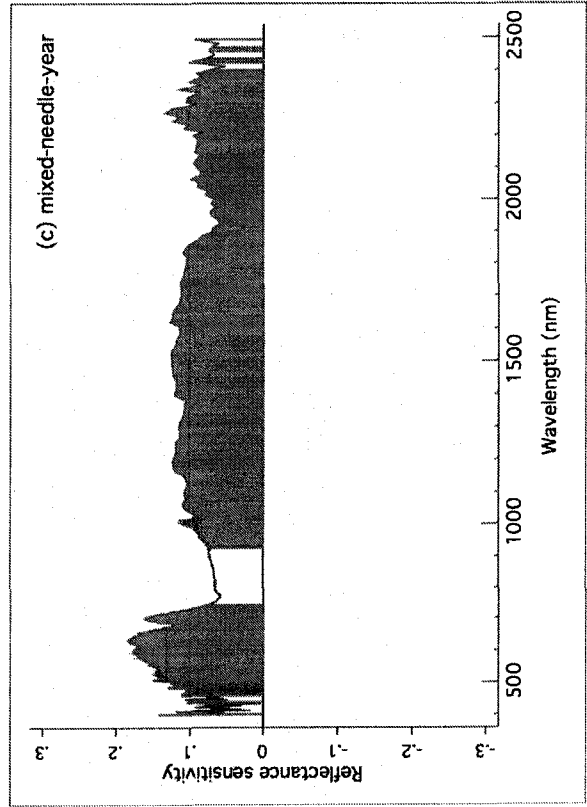
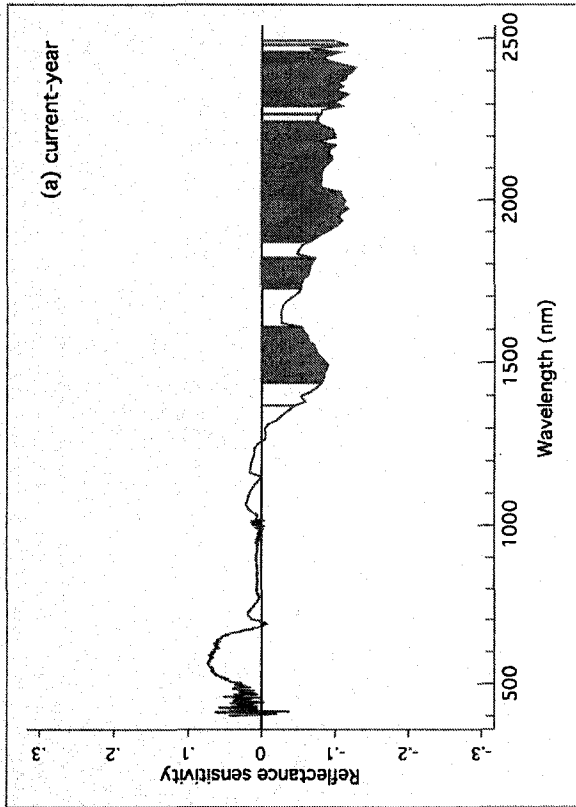
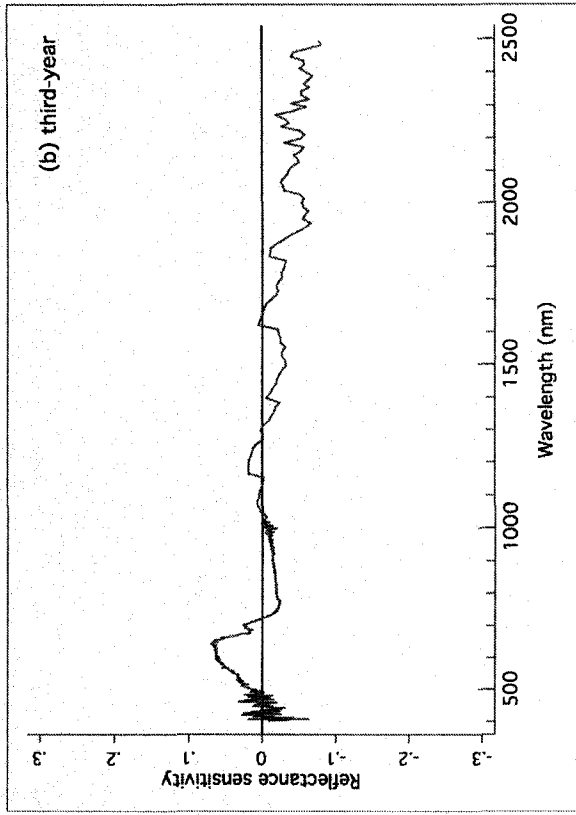


Figure 11. Reflectance sensitivity curves showing the strength of differences between Ca-amended and reference needles, as a fraction of reference reflectance at each wavelength, for (a) current-year (b) third-year (c) mixed-needle-year samples. Shaded areas of the spectrum indicate significant differences ( $P < 0.05$ ) between treatments.

## CHAPTER III

### **Measurement of stand spectral responses following calcium application to a small forested watershed using Landsat TM imagery.**

**Abstract.** Imagery collected from the Landsat satellites was evaluated over an 8-year period preceding and following the 1999 application of 1.2 metric tons Ca ha<sup>-1</sup> to watershed 1 at the Hubbard Brook Experimental Forest. Landsat data were selected from August/September near-anniversary dates in 1999, 2001, 2005, and 2007, and normalized to the 1999 base image to conduct a before-after-control-impact assessment of the spectral effects of Ca re-fertilization of a forest ecosystem. In spruce-fir stands, reflectance properties in the visible bands 1 and 3, as well as the infrared band 7 appear significantly decreased over 8 years relative to the reference area. This is suggestive of increasing contributions of non-photosynthetic and reflective material to the overall stand spectrum, e.g. soil, rock, and woody debris, and corresponds to a period of declining stand density in the reference area. The sustained increase we observed in the near-infrared band 4 in the Ca-amended watershed does not conform to this stand thinning hypothesis, and is probably related to changes in conifer physiology. Increased near-infrared reflectance has been tied to the accumulation of excess Ca as birefringent Ca-oxalate crystals in both red spruce (*Picea rubens* Sarg.) and balsam fir (*Abies balsamea* L.) in these stands, and this may explain the increased band 4 signal despite a canopy which has a relatively lower ground reflectance component. A ratio of Landsat band 4 to band 7 (TM4/7) could help determine areas of increased Ca supply in coniferous forests by normalizing near-infrared reflectance increases for changes in canopy/ground cover.



Deciduous pixel changes are also presented for reference and Ca-treated watersheds.

## **Introduction**

Forest systems are valued for their diversity, forest products, carbon storage capacity, stability, and regenerative potential. Understanding forests in the context of nutrient cycles and constraints is necessary for their management and maintenance. Across areas of eastern North America and Europe these systems may be particularly sensitive to availability of calcium (Ca), due to its role as a macronutrient, along with recent trends in soil acidification and base cation depletion (Federer et al., 1989; Likens et al., 1996; Krám et al., 1997; Driscoll et al., 2001; Jandl et al., 2004). There has been considerable effort to quantify fluxes of Ca in forest ecosystems at the landscape level, even as concurrent studies focus on the specific mechanisms of Ca physiology in individual trees and tissues (Likens et al., 1998; Bailey et al., 2003; Borer et al., 2005; Halman et al., 2008).

Although Ca is a required plant nutrient, influential to forest ecosystem processes (McLaughlin and Wimmer, 1999; Horsley et al., 2002; Juice et al., 2006), its biogeochemistry amid various perturbations is complex and in some cases poorly understood at large spatial and temporal scales (Lawrence et al., 1997; Yanai et al., 1999; Bullen and Bailey, 2005). The twentieth century's legacy of acid precipitation has been identified as the primary cause of Ca deficiency in northeastern forests (Driscoll et al., 2001). In forests, the belowground pool of available Ca is adsorbed to negatively charged soil exchange sites. Low pH water delivers hydrogen ions ( $H^+$ ) that displace exchangeable calcium ( $Ca^{2+}$ ) from the soil matrix, and results in Ca leaching losses

(Federer et al., 1989). Increased Al mobility is another effect of low pH soils that hinders fine root nutrient uptake, and may be directly toxic to trees (Shortle and Smith, 1988; Delhaize and Ryan, 1995).

In research at the Hubbard Brook Experimental Forest (HBEF), Likens et al. (1998) estimated that from 1940-1995 the exchangeable soil Ca pool of a typical Northern Hardwood Forest system diminished by roughly 70 percent. Studies have cited Ca leaching, either from soils or directly from foliage as a threat to northeastern coniferous forests involving Al toxicity (Shortle and Smith, 1988; Borer et al., 2004), cold tolerance (Halman et al., 2008), photosynthetic efficiency (Borer et al., 2005; Boyce, 2007), mechanical stresses (McLaughlin and Wimmer, 1999), or a combination of these and other factors (DeHayes et al., 1999; Schaberg et al., 2001).

A recent large-scale fertilization has been designed to experimentally study Ca processes in a small ecosystem. In October of 1999, wollastonite ( $\text{CaSiO}_3$ ) was added to an entire watershed (WS1) at HBEF in order to mitigate soil Ca to approximately pre acid rain levels, and facilitate direct comparison with adjacent stands (WS6) of ambient soil Ca levels (Peters et al., 2004). Effects measured in fertilized stands thus far include an increase in sugar maple (*Acer saccharum* Marsh.) crown vigor and understory regeneration (Juice et al., 2006), and decreased freezing damage in red spruce (*Picea rubens* Sarg.) at higher elevations (Hawley et al., 2006). Measurements of foliar Ca begun in 1999 have shown immediate and lasting increases of total foliar Ca levels in the treated watershed spruce ( $P < 0.01$ ; Chapter I) and fir (Hubbard Brook Ecosystem Study, 2008a) following a pattern of correlation between soil and foliar Ca pools (McNulty et al., 1991; Littke and Zabowski, 2007).

High spectral resolution laboratory measurements of red spruce foliage in the Ca-treated and an adjacent reference watershed from HBEF have shown a significant Ca-treatment effect (Chapter II). In laboratory measurements of mixed-needle samples from WS1, there was increased reflectance in broad portions of the spectrum from 400-2500 nm, and significantly ( $P < 0.10$ ) higher reflectance in all six Landsat band regions. Laboratory spectra have proven useful in evaluating the potential for remote sensing of foliar chemistry and soil nutrients (Peterson et al., 1988; Curran et al., 1992; Mutanga et al., 2005), and constructing forest canopy and soil nutrient models at large spatial scales (Martin and Aber, 1997; Ollinger et al., 2002; Ollinger and Smith; 2005). The present study is an initial evaluation of Landsat data collected from four dates: one pre-treatment, and three post-treatment (Table 9), in order to explore the utility of multispectral data in the identification of a spruce-fir stand of elevated Ca supply. We anticipate the multispectral reflectance response of a Ca-amended ~2.5 ha spruce-fir stand will parallel the laboratory hyperspectral response of broadly increasing foliar reflectance measured directly in red spruce.

## **Methods**

### *Site description and experimental background*

Work was conducted at the Hubbard Brook Experimental Forest (HBEF), located in West Thornton, in the White Mountain region of New Hampshire (43 ° 56' N, 71 ° 45' W; Figures 12 and 13). The HBEF is part of the Long-Term Ecological Research (LTER) network and has been extensively characterized in its climate, hydrology, geology, soils, and biota (Likens and Bormann, 1995). Prevalent tree species in this Northern Hardwood

community include American beech (*Fagus grandifolia* Ehrh.), yellow birch (*Betula alleghaniensis* Michx.) and sugar maple (*Acer saccharum* Marsh.) at elevations below ~700 m, with red spruce (*Picea rubens* Sarg.), balsam fir (*Abies balsamea* L.), and paper birch (*Betula papyrifera* Marsh.) more common at higher elevations, and on north-facing slopes. Bedrock at the HBEF is granitic (schists, quartzites), with well-drained, nutrient-poor Spodosol soils (typic Haplorthods) forming from a glacial till substrate (Barton et al., 1997; Bohlen et al., 2001).

The forest receives approximately 140 cm of precipitation annually, with deep winter snowpacks contributing about 30 cm of this (Juice et al., 2006). Average summer temperatures are 19 °C (July), while winters (January) average -9 °C (Bohlen et al., 2001). A Ca-poor parent material and moist climate result in poorly buffered soils (pH commonly < 4.5) with low available soil nutrient content below thick organic horizons (Fisk et al., 2006). A detailed summary of the Ca biogeochemical processes and pools at HBEF is available (Likens et al., 1998), and is supported by extensive online resources (Hubbard Brook Ecosystem Study, 2008b).

Experimental manipulations of entire watersheds at Hubbard Brook have focused on ecosystem processes such as hydrologic export, nutrient cycling and storage, and response to timber harvest techniques (Johnson, 1995; Likens et al., 1996; 1998). The most recent manipulation is the wollastonite ( $\text{CaSiO}_3$ ) amendment of an 11.8-ha watershed (WS1) in October of 1999. The application rate of 0.12 kg Ca m<sup>-2</sup> was chosen in order to replenish soil pools of the Ca estimated to have been removed by acidic precipitation over the previous 50 years (Hawley et al., 2006). The soluble mineral wollastonite form was distributed by helicopter after leaf drop, on 19 and 21 October

1999 (Peters et al., 2004). A single watershed (WS6) has remained un-manipulated throughout the HBEF study, functioning as a biogeochemical reference watershed, about 1 km to the west of the Ca-treated watershed. Distinct from WS6 is the adjacent "west of six" (Wo6) area, which is of similar aspect, elevation, and composition; used for destructive foliar sampling in this study.

#### *Plot selection and foliar chemistry*

Six cluster plots of three canopy-dominant or co-dominant spruce trees in each watershed were selected (total  $n = 36$ ). Selection was random, but an effort was made to choose individuals of visually healthy appearance from within a continuous stand of predominantly spruce and fir composition along the valley ridge (see aerial photo, Figure 14; ground photo, Figure 15). A differential global positioning system (Pathfinder GPS, Trimble Inc.\*, Sunnyvale, CA) was used to record the locations of trees. Base station data for differential correction was acquired from a New Hampshire Department of Transportation receiver, located in Concord, NH (about 85 km from HBEF). Single trees were initially chosen to anchor each plot, and GPS coordinates and Landsat imagery were then used to co-locate two additional trees within the same 28.5 m pixels (see below, section "Landsat imagery processing"). A more detailed biometric description of plots, including DBH, height, live-crown ratio, and needle retention is provided in a separate study (Chapter I).

On 13 and 14 August 2007, needles were sampled from WS1 and Wo6 following methods described separately (Chapter I). Chemical analyses of Ca, magnesium, strontium, aluminum, iron, manganese, phosphorus, potassium, and oxalic acid were

---

\* Use of brand names is for clarity and does not imply endorsement.

done on needles from each sample (Chapter I).

### *Laboratory spectra*

All foliar samples were scanned using a GER 2600 portable laboratory spectroradiometer (Geophysical Environmental Research Corp.\* , Millbrook, NY) to provide comparative hyperspectral characterization of spruce needles from within WS1 and Wo6 areas.

Spectra were produced at a bandwidth sampling resolution of 1.5-nm in the visible and near-infrared regions (400-1020 nm), and 15-nm resolution in longer infrared (1020-2580 nm). Landsat band 1-5 and 7 reflectance was simulated for comparison with multispectral data. Complete methodology and discussion of laboratory spectra from the two watersheds are presented in a separate paper (Chapter II).

### *Landsat imagery processing*

Image selection. Landsat 7 images collected after 31 May 2003 are problematic due to a scan-line corrector error that affects the outer regions of each scene, where the Hubbard Brook valley is located. We selected Landsat 5 Thematic Mapper (TM) and pre-2003 Landsat 7 Enhanced Thematic Mapper (ETM+) scenes of 28.5 m spatial resolution for 4 approximate anniversary dates over north-central New England (Table 9, Figure 12). Late August was identified as the ideal period for imagery acquisition, since at this time, spruce have completed the rapid physiological allocation of nutrients to produce new needle biomass, and we would expect low spectral variation due to phenology. However, the selection was limited by availability of cloud-free data from the 16-day Landsat repeat-capture cycle, and we considered an acceptable window extending from the

---

\* Use of brand names is for clarity and does not imply endorsement.

completion of new needle flush in late July, to the onset of autumn senescence and decreased photosynthetic rates in October (Fowells, 1965). Landsat 5 imagery was determined to be of acceptable quality, despite a minor striping anomaly in bands 1-3 caused by inter-detector (within-scan) variability. Visible striping of these bands was found to have an average difference of 1 digital number, or about 0.2 % reflectance, within the study area of HBEF. All image processing was done using ERDAS Imagine 9 (ERDAS Inc.\* , Norcross, GA).

Registration and rectification. The earliest Landsat pre-treatment scene (1999) was selected as the base image for geometric rectification. The image was initially evaluated to determine the extent of geometric rectification necessary using a USGS Digital ortho-quadrangle (DOQ) aerial photograph of Woodstock, NH, acquired in the spring of 1993 (Figure 14). Four ground control points were collected with Trimble GPS Pathfinder equipment at corners of a rain gauge clearing in the Wo6 area, then compared to corner points of the rain gauge clearing visible on the DOQ (Figure 16). Visual inspection (ERDAS Imagine, image-swipe tool) showed that the close spatial agreement of these four local ground control points with the aerial photograph was consistent throughout the DOQ region and allowed the DOQ to serve as a local reference image.

The 1999 Landsat and DOQ images were co-registered in a single projection plane, and spatial registration error was determined using a series of 15 ground control points collected both from within HBEF and throughout the scene with GPS. The root-mean-square registration error was 13.5 m (about 0.5 pixel) over the entire scene, and 11.4 m (about 0.35 pixel) for the subset of four points in the Hubbard Brook study area. The three subsequent Landsat scenes were referenced to the base image in order to

---

\* Use of brand names is for clarity and does not imply endorsement.

compose a four-date multi-image. No geometric rectification was done for either of the 1999 or 2001 images. Data from 2005 and 2007 were rectified using first-order polynomial transformations, and all scenes were inspected to ensure alignment of visible features.

Instrument cross-calibration. Data collected from the ETM+ and TM sensors are not suited for direct comparison, due to differences in radiometric response (Teillet et al., 2001). In order to allow comparison of spectral information across dates of the multi-image, we performed a linear cross-calibration of Landsat 5 TM radiometric response data (digital numbers) to the equivalent Landsat 7 ETM+ data following Vogelmann et al. (2001).

Radiometric correction. All data were radiometrically corrected to convert raw instrument response (digital number) to percent reflectance (Landsat 7 Science Data Users Handbook, 2006). The spectral effects of atmospheric scattering and absorbance were then corrected using a dark-object subtraction, whereby very dark features (such as lakes) from within the scene are taken as non-reflective. The corresponding minimum scene-wide reflectance values can then be subtracted from each pixel in a scaling computation (Song et al., 2001; Paolini et al., 2006).

Image normalization. In order to allow direct inter-annual comparison of spectral response, relative radiometric correction was done using features visually selected from Landsat imagery. A total of 17 features representing a wide range of reflectance were selected, including: 5 lakes, 4 exposed talus/scree fields, 4 upland deciduous stands, and 4 lowland coniferous stands. For the 1999-2001 image pair, only 12 of these normalization targets were available due to cloud cover. In each band, a linear



relationship was established between reflectance for three image pairs: 1999-2001, 1999-2005, and 1999-2007 ( $R^2$  values presented in Table 10). Relative correction following Hall et al. (1991) produced reflectance data from 2001, 2005, and 2007, normalized to the spectral response of the base image.

Pixel extraction. Watershed boundary maps were acquired from the Hubbard Brook online repository (Hubbard Brook Ecosystem Study, 2008c), and rectified using GPS ground control data. In each watershed, two zones were delineated corresponding to coniferous and deciduous canopy using aerial photography (DOQ), which was acquired prior to spring leaf-out. A pixelated area of interest was visually selected from each zone in both WS1 and Wo6/WS6 (hereafter referred to simply as WS6 in discussion of Landsat data), and included coniferous plot pixels established in ground sampling (see Figures 14 and 17). A total of 65 pixels were used in the coniferous comparison, and 321 pixels in the deciduous, representing areas of 5.3 and 26 ha, respectively.

#### *Statistical analysis.*

All analyses were performed on unsmoothed reflectance data, using the Stata 10 data analysis software package (StataCorp\*, College Station, TX). Laboratory chemistry and laboratory hyperspectral measurements were analyzed for significant differences with the Student's t-test, nested within needle age class. A two-way factorial ANOVA was performed to assess the relationship between Landsat pixel reflectance data and year, treatment, and interactive effects of treatment by year.

## **Results**

---

\* Use of brand names is for clarity and does not imply endorsement.

### *Laboratory measurements*

Data showing the increased foliar Ca, Sr, and oxalate content of trees in WS1, along with strong correlation between Ca and oxalate, are presented in a preceding paper (Chapter I). Hyperspectral measurements of mixed-needle-year samples indicated the needles from Ca-treated sites had a significantly higher ( $P < 0.05$ ) percent reflectance in most areas of the spectrum including the visible and far-red (400-739 nm), and near and short-wave infrared (928-2500 nm), but excluding the near infrared region from 740-927 nm (Figure 18). The simulated Landsat band reflectance was significantly higher ( $P < 0.10$ ) in WS1 samples for all band regions 1-5 and 7 (Figure 18). A complete treatment of these hyperspectral results is presented (Chapter II), including a full range of vegetation stress indices.

### *Image differencing and inter-annual comparison*

A normalized Landsat data comparison between watersheds showed significant trends of treated WS1 reflectance compared to WS6 for both coniferous and deciduous pixels (Figures 19 and 20, respectively). Factorial ANOVAs showed a significant ( $P < 0.05$ ) treatment by year effect in four of six bands in both coniferous and deciduous data (Tables 11 and 12, respectively). Notable trends in the Ca-treated pixels include: sustained increase of infrared (Figure 19, band 4) reflectance in conifers, and a diminished visible reflectance in WS1 compared to WS6 in both deciduous and conifers (Figures 19 and 20, bands 1-3). In coniferous pixels, the reference area had lower band 3 reflectance than the Ca-treated in 1999, whereas the most recent data (2005 and 2007) show this pattern has reversed, with higher band 3 reflectance in the reference watershed.

A summary of net change in percent reflectance from 1999 to 2007, the two dates nearest an eight-year anniversary, is also presented (Tables 11 and 12). Data from pre- and post-treatment indicate that reflectance of coniferous pixels decreased significantly in band 1, band 3, and band 7, while that of band 4 increased. Deciduous Ca-treated pixels show a trend of decreasing reflectance in each of bands 1-3, and 7, compared to the reference data.

The multispectral moisture stress index of Landsat bands 5 and 4 (TM5/4) showed consistent and significant decreases in the coniferous pixels between 1999 and 2007 (Table 13). Calcium-treatment by year effects on the ratio in deciduous zones were also significant ( $P = 0.002$ ). Overall trends of decreased TM5/4 between 1999 and 2007 were seen in Ca-amended deciduous zones, however, the magnitude of the decrease was much less than coniferous zones, and similar in reference and Ca-amended watersheds (Table 14). The normalized difference vegetation index (NDVI) increased in WS1 coniferous pixels compared to little change between 1999 and 2007 in WS6 pixels. Inter-annual differences (2007-1999) in deciduous NDVI values were also comparable between the two watersheds (Table 14), although ANOVA indicates there was a significant year by treatment effect.

## **Discussion**

The Ca application at Hubbard Brook allows the direct comparison of multispectral data gathered from a stand characterized by recharged soil Ca (WS1), and one with base-poor soil conditions (WS6) typical of the White Mountain region. The two watersheds have the same aspect and elevation, and the close proximity eliminates atmospheric variables.

Geometrically rectified, co-registered data spanning eight years were normalized to a single pre-treatment base image in 1999, and showed comparable reflectance values from year to year. The impacts of disturbance, e.g. the New England ice storm of February 1998 (Boyce et al., 2003), and unattributed species decline, e.g. increasing mortality of paper birch (Battles JJ, unpub. data; Rock BN, personal observation), are thus taken to be approximately equal in stands of both WS1 and WS6. This discussion focuses primarily on data from coniferous stands, which may be related to previous work on red spruce needle chemistry and hyperspectral characteristics following the Ca addition (Chapter I; II).

#### *Stand spectral effects*

Previous work at HBEF has shown the effects of Ca application in enhanced vigor of three tree species: sugar maple (Juice et al., 2006; Huggett et al., 2007), balsam fir (Boyce, 2007), and red spruce (Hawley et al., 2006; Boyce, 2007; Halman et al., 2008). Parallel studies have made direct chemical and hyperspectral measurements of red spruce needles and boughs from WS1 and WS6, finding accrual of the applied Ca as extracellular Ca-oxalate in multiple needle years (Chapter I). The sequestration of excess Ca as crystal Ca-oxalate has been hypothesized as the cause of increased reflectance measured across the entire visible and short-wave infrared spectrum of mixed-needle boughs (Figure 18), and the possible cause of spectral index stress response patterns in these needles (Chapter II).

The pan-spectral reflectance increases seen in spruce needles at hyperspectral resolution were not observed in the Landsat satellite data from coniferous pixels. The

significant effects observed in WS1 coniferous and deciduous data from 1999 and 2007 amount to increased near-infrared reflectance, and decreases in the reflectance of visible bands 1, 2 (deciduous only), and 3, and the infrared band 7. Increases in the band 4 signal were strong in the conifer pixels ( $P = 0.01$ ) and marginally significant in the deciduous ( $P = 0.06$ ).

There have been measurements of increased visible/infrared reflectance responses to the Ca addition in both conifer species present on the ridges of HBEF: spruce (Chapter II) and fir (McCarthy PM, unpub. data). The measurement of *in situ* forest spectra via analysis of Landsat TM/ETM+ data, however, must take into account factors independent of the spectral properties of constituent species. These factors include canopy architecture, shading, and contributions of ground reflectance (Williams, 1991). There is also the likelihood of a mixed vegetation signal in spruce-fir stands due to herbaceous ground cover or the encroaching broadleaved species sometimes present at upper elevations in the Hubbard Brook Valley, e.g. paper birch, American beech, or red maple (*Acer rubrum* L.). Surveys done in WS1 and WS6 following the Ca-addition did not show a net effect on the overall herbaceous cover (Siccama TG and Denny EG, unpub. data), therefore, canopy-level effects are probably more important in interpreting these results. Complete forest inventories done at 5-year intervals in the coniferous zones of WS1 (1996-2006) and WS6 (1997-2007) show a roughly 15 % decrease in live deciduous and coniferous stems greater than 10 cm DBH in WS6, compared to constant levels in WS1 (Battles JJ, unpub. data). One effect of a disturbed or broken canopy is greater visible spectral reflectance due to the increased contribution of non-photosynthetic non-absorbent material, i.e. woody debris, standing snags, soil and rocks, to the overall

spectral signal (Colwell, 1974; Entcheva Campbell et al., 2004). A parallel effect occurs with the increased signals in the infrared bands 4, 5, and 7 due to the exposure of increased level ground (Figure 13), and work by Baret et al. (1995) has shown positive correlation between canopy gaps and infrared reflectance. We hypothesize that trends of higher reflectance in the pigment associated visible bands 1, 2, and 3, as well as the infrared band 7 followed from the decline of some species in the coniferous zone of the reference watershed, particularly paper birch. Future Landsat work could include a spectral un-mixing analysis to ascertain the spectral contribution of different vegetation and soil components.

#### *Near-infrared reflectance increases*

The increased near-infrared reflectance seen in WS1 conifers, compared to the relatively stable reflectance of WS6 conifers, suggests effects of other canopy processes besides the opening of gaps in WS6. Level ground features are highly reflective in the infrared portion of the spectrum, and we would anticipate increased band 4 reflectance as the spruce-fir WS6 canopy is thinning, rather than the opposite trend observed.

A previous study of the laboratory spectral effects of the WS1 Ca-amendment in fresh red spruce foliage (Chapter II) offers two pieces of evidence that may tie the infrared signal to Ca physiology in spruce at HBEF. First, the infrared region of band 4 (760-900 nm) is a region of high variation (s.d. > 7 % reflectance) in laboratory scans, but nonetheless showed a marginally significant ( $P = 0.08$ ) positive response to the Ca-treatment. The same study also found that in mixed needle year samples, foliar oxalate positively correlated more strongly with band 4 than with any other simulated Landsat

band. Direct observation by Gausman (1977) has shown the highly reflective properties of an extracellular crystal deposit in *Zebrina pendula* in the near-infrared (850 nm), and this plant has been identified as producing Ca-oxalate crystals (Loetsch and Kinzel, 1971). The tendency of both spruce and fir at Hubbard Brook to form extensive amounts of cell wall Ca-oxalate crystal deposits (Chapter I; McCarthy PM, pers. obs.), along with trends of improving red spruce vigor (Hawley et al., 2006; Halman et al., 2008), and overall conifer density (Battles JJ, pers. comm.) suggest there is an infrared-reflecting evergreen component responsible for the observed response in band 4 data, possibly Ca-oxalate.

In addition, Halman et al. (2008) have measured greater sugar and antioxidant concentrations in WS1 spruce needles. Boyce (2007) has measured greater maximum leaf fluorescence in WS1, which relates to the down-regulation of photosynthesis (fluorescence quenching) over winters (Krause and Weis, 1991; Adams and Demming-Adams, 1994) and is indicative of higher photosynthetic efficiency. The benefit of Ca to physiological processes such as inter-cellular signal transduction (Borer et al., 2005), cold-adaptive down-regulation of photosynthesis (Halman et al., 2008), wound repair and recovery, and wood structural integrity (McLaughlin and Wimmer, 1999) could have led to a higher biomass increment in these trees, and subsequent increases in the band 4 infrared signal in the years following the Ca treatment. A previous study (Chapter I) did not find evidence of radial growth effects in the spruce of WS1 compared to Wo6.

#### *Indications of stress*

An increase in stand normalized difference vegetation index (NDVI) seen at the

coniferous pixel level, along with decreasing moisture stress signal (TM5/4) from 1999 to 2007 suggests improved health at the stand level following the Ca amendment. The Landsat Thematic mapper 5/4 band ratio has been employed in past studies, showing positive correlations with crown-level insect damage (Vogelmann and Rock, 1989) and forest damage (Rock et al., 1986; Vogelmann and Rock, 1988), and NDVI is one measure of green plant biomass signal (Rouse et al., 1973). These effects were not measured in hyperspectral data collected in the laboratory, and there may be a complex factors at work *in situ* giving the WS1 stands a comparative advantage in cold tolerance, photosynthetic efficiency, and regulation of physiological processes (Hawley et al., 2006; Boyce, 2007; Halman et al., 2008).

Coniferous Landsat pixels from WS1 also showed a relatively constant red-absorption characteristic in band 3 across the eight years analyzed, compared to that of WS6, which sharply increased between 2001 and 2005 implying a decrease in chlorophyll at the pixel level. In 1999, WS1 had the higher band 3 value of the two watersheds, while in 2007 WS6 had increased and surpassed it. Studies at HBEF have documented the connection between Ca and resistance to winter-injury, where current-year needles experience cold stress, become reddened and desiccated, and eventually die (Hawley et al., 2006). The winter of 2002-2003 was a year of particularly high winter injury (Lazarus et al., 2006), and could be implicated in our observation of a roughly 14 % increase in WS6 red reflectance during the 4-year period from 2001 to 2005, while red reflectance remained unchanged in WS1.



## Summary

The Ca fertilization of 1999 has had significant effects on the satellite-measured reflectance properties of the conifer and deciduous stands of watershed 1 at Hubbard Brook. Hyperspectral effects measured in laboratory work on red spruce were not seen in Landsat spectral data, with the exception of the near-infrared region (band 4) related to plant structural reflectance and refraction. In this region, Ca-treated pixels showed a sustained increase in reflectance from 1999 to 2007 that was comparable in magnitude to increases measured in fresh needle samples in the laboratory. Measurements linking needle infrared reflectance to bound oxalate crystal content in spruce suggest this is the result of increased foliar scattering-reflectance properties in the near-infrared. The decreased reflectance in WS1 conifer pixels' visible bands 1 and 3, relative to that of WS6, may be due to changes in chlorophyll levels due to a measured decrease in stand density in the reference area, compared to a Ca-treated stand that was increasingly coniferous and of constant density. We suggest the Landsat infrared bands 4 and 7 (TM4/TM7) as a potential Ca response ratio to measure changing Ca supply in coniferous forests, while normalizing for changes in canopy/ground cover.

## Literature cited

- Adams WW and Demmig-Adams B (1994) Carotenoid composition and down regulation of photosystem II in three conifer species during the winter. *Physiologia Plantarum* 92: 451-458.
- Bailey SW, Buso DC, Likens GE (2003) Implications of sodium mass balance for interpreting the calcium cycle of a forested ecosystem. *Ecology* 84: 471-484.
- Baret F, Clevers JGPW, Steven MD (1995) The robustness of canopy gap fraction estimates from red and near-infrared reflectances: a comparison of approaches. *Remote Sensing of Environment* 54: 141-151.
- Barton CC, Camerlo RH, Bailey SW (1997) Bedrock geologic map of the Hubbard Brook Experimental Forest and maps of fractures and geology in roadcuts along interstate 93, Grafton County, New Hampshire, Sheet 1, Scale 1:12,000; Sheet 2, Scale 1:200: U.S. Geological Survey Miscellaneous Investigations Series Map I-2562.
- Bohlen PJ, Groffman PM, Driscoll CT, Fahey TJ, Siccama TG (2001) Plant-soil-microbial interactions in a northern hardwood forest. *Ecology*, 82: 965-978.
- Borer CH, Schaberg PG, DeHayes DH, Hawley GJ (2004) Accretion, partitioning, and sequestration of calcium and aluminum in red spruce foliage: implications for tree health. *Tree Physiology* 24: 929-939.
- Borer CH, Schaberg PG, DeHayes DH (2005) Acidic mist reduces foliar membrane-associated calcium and impairs stomatal responsiveness in red spruce. *Tree Physiology* 25: 673-680.
- Boyce RL, Friedland AJ, Vostral CB, Perkins TD (2003) Effects of a major ice storm on four New England conifers. *Ecoscience* 10: 342-350.
- Boyce RL (2007) Chlorophyll fluorescence response of red spruce and balsam fir to a watershed calcium fertilization experiment in New Hampshire. *Canadian Journal of Forest Research* 37: 1518-1522.
- Bullen TD and Bailey SW (2005) Identifying calcium sources at an acid deposition-impacted spruce forest: a strontium isotope, alkaline earth element multi-tracer approach. *Biogeochemistry* 74: 63-99.
- Colwell (1974) Vegetation canopy reflectance. *Remote Sensing of Environment* 3: 175-183.
- Curran PJ, Dungan JL, Macler BA, Plummer SE, Peterson DL (1992) Reflectance spectroscopy of fresh whole leaves for the estimation of chemical concentration.

Remote Sensing of Environment 39: 153-166.

DeHayes DH, Schaberg PG, Hawley GJ, Strimbeck GR (1999) Acid rain impacts on calcium nutrition and forest health. *Bioscience* 49: 789-800.

Delhaize E and Ryan PR (1995) Aluminum toxicity and tolerance in plants. *Plant Physiology* 107: 315-321.

Driscoll CT, Lawrence GB, Bulger AJ, Butler TJ, Cronan CS, Eagar C, Lambert KF, Likens GE, Stoddard JL, Weathers KL (2001) Acidic deposition in the northeastern United States: sources and inputs, ecosystem effects, and management strategies. *Bioscience* 51: 180-198.

Entcheva Campbell PK, Rock BN, Martin ME, Neefus CD, Irons JR, Middletown EM, Albrechtová J (2004) Detection of initial damage in Norway spruce canopies using hyperspectral airborne data. *International Journal of Remote Sensing* 25: 5557-5583.

Federer CA, Hornbeck JW, Tritton LM, Martin CW, Pierce RS, Smith CT (1989) Long-term depletion of calcium and other nutrients in eastern US forests. *Environmental Management* 13: 593-601.

Fisk MC, Kessler WR, Goodale A, Fahey TJ, Groffman PM, Driscoll CT (2006) Landscape variation in microarthropod response to calcium addition in a northern hardwood forest ecosystem. *Pedobiologia* 50: 69-78.

Fowells HA (ed) (1965) *Silvics of forest trees of the United States*. USDA Forest Service, Washington D.C.

Gausman HW (1977) Reflectance of leaf components. *Remote Sensing of Environment* 6: 1-9.

Hall FG, Strebel DE, Nickeson JE, Goetz SJ (1991) Radiometric rectification: toward a common radiometric response among multi-data, multi-sensor images. *Remote Sensing of Environment* 35: 11-27.

Halman JM, Schaberg PG, Hawley GJ, Eagar C (2008) Calcium addition at the Hubbard Brook Experimental Forest increases sugar storage, antioxidant activity and cold tolerance in native red spruce (*Picea rubens*). *Tree Physiology* 28: 855-862.

Hawley GJ, Schaberg PG, Eagar C, Borer CH (2006) Calcium addition at the Hubbard Brook Experimental Forest reduced winter injury to red spruce in a high-injury year. *Canadian Journal of Forest Research* 36: 2544-2549.

Horsley SB, Long RP, Bailey SW, Hallett RA, Wargo PM (2002) Health of eastern North American sugar maple forests and factors affecting decline. *Northern Journal of*

Applied Forestry 19: 34-44.

Hubbard Brook Ecosystem Study (2008a) Watershed 1 and 6 temporal canopy leaf chemistry. <http://www.hubbardbrook.org/data/> Cited 15 September 2006

Hubbard Brook Ecosystem Study (2008b) Hubbard Brook Ecosystem Study. <http://www.hubbardbrook.org/> Cited 20 September 2008

Hubbard Brook Ecosystem Study (2008c) Hubbard Brook GIS coverages. <http://www.hubbardbrook.org/gis/> Cited 5 November 2008

Huggett BA, Schaberg PG, Hawley GJ, Eagar C (2007) Long-term calcium addition increases growth release, wound closure, and health of sugar maple (*Acer saccharum*) trees at the Hubbard Brook Experimental Forest. *Canadian Journal of Forest Research* 37: 1692-1700.

Jandl R, Alewell C, Prietzel J (2004) Calcium loss in Central European forest soils. *Soil Science Society of America Journal* 68: 588-595.

Johnson CE (1995) Soil nitrogen status eight years after whole-tree clear-cutting. *Canadian Journal of Forest Research* 25: 1346-1355.

Juice SM, Fahey TJ, Siccama TG, Driscoll CT, Denny EG, Eagar C, Cleavitt NL, Minocha R, Richardson AD (2006) Response of sugar maple to calcium addition to northern hardwood forest. *Ecology* 87:1267-1280.

Krám P, Hruška J, Wenner BS, Driscoll CT, Johnson CE (1997) The biogeochemistry of basic cations in two forest catchments with contrasting lithology in the Czech Republic. *Biogeochemistry* 37:173-202.

Krause GH and Weis E (1991) Chlorophyll fluorescence and photosynthesis: the basics. *Annual Review of Plant Physiology and Plant Molecular Biology* 42: 313-349.

Landsat 7 Science Data Users Handbook (2006) Chapter 11 - Data Products. [http://landsathandbook.gsfc.nasa.gov/handbook/handbook\\_htmls/chapter11/chapter11.html/](http://landsathandbook.gsfc.nasa.gov/handbook/handbook_htmls/chapter11/chapter11.html/) Cited 31 October 2006

Lawrence GB, David MB, Bailey SW, Shortle WC (1997) Assessment of soil calcium status in red spruce forests in the northeastern United States. *Biogeochemistry* 38: 19-39.

Lazarus BE, Schaberg PG, Hawley GJ, DeHayes DH (2006) Landscape patterns of winter injury to red spruce foliage in a year of heavy region-wide injury. *Canadian Journal of Forest Research* 36: 142-152.

Likens GE and Bormann FH (1995) *Biogeochemistry of a forested ecosystem*, 2nd ed.

Springer-Verlag, New York.

- Likens GE, Driscoll CT, Buso DC (1996) Long-term effects of acid rain: response and recovery of a forest ecosystem. *Science* 272: 244-246.
- Likens GE, Driscoll CT, Buso DC, Siccama TG, Johnson CE, Lovett GM, Fahey TJ, Reiners WA, Ryan DF, Martin CW, Bailey SW (1998) The biogeochemistry of calcium at Hubbard Brook. *Biogeochemistry* 41: 89-173.
- Littke KM and Zabowski D (2007) Influence of calcium fertilization on Douglas-fir foliar nutrition, soil nutrient availability, and sinuosity in coastal Washington. *Forest Ecology and Management* 247: 140-148.
- Loetsch B and Kinzel H (1971) The calcium requirement of oxalate producing plants. *Biochemie und Physiologie der Pflanzen* 162: 209-219.
- Martin ME and Aber JD (1997) High spectral resolution remote sensing of forest canopy lignin, nitrogen, and ecosystem processes. *Ecological Applications* 7: 431-443.
- McLaughlin SB and Wimmer R (1999) Calcium physiology and terrestrial ecosystem processes. *New Phytologist* 142: 373-417.
- McNulty SG, Aber JD, Boone RD (1991) Spatial changes in forest floor and foliar chemistry of spruce-fir forests across New England. *Biogeochemistry* 14: 13-29.
- Mutanga O, Skidmore AK, Kumar L, Ferwerda J (2005) Estimating tropical pasture quality at canopy level using band depth analysis with continuum removal in the visible domain. *International Journal of Remote Sensing* 26:1093-1108.
- Ollinger SV, Smith ML, Martin ME, Hallett RA, Goodale CL, Aber JD (2002) Regional variation in foliar chemistry and N cycling among forests of diverse history and composition. *Ecology* 83: 339-355.
- Ollinger SV and Smith ML (2005) Net primary production and canopy nitrogen in a temperate forest landscape: an analysis using imaging spectroscopy, modeling, and field data. *Ecosystems* 8: 760-778.
- Paolini L, Grings F, Sobrino JA, Jiménez Muñoz JC, Karszenbaum H (2006) Radiometric correction effects in Landsat multi-date/multi-sensor change detection studies. *International Journal of Remote Sensing* 27: 685-704.
- Peters SC, Blum JD, Driscoll CT, Likens GE (2004) Dissolution of wollastonite during the experimental manipulation of Hubbard Brook watershed 1. *Biogeochemistry* 67: 309-329.
- Peterson DL, Aber JD, Matson PA, Card DH, Swanberg N, Wessman C, Spanner M

- (1988) Remote sensing of forest canopy and leaf biochemical contents. *Remote Sensing of Environment* 24: 85-108.
- Rock BN, Vogelmann JE, Williams DL, Vogelmann AF, Hoshizaki T (1986) Remote detection of forest damage. *Bioscience* 36: 439-445.
- Rouse JW, Haas RH, Schell JA, Deening DW (1973) Monitoring vegetation systems in the great plains with ERTS, Third ERTS Symposium, NASA SP-351 I: 309-317.
- Schaberg PG, DeHayes DH, Hawley GJ (2001) Anthropogenic calcium depletion: a unique threat to forest ecosystem health? *Ecosystem Health* 7: 214-228.
- Shortle WC and Smith KT (1988) Aluminum-induced calcium deficiency syndrome in declining red spruce. *Science* 240: 1017-1018.
- Song C, Woodcock CE, Seto KC, Pax-Lenney M, Macomber SA (2001) Classification and change detection using Landsat TM data: when and how to correct atmospheric effects? *Remote Sensing of Environment* 75: 230-244.
- Teillet PM, Barker JL, Markham BL, Irish RR, Fedosejevs G, Storey JC (2001) Radiometric cross-calibration of the Landsat-7 ETM+ and Landsat-5 TM sensors based on tandem data sets. *Remote Sensing of Environment* 78: 39-54.
- Vogelmann JE and Rock BN (1988) Assessing forest damage in high-elevation coniferous forests in Vermont and New Hampshire using Thematic Mapper data. *Remote Sensing of Environment* 24: 227-246.
- Vogelmann JE and Rock BN (1989) Use of thematic mapper data for the detection of forest damage caused by the pear thrips. *Remote Sensing of Environment* 30: 217-225.
- Vogelmann JE, Helder DH, Morfitt R, Choate MJ, Merchant JW, Bulley H (2001) Effects of Landsat 5 Thematic Mapper and Landsat 7 Enhanced Thematic Mapper Plus radiometric and geometric calibrations and corrections on landscape characterization. *Remote Sensing of Environment* 78: 55-70.
- Williams DL (1991) A comparison of spectral reflectance properties at the needle, branch, and canopy level for selected conifer species. *Remote Sensing of Environment* 35:79-93.
- Yanai RD, Siccama TG, Arthur MA, Federer CA, Friedland AJ (1999) Accumulation and depletion of base cations in forest floors in the northeastern United States. *Ecology* 80: 2774-2787.

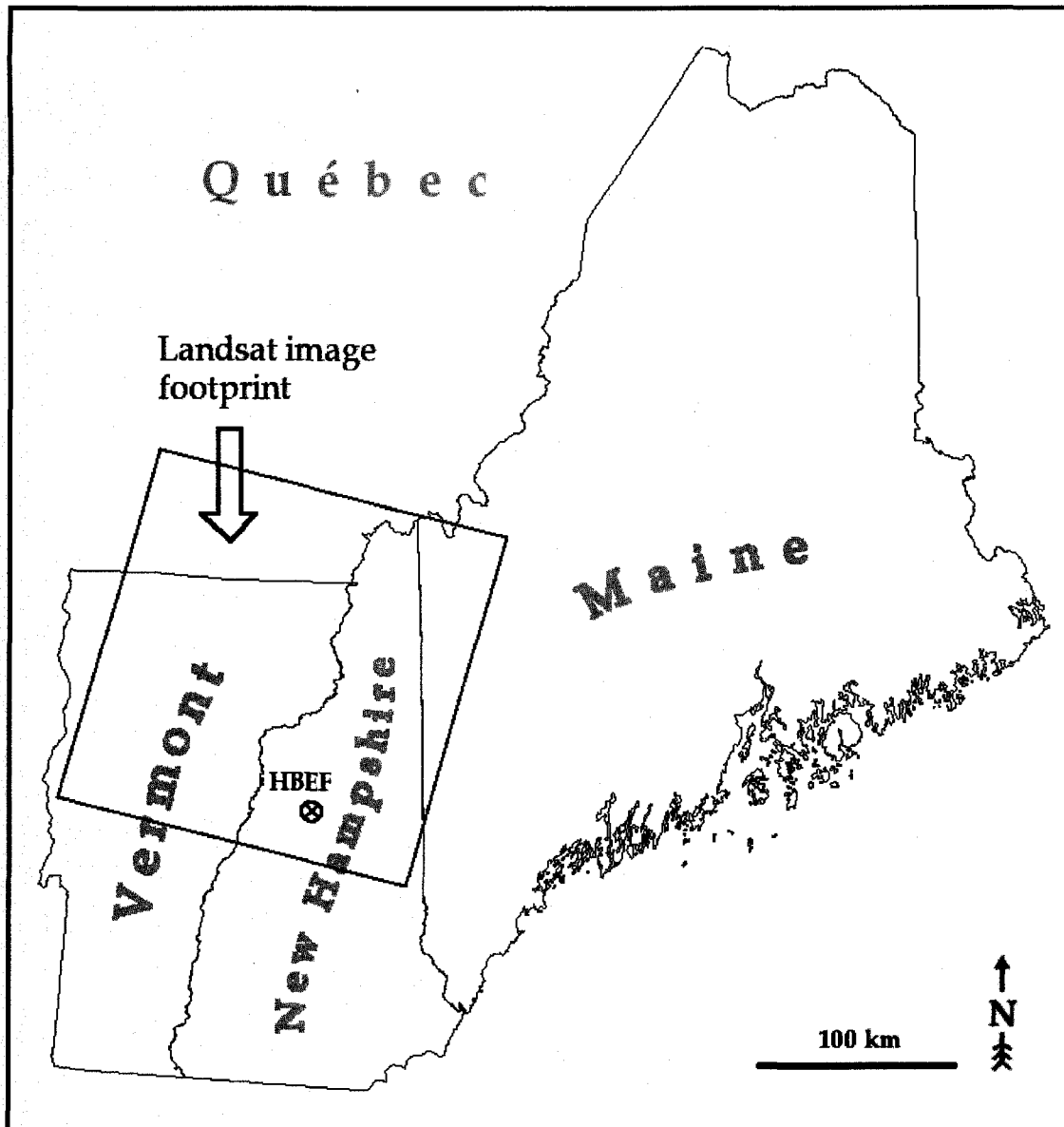


Figure 12. Map showing the location of multispectral data from Landsat 5 and Landsat 7, worldwide reference system (WRS) path 13, row 29. The Hubbard Brook Experimental Forest (HBEF) sits in the southeast corner of the scene.

| Acquisition date  | Time  | Satellite | Sensor | Path / Row | % Cloud cover |
|-------------------|-------|-----------|--------|------------|---------------|
| 31 August 1999    | 15:25 | Landsat 7 | ETM+   | 13 / 29    | 0             |
| 4 August 2001     | 15:21 | Landsat 7 | ETM+   | 13 / 29    | 18            |
| 24 September 2005 | 15:20 | Landsat 5 | TM     | 13 / 29    | 0             |
| 29 August 2007    | 15:25 | Landsat 5 | TM     | 13 / 29    | 1             |

Table 9. List of Landsat scenery used.

| Band | Image pair: | 1999 – 2001 | 1999 – 2005 | 1999 – 2007 |
|------|-------------|-------------|-------------|-------------|
| 1    |             | 0.966       | 0.988       | 0.970       |
| 2    |             | 0.994       | 0.992       | 0.990       |
| 3    |             | 0.998       | 0.982       | 0.995       |
| 4    |             | 0.992       | 0.992       | 0.993       |
| 5    |             | 0.993       | 0.994       | 0.999       |
| 7    |             | 0.996       | 0.994       | 0.999       |

Table 10.  $R^2$  values for Landsat image-pair normalization, by band.

| Reflectance difference | Band 1  | Band 2  | Band 3  | Band 4  | Band 5  | Band 7 |
|------------------------|---------|---------|---------|---------|---------|--------|
| WS1: 2007-1999         | -0.0506 | -0.192  | -0.111  | 5.48    | -0.456  | -0.531 |
| WS6: 2007-1999         | 0.267   | -0.0048 | 0.350   | 2.02    | 0.575   | 0.321  |
| Treatment              | 0.036   | < 0.001 | 0.785   | < 0.001 | < 0.001 | 0.011  |
| Year                   | < 0.001 | < 0.001 | < 0.001 | < 0.001 | 0.277   | 0.005  |
| Year * Treatment       | 0.040   | 0.402   | 0.002   | 0.012   | 0.614   | 0.040  |

Table 11. Change in coniferous Landsat reflectance signature of watersheds 1 and 6 at HBEF, 1999 to 2007. Differences of mean pixel reflectance are presented for Ca-treated (WS1;  $n = 32$ ) and reference (WS6;  $n = 33$ ). Resulting  $P$  values for F-tests of significance from ANOVAs are also shown, by band.

| Reflectance difference | Band 1  | Band 2  | Band 3  | Band 4  | Band 5  | Band 7  |
|------------------------|---------|---------|---------|---------|---------|---------|
| WS1: 2007-1999         | 0.169   | -0.166  | 0.0377  | 3.94    | -0.0759 | -0.296  |
| WS6: 2007-1999         | 0.359   | 0.0275  | 0.148   | 3.82    | 0.225   | -0.0659 |
| Treatment              | 0.028   | < 0.001 | < 0.001 | < 0.001 | < 0.001 | < 0.001 |
| Year                   | < 0.001 | < 0.001 | < 0.001 | < 0.001 | < 0.001 | < 0.001 |
| Year * Treatment       | 0.011   | < 0.001 | < 0.001 | 0.060   | 0.236   | 0.036   |

Table 12. Change in deciduous Landsat reflectance signature of watersheds 1 and 6 at HBEF, 1999 to 2007. Differences of mean pixel reflectance are presented for Ca-treated (WS1;  $n = 156$ ) and reference (WS6;  $n = 165$ ). Resulting  $P$  values for F-tests of significance from ANOVAs are also shown, by band.



| Index               | Landsat 5 / 4 |       | NDVI    |       |
|---------------------|---------------|-------|---------|-------|
|                     | WS1           | WS6   | WS1     | WS6   |
| Year                |               |       |         |       |
| 1999                | 0.482         | 0.434 | 0.787   | 0.786 |
| 2001                | 0.448         | 0.425 | 0.813   | 0.813 |
| 2005                | 0.440         | 0.490 | 0.798   | 0.759 |
| 2007                | 0.400         | 0.426 | 0.819   | 0.788 |
| Year                | < 0.001       |       | < 0.001 |       |
| Ca-treatment        | 0.853         |       | < 0.001 |       |
| Year * Ca-treatment | < 0.001       |       | < 0.001 |       |

*Table 13.* Descriptive indices from coniferous pixels in Ca-treated (WS1) and reference (WS6) areas extracted from four Landsat scenes. *P* values are also listed for a two-way factorial ANOVA for each index.

| Index               | Landsat 5 / 4 |       | NDVI    |       |
|---------------------|---------------|-------|---------|-------|
|                     | WS1           | WS6   | WS1     | WS6   |
| Year                |               |       |         |       |
| 1999                | 0.479         | 0.472 | 0.822   | 0.827 |
| 2001                | 0.434         | 0.450 | 0.843   | 0.841 |
| 2005                | 0.442         | 0.441 | 0.834   | 0.827 |
| 2007                | 0.431         | 0.434 | 0.836   | 0.836 |
| Year                | < 0.001       |       | < 0.001 |       |
| Ca-treatment        | 0.240         |       | 0.393   |       |
| Year * Ca-treatment | 0.002         |       | 0.002   |       |

*Table 14.* Descriptive indices from deciduous pixels in Ca-treated (WS1) and reference (WS6) areas extracted from four Landsat scenes. *P* values are also listed for a two-way factorial ANOVA for each index.



*Figure 13.* Infrared-color (bands 7:4:3 corresponding to R:G:B) Landsat 7 ETM+ image of the Hubbard Brook Experimental Forest, acquired 31 August 1999. Level areas of high infrared reflectance appear a pinkish color, water bodies are dark blue, and vegetation ranges from light green (deciduous character), to darker (coniferous). Watersheds 1 and 6 are shown on the south-facing slope. The Pemigewasset river and interstate-93 are also visible running north-south, just east of Mirror Lake.



*Figure 14.* Digital ortho-quadrangle (DOQ) image of the experimental watersheds at HBEF. Image was taken during the spring of 1993 before deciduous leaf-out, and the darkened spruce-fir stands are visible along the ridge in the northwest corner. Boxes show the locations of 28.5-m Landsat pixels ( $n = 65$ ) covering the spruce-fir zone in the two watersheds.



*Figure 15.* May 2008 photo of spruce-fir ridge zone of Hubbard Brook showing unclosed, predominantly conifer canopy. Note the white birch snag in the foreground, a common sight in these plots.

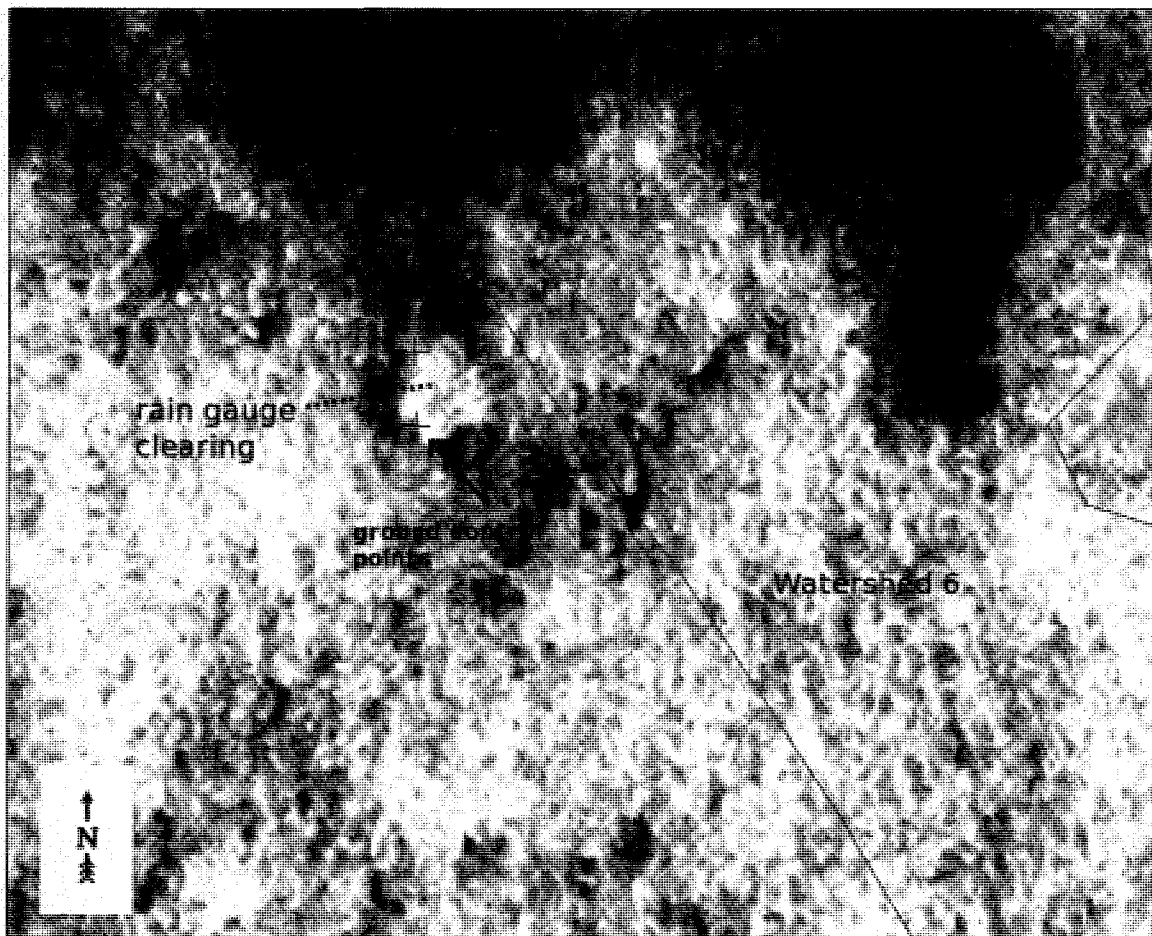


*Figure 16.* Digital ortho-quadangle (DOQ) image acquired before spring leaf-out, showing the area west of watershed 6, and GPS ground control points collected at the corners of a rain gauge clearing, approximately one Landsat pixel in size.

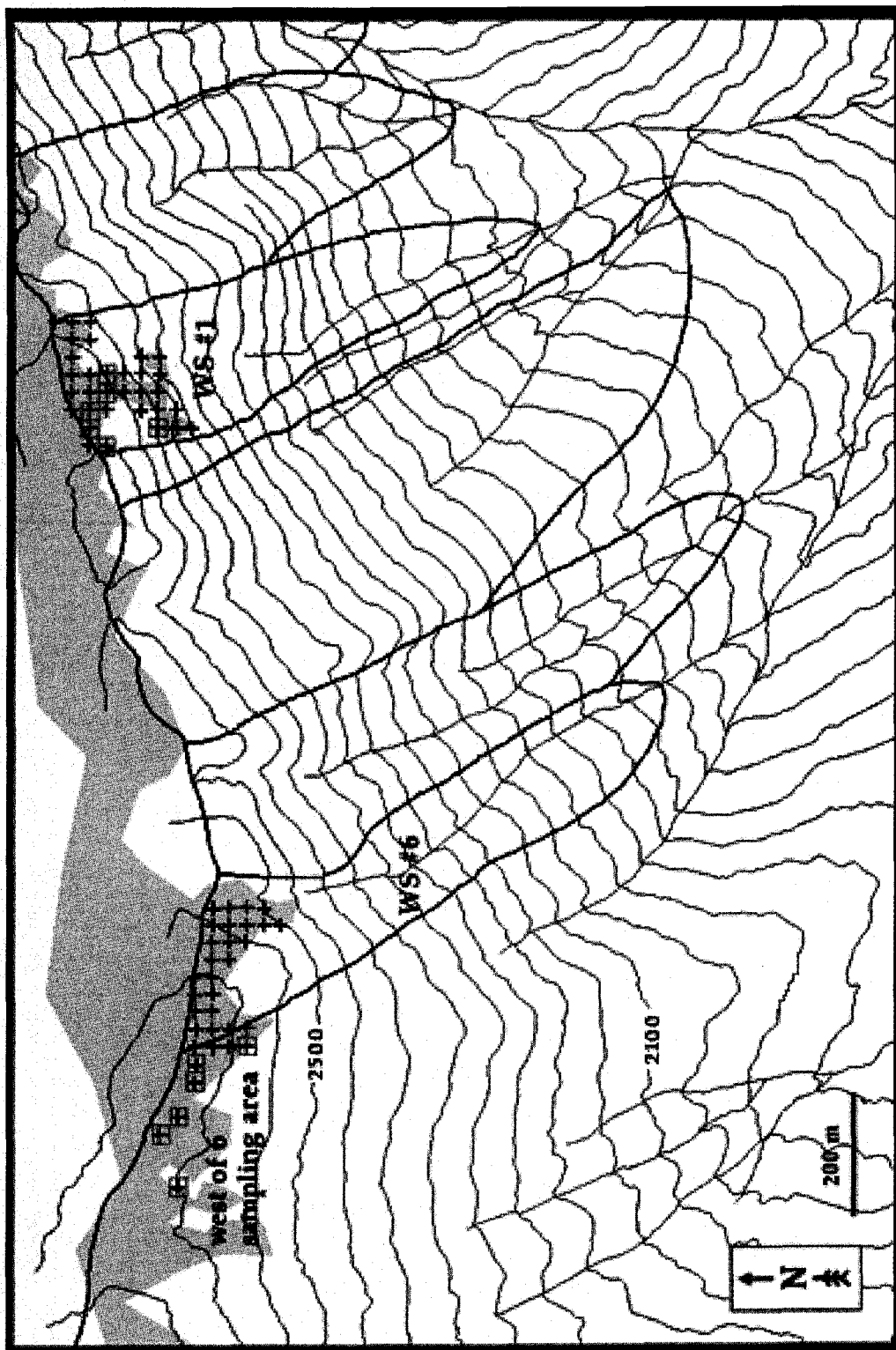


Figure 17. Ca-treated (WS1) and reference (WS6) areas at HBEF. Topographic contour lines are spaced at 50 ft. Crosshairs indicate centers of extracted coniferous Landsat 28.5-m pixels, and boxes indicate ground sampling plots. All pixels and plots reside within the spruce-fir community (shaded gray) along the ridge.

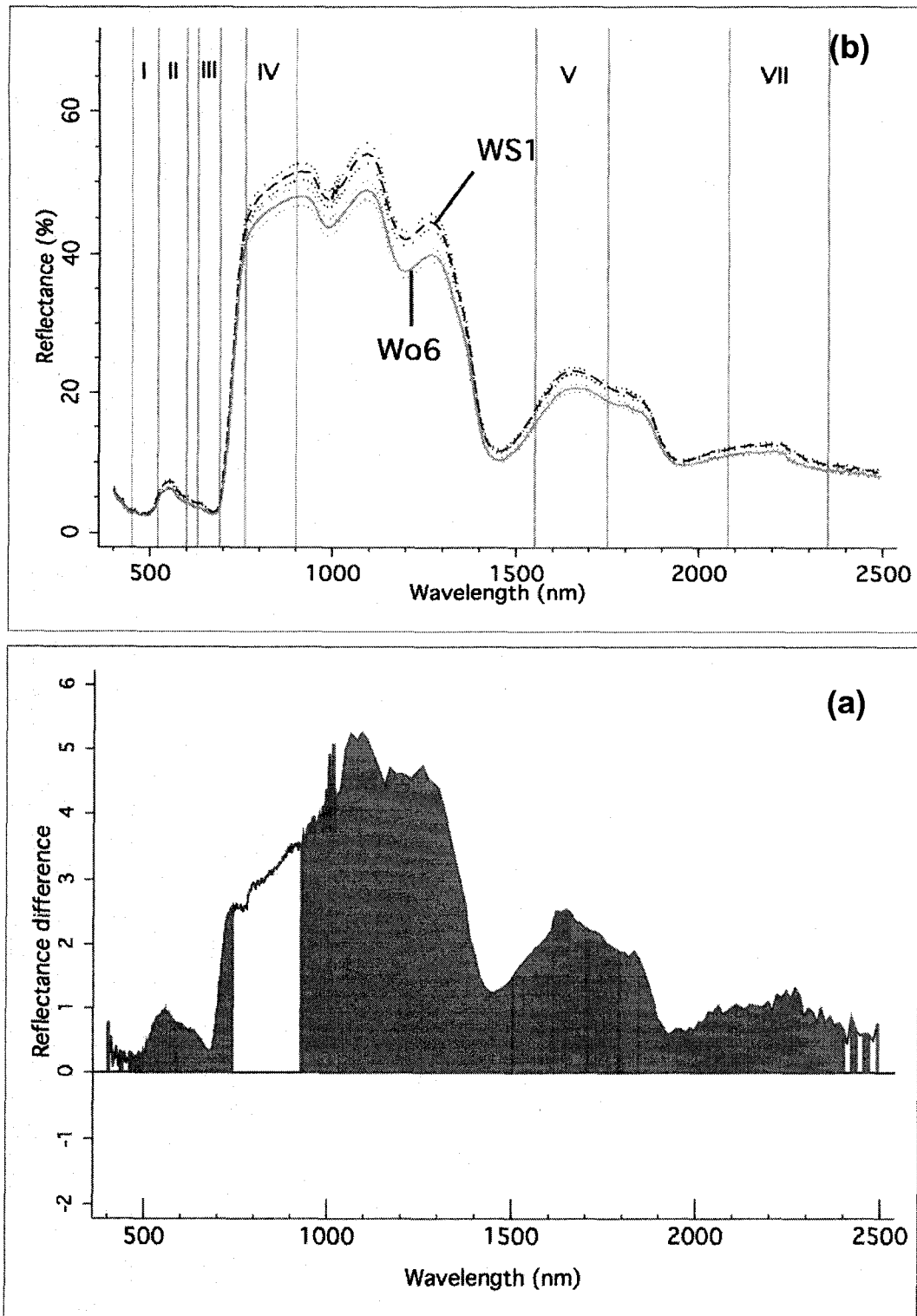


Figure 18. (a) Mean ( $n = 18$ ) reflectance curves for Ca-treated (WS1) and reference (Wo6) needles in mixed-needle year boughs sampled at HBEF. Finely dotted lines show  $\pm$  standard error of measurement for each age class. Landsat band regions 1-5 and 7 are indicated by Roman numerals. (b) Reflectance difference curve (WS1 - Wo6); shaded regions significantly ( $P < 0.05$ ) differed in a Student's t-test.

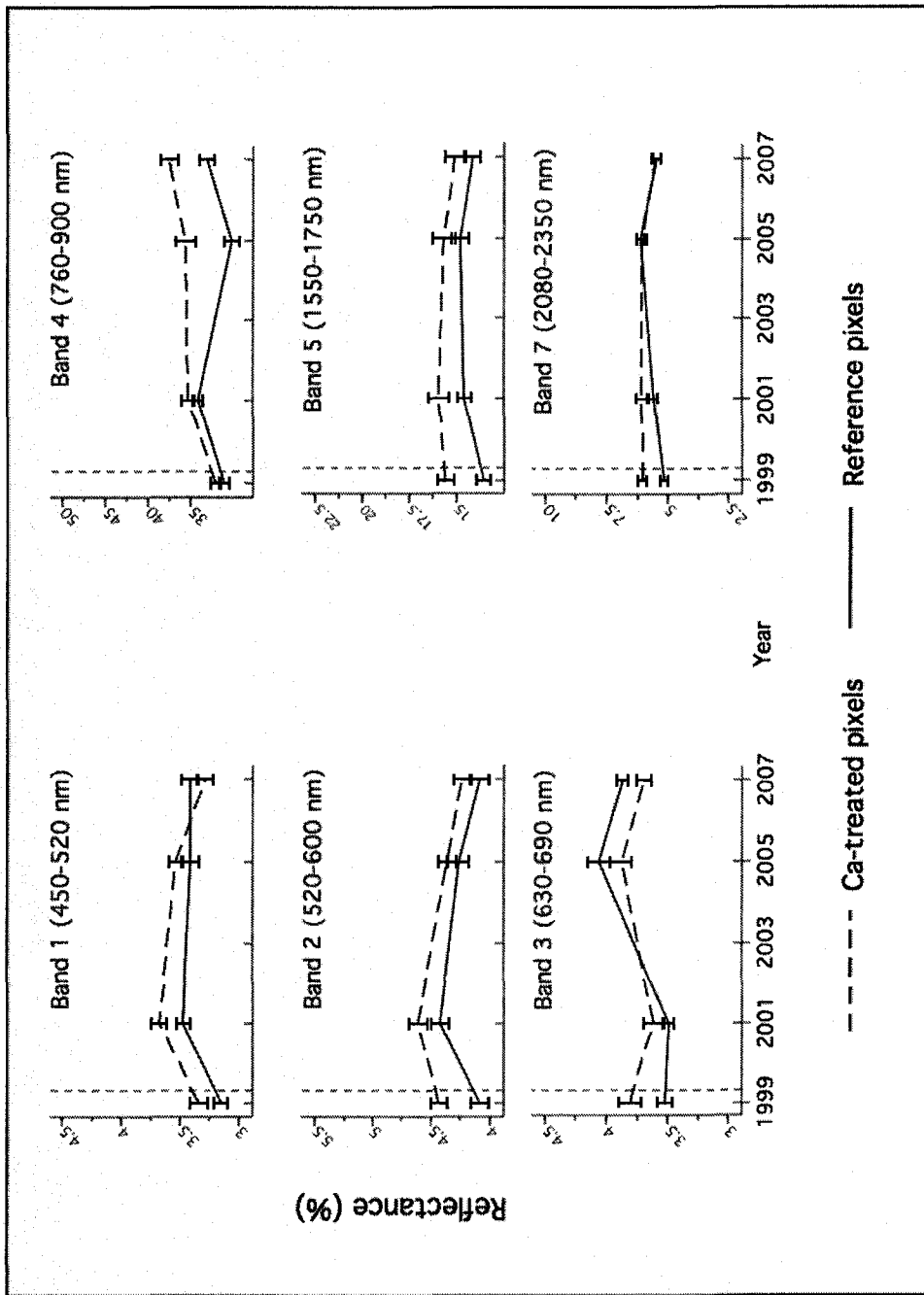


Figure 19. Change in normalized band reflectance from 1999-2007 in coniferous pixels extracted from watershed 1 (n = 32) and watershed 6 (n = 33). The vertical dashed line indicates the date of Ca fertilization, October 1999. Bars indicate +/- one standard error.



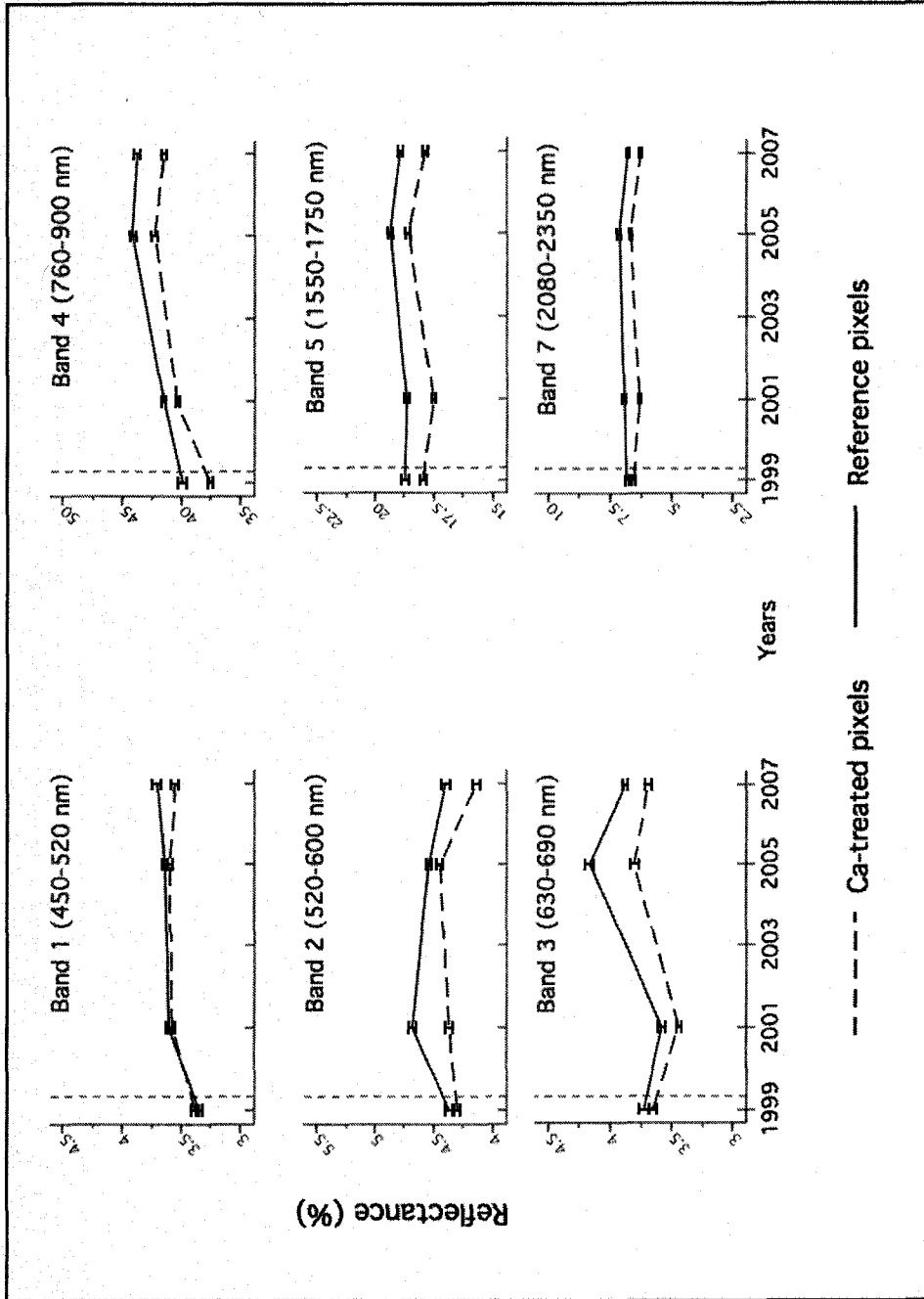


Figure 20. Change in normalized band reflectance from 1999-2007 in deciduous Landsat pixels extracted from watershed 1 (n = 156) and watershed 6 (n = 165). The vertical dashed line indicates the date of Ca fertilization, October 1999. Bars indicate +/- one standard error.

## CONCLUSION

The abundant soil Ca pool produced by the whole-watershed wollastonite application has resulted in increased foliar Ca and oxalate levels in red spruce. Several vegetation health indices measured from laboratory spectra show a surfeit of Ca resulted in a physiological stress for the Ca-amended trees. The pan-spectral reflectance increases seen in Ca-treated bough samples suggest the accumulation of crystal Ca-oxalate deposits over multiple growing seasons has enhanced foliar refraction and reflectance, and correlations were seen between foliar oxalate content and infrared reflectance. Stand level processes related to tree mortality and conifer/deciduous canopy fraction complicate the extrapolation of laboratory spectra to larger scales, and the laboratory hyperspectral signs of foliar stress were not measured by Landsat data or stand inventories corresponding to spruce-fir pixels. Nonetheless, there were several signs of an increased near-infrared response that was common to Ca-treated spectra in both laboratory and satellite data. Future work is needed for the evaluation of multispectral response ratios (e.g. Landsat TM4/TM7) over known Ca gradients, or the un-mixing of spectral components in the Ca-treated spruce-fir zone of Hubbard Brook.